ANALYSIS OF SAHARAN DESERT DUST TRANSPORT TO THE ANATOLIAN PENINSULA: A MEGACITY PERSPECTIVE

by

GÜL AKINÇ

BS. in Env. Eng., Dokuz Eylül University, 2005

Submitted to the Institute of Environmental Sciences in partial fulfillment of the requirements for the degree of

Master of Science

in

Environmental Technologies

Boğaziçi University

2010

ACKNOWLEDGEMENTS

This study would not have been possible without the guidance and the help of several individuals who contributed and extended their valuable efforts in the preparation and completion of this thesis.

First, I would like to thank my thesis supervisors; Prof. Dr. Orhan Yenigün and Assoc. Prof. Dr. Tayfun Kındap for their spectacular guidance and support during the thesis preparation period.

The guidance of the Eurasia Institute of Earth Sciences Climate Research Group, under the leadership of Assoc. Prof. Dr. Tayfun Kındap and Assoc. Prof. Dr. Alper Ünal, was the driving force of this study. I am also thankful to Assoc. Prof. Dr. Alper Ünal, who shares his valuable atmospheric science knowledge with me.

I would like to thank the thesis committee members: Prof. Dr. Selahattin İncecik, Assoc. Prof. Dr. Nadim Copty and Assist. Prof. Dr. Başak Güven for their precious suggestions.

I should thank Dr. Ulaş İm, who shared his precious insights and his technological (model) background with me. I am really thankful to him for having directed me in a correct way.

Behind this study, there is a hidden hero. No words can express how I can thank to him for his patient encouragement. I am so grateful to Deniz Ural for his IT support & shared meteorological information. Also, I should thank him for his reliable friendship. Thank you for everything Deniz.

I am grateful to Seden Baltacıbaşı for the help on executing the map displaying programs and for her sweet friendship.

Finally, I offer my regards and blessings to my special family. Thank you for your lovely moral support!

ANALYSIS OF SAHARAN DESERT DUST TRANSPORT TO THE ANATOLIAN PENINSULA: A MEGACITY PERSPECTIVE

Mineral dust is one of the most significant constituent among the air pollutants. Besides its negative effects on human health, it influences the radiation balance of the Earth. The greatest source of mineral dust over the world is known as the Saharan Desert. The lifted dust from the Saharan region has been distributed over many parts of the Northern Hemisphere. Especially, during the spring period, the desert dust has been transported to the eastern Mediterranean region. From this point of view, contribution of Saharan Desert dust to the Istanbul's coarse particulate matter levels has been investigated. To find out the clues of the transport, a numerical meteorological model called Weather Research and Forecasting has been run for the month of April in year 2008. The meteorological patterns of the model domain such as distribution of horizontal and vertical wind vectors, backward trajectory analysis of Istanbul have been examined to decide on the transport. In addition to the WRF model outputs, three additional models have been used to support the model data. Results of WRF and the other supportive models indicate that during the spring, there is an obvious contribution of Saharan Desert dust to the high PM10 levels of Istanbul.

SAHRA ÇÖL TOZLARININ ANADOLU YARIMADASI'NA TAŞINIM ANALİZİ: MEGAŞEHİR PERSPEKTİFİNDEN

Mineral toz, hava kirleticileri içersinde ciddi önem arz etmektedir. Dünya üzerindeki en büyük mineral toz kaynağı ise Sahra Çöl bölgesi olarak adlandırılmaktadır. Yapılan araştırmalar göstermektedir ki Sahra Çöl'ünden kuzey yarımküredeki pek çok alana mineral toz taşınımı gerçekleşmektedir (Engelstaedter, 2006). Bahsi geçen taşınım istikametlerinden biri Doğu Akdeniz-Orta Doğu güzergahıdır. Bu bağlamda, Sahra Çöl tozlarının Türkiye ve Anadolu Yarımadası üzerine potansiyel taşınabilirliği bu çalışmanın temelini oluşturmaktadır. İlkbahar aylarında Akdeniz bölgesinde tespit edilen Sahra Çölü tozlarının, İstanbul'un ölçümlenen yüksek partikül madde konsantrasyonlarının önemli bir sebebi olup olmadığı araştırılmıştır. Taşınımın tespit edilebilmesi için, Weather Research and Forescasting (WRF) isimli numerik meteorolojik modelden faydalanılmıştır. İstanbul'un 4 ciddi hava kirliliği episodu deneyimlediği 2008 Nisan ayı baz alınarak, WRF modeli aracılığıyla Sahra Çölü ve Anadolu Yarımadası'nı kapsayan bir çalışma alanı içerecek şekilde; yatay ve düşey atmosferde rüzgar dağılımları, geri yörünge analizleri, yağış haritaları üretilmiştir. Elde edilen meteorolojik bulgular, 2008 Nisan ayı içersinde pek çok kez meteolojik koşulların Sahra Çöl tozlarının Anadolu Yarımadasına taşınımını elverişli kıldığını göstermektedir. WRF'a ek olarak üç ayrı destekleyici modelin de bahsi geçen dönem ve alanlarda mineral toz taşınımını destekler nitelikte sonuçlar ortaya koyduğu tespit edilmiştir.

TABLE OF CONTENTS

LIST OF FIGURES

LIST OF TABLES

LIST OF SYMBOLS/ABBREVIATIONS

Symbol	Explanation
ABM	Australia's Bureau of Meteorology
AD	The region of Adrar Mountains
AI	The region of Air Mountains
AK	The region of Akhdar Mountains
AOD	Aerosol Optical Depth
ARL	Air Resources Laboratory
AT	The region of Atlas Mountains
AVHRR	Advanced Very High Resolution Radiometer
BSC	Barcelona Supercomputing Center
BL	Boundary layer
BO	The region of Bodélé Depression
COAMPS	The Coupled Ocean/Atmosphere Mesoscale Prediction System
COD	Cloud Optical Depth
DREAM	The Dust Regional Atmospheric Model
DSA	Dust Source Activation
E	A cardinal wind direction representing east
ENE	A wind direction representing east north - east
EPA	The United States Environmental Protection Agency
EU	The European Union
EI	Episode I
EII	Episode II
EIII	Episode III
EIV	Episode IV
FAO	Food and Agriculture Organization
GES-DISC	Goddard Earth Sciences Data and Information Services Center
Giovanni	The GES-DISC Interactive Online Visualization and Analysis Infrastructure
GOCART	The Goddard Chemistry Aerosol Radiation and Transport
H	High-pressure area
HYSPLIT	The Hybrid Single Particle Lagrangian Integrated Trajectory Model

IDDI	Infrared Difference Dust Index
IMM	Istanbul Metropolitan Municipality
IR	Infrared
ITCZ	The Inter-Tropical Convergence Zone
KO	The region of Kordofan
L	Low-pressure area
lat	Latitude
LLJ	Low-level jet
lon	Longitude
MISR	Multi-angle Imaging SpectroRadiometer
MM5	The Fifth-Generation NCAR / Penn State Mesoscale Model 5
MODIS	The Moderate Resolution Imaging Spectroradiometer
MSG	Meteosat Second Generation
N	A cardinal wind direction representing north
NCEP	National Centers for Environmental Prediction
NCAR	The National Center for Atmospheric Research
NID	The Naval Intelligence Division
NE	An ordinal wind direction between north and east
NOAA	The National Oceanic and Atmospheric Administration
NU	The region of Red Sea and Nubian Mountains
NWP	Numerical Weather Prediction
Obs	Observations
OMI	Ozone Monitoring Instrument
OU	The region of Quaddai Mountains
PM_{10}	Coarse Particulate Matter
PSU	Penn State University
RAMS	The Regional Atmospheric Modeling System
S	A cardinal wind direction representing south
SAL	Saharan Air Layer
SAMUM	Saharan Mineral Dust Experiment
SE	An ordinal wind direction between south and east
SEVIRI	Spinning Enhanced Visible and Infrared Imager
SW	An ordinal wind direction between south and west

TOMS AI	Total Ozone Mapping Spectrometer - Aerosol Index
TSMS	Turkish State Meteorological Service
USGS	The United States Geological Survey
UTC	Universal Time Coordinated
UV	Ultraviolet light
W	A cardinal wind direction representing west
WRF	The Weather Research and Forecasting Model
WS	The region of Western Sahara

1. INTRODUCTION

1.1. The Significance of Mineral Dust as an Atmospheric Pollutant

Mineral dust is a class of aerosols which results from wind activities on soil particles (Seinfeld, 2006). Figure 1.1 gives the global emission estimates of major dust classes. After seasalts, mineral dust is the second greatest aerosol source of the world.

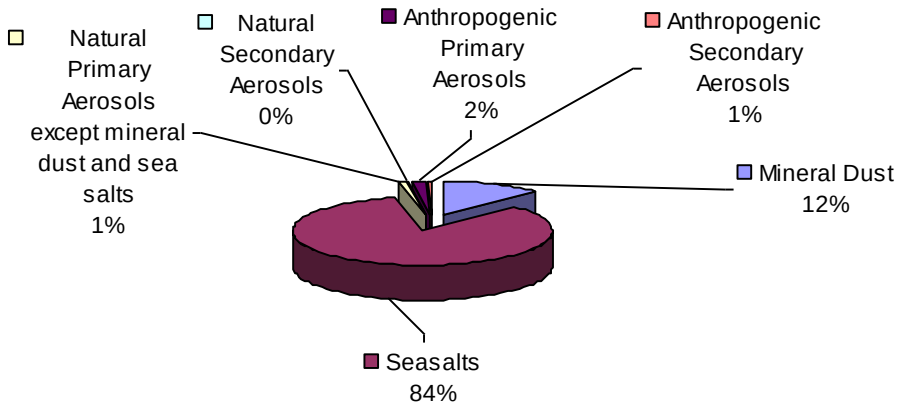

Figure 1.1. Global emission estimates of major dust classes.

Besides being a considerable air pollutant source, mineral aerosols have attracted the attention of the researchers because of aerosols significant impacts on human health and environment. Particulate pollution is related with a variety of health problems, including (EPA, 2010) :

- increased respiratory symptoms, such as irritation of the airways, coughing, or difficulty breathing,
- decreased lung function,
- aggravated asthma,
- development of chronic bronchitis,
- irregular heartbeat,
- nonfatal heart attacks, and
- premature death in people with heart and lung disease.

Effects of aerosols on environment can be listed as (EPA, 2010);

- visibility reduction,
- environmental damage (Transported particles over the lakes and streams make them acidic. Aerosols change the nutrient balance in coastal waters and large river basins.They deplete the nutrients in soil, damage sensitive forests and farm crops, affect the diversity of the ecosystems.),
- aesthetic damage: Particle pollution can damage stone & other materials, including culturally important objects such as statues and monuments.

Atmospheric aerosol's effects on climate and environment can be listed as (Goudie et al., 2001.);

- they may influence air temperatures through the absorption and scattering of solar radiation. They modify short-wave solar radiation transmitted through the earth's surface and long-wave infra-red radiation emitted to space. The balance between these two tendencies identifies whether cooling or warming occurs. Therefore, they affect the radiation balance of the Earth,
- dust may cause ocean cooling,
- changes in atmospheric temperatures and in concentrations of potential condensation nuclei may influence convectional activity and cloud formation. These modify rainfall amounts,
- mineral dust is an effective substrate for transporting disease-spreading spores which can cause epidemics (in Caribbean region, particularly),
- aerosols may affect soil formation (High carbonate content of dust forms calcretes),
- dust has a role in the delivery of sediments to oceans.

Due to these significant impacts of dust on human health and the environment, one of the most abundant type of aerosols; mineral dust, come into prominence. The greatest source of this ample dust is known as the Saharan Desert region of the North Africa.

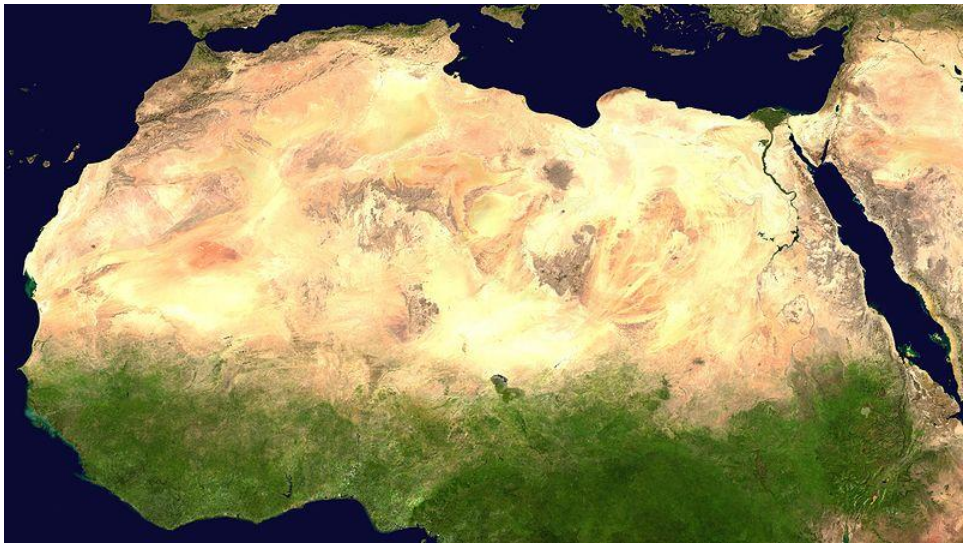

Figure 1.2. A satellite image of Saharan Desert by NASA World Wind.

The export of desert aerosols from the Saharan Desert region reaches to areas of several 100 000km^2. Saharan dust may be considered as being distributed over the great regions of the Northern Hemisphere. Since distances of Saharan dust transport approach 10 000 km, it can be concluded that desert dust is obviously omnipresent within the atmosphere (SAMUM).

The transport pathways of Saharan desert aerosols have been defined by several researchers (Engelstaedter et al., 2006). One of these major pathways of Sahara is identified as the way towards the Eastern Mediterranean (Kocak et al., 2007; Kocak et al., 2009). The studies indicate that Saharan Desert is the potential aerosol source of the particulate matter events of Erdemli which is a rural site of Turkey, located on the coast of the Eastern Mediterranean .

Contribution of Saharan Desert dust to the coarse Particulate Matter (PM10) levels of the southern Turkey brings into question the potential contribution of Saharan mineral aerosols to the high PM levels of Istanbul. The data on daily concentrations of ambient coarse Particulate Matter (PM10) points out that Istanbul had experienced significant particulate matter episodes during the month of April in year 2008 (Fig 1.3).

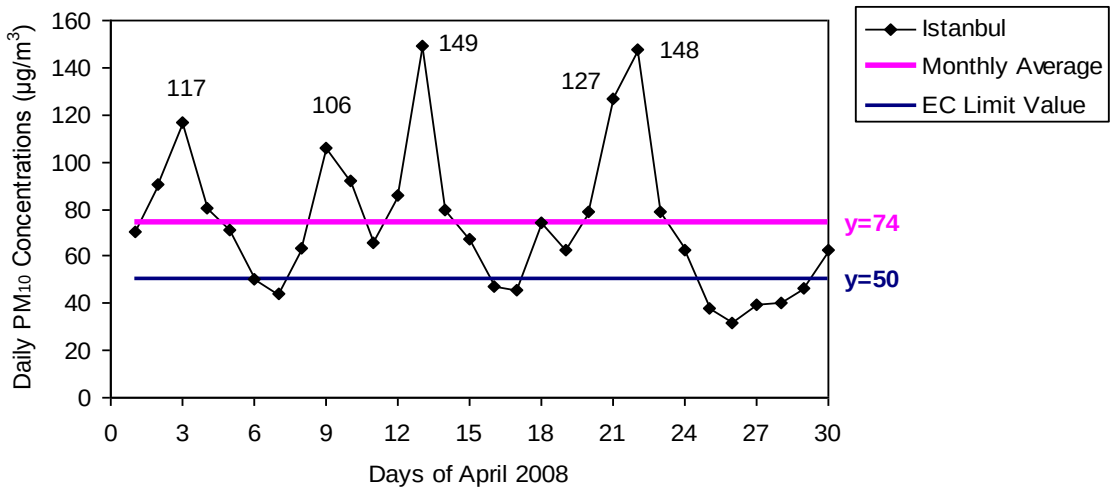

Figure 1.3. Daily PM10 concentrations of the month of April in year 2008.

The directives of European Commision; Council Directive 96/62/EC and Council Directive 1999/30/EC set the PM10 annual average concentration limit value as 40 ($\mu g/m^3$), and the daily PM10 concentration limit value as 50 ($\mu g/m^3$). According to the directives, the daily PM10 limit value 50 ($\mu g/m^3$) should not be exceeded more than 35 times per calender year. However, as it can be seen from Fig 1.3, only the month April itself includes 22 days exceeding the limit value of the EC directives. Therefore, these suspiciously high PM levels of Istanbul has been the starting point of this study. Although the antropogenic sources of Istanbul contributes to the PM levels, natural sources of dust may contribute to these extreme levels of the particulates. It has been known that, during the spring, favorable meteorological conditions play a role to carry dust towards the Mediterranean region (Engelstaedter et al., 2006).

Therefore, in order to prove the potential contribution of Saharan Desert dust to Istanbul's high levels of PM during April 2008, a numerical meteorological model called Weather Research and Forecasting (WRF) was run. The study domain has been selected to include both the Saharan Desert Region and Turkey. The output graphics of the meteorological parameters (such as horizontal and vertical distribution of wind vectors, temperature, geopotential height, precipitation) and backward trajectory analysis of Istanbul have been used to show the evidence of the transport of desert dust towards the Marmara Region of Turkey. Alternative methods, which will be described in the following sections, have been used to support the results of the WRF model.

1.2. Characteristics of Saharan Desert & Desert Dust

1.2.1. General Information on Saharan Desert

Saharan Desert, which is mentioned as the technically third greatest desert in the world, is also the major global dust source of the planet. It is located on the continent of Africa and represents over 40% of the continent. The driest and hottest areas of Earth exist in this region. Extremely arid, arid and semi-arid areas can be listed as the composers of the Saharan Desert land types (Warner, 2004).

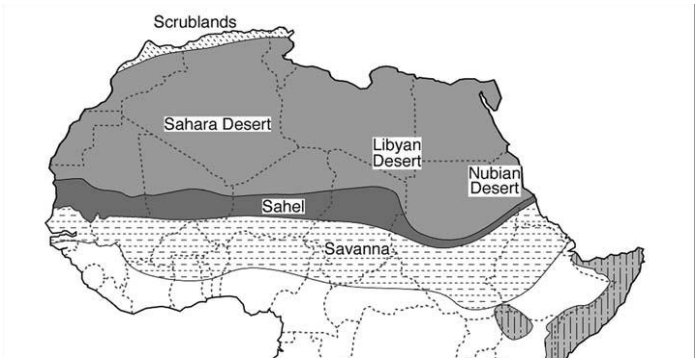

Figure 1.4. North African Deserts including the Saharan Desert (Warner, 2004).

The desert area covers from 5°N to the Mediterranean coast and from the Atlantic coast in the west to the Red Sea in the east. It spans 1500 km between north-south direction and 5000 km between west-east directions. The total area of Sahara is approximately 9 400 000 km^2.

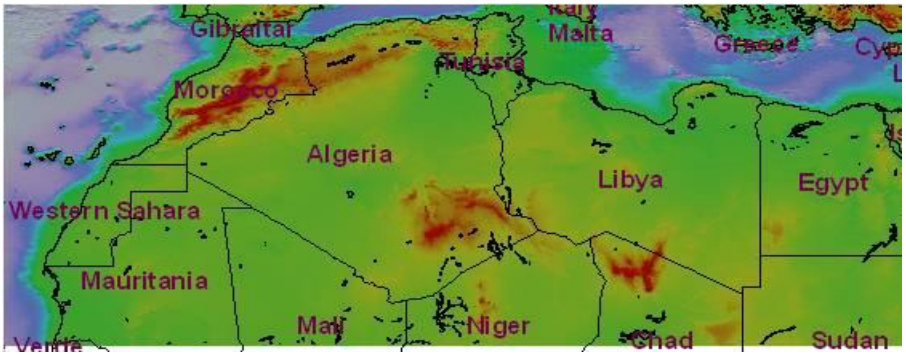

Figure 1.5. The countries of Africa covered by the Saharan Desert.

The countries covered by Sahara can be listed as: Algeria, Chad, Egypt, Libya, Mali, Mauritania, Morocco, Niger, Western Sahara, Sudan and Tunisia (Fig 1.5).

1.2.2. Physiographical Characteristics of Sahara

The geomorphology of Saharan Desert has a significant role in influencing the mineral aerosol sources of the region. Sahara includes several soil- derived aerosol source areas, usually distinct from each other. The source areas of mineral dust is expected to be related with paleo or fluvial deposits associated with geomorphologic elements i.e. periodically flooded or dry lakes, drainage systems, wadis, alluvial fans or playas. It is considered that these sediments are collected at topographic depressions. They are expected to be transported from the surrounding mountains or high elevated areas to the depressions. Then, the favorable wind speed initiates the transportation of the materials. Interestingly, large dune systems of Africa are not expected to be the major sources of mineral dust (Engelstaedter, 2006). In addition to comprising source of the dust, mountains also have effect on transport of the desert dust. The gaps between the main mountain regions act as channels for the airmass transport (Kallos et al., 2007). Since of the significance of the topographic features, the major elements of the geomorphology and some geomorphologic terms are explained in the following sections.

1.2.2.1. Mountain Regions. Main major Saharan mountain regions are defined as:

- Atlas Mountains in Morocco,
- The Hoggart Massif in southeast Algeria,
- The Air Mountains in Niger,
- The Tibesti and Ennedi Mountains in Chad (Engelstaedter, 2006).

These mountain regions are shown in Figure 1.6.

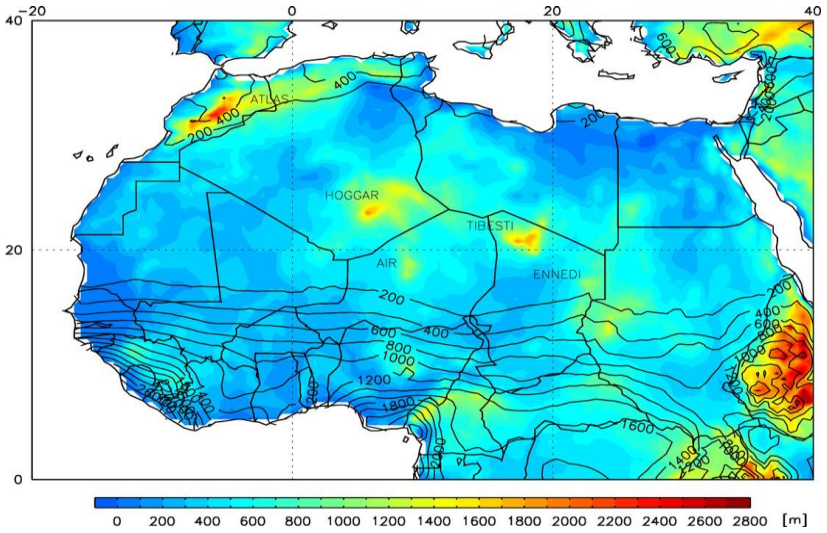

Figure 1.6. Main Saharan mountain regions (Engelstaedter, 2006).

1.2.2.2. Other Topographic Features. One of the most important feature of the Saharan region can be stated as the topographic depression. Depression is defined as a type of land, sunken or depressed below its surrounding area. Topographic Depressions located in the Sahara Desert region are the Bodélé Depression in Chad (Fig. 1.7) and Qattara Depression in western Egypt. Table 1.1 shows some important topographic features, observed in Saharan Desert Region.

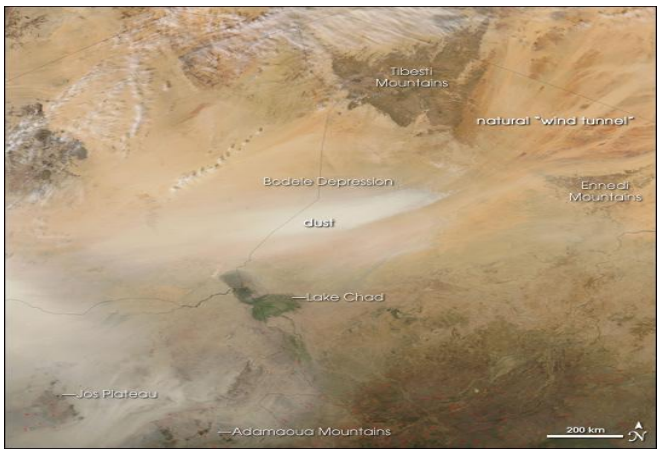

Figure 1.7. Bodélé dust storm (Bodélé Depression | earthobservatory.nasa.gov).

Table 1.1. Some topographic features observed in Sahara region.

Topographic Features	Definitions
Wadis	Dry eroded water courses
Regs	smooth plains of dense, cemented fine gravel in the western Sahara
Serir	smooth plains of dense, cemented fine gravel in the eastern Sahara
Hammadas (or hamadas)	a type of desert landscape including largely barren, hard, rocky plateaus, with a little sand.
Ergs	Sand seas

Approximately 80% of Sahara is made up of rock, gravel or pebble, and sand surfaces. Sand represents nearly 15-20% of the total (Warner, 2004).

1.2.3. Threshold Wind Velocities for Saharan Dust Mobilization. Transportation of desert dust starts with the lifting of fine deflatable material from ground when surface wind velocity exceeds a certain threshold wind speed (Engelstaedter, 2006). This threshold value depends on surface roughness elements, grain size and soil moisture. Several experiments have been made to determine the threshold velocity of dust mobilization. Table 1.2 summarizes the results of the threshold wind speed experiments for Sahara dust activation.

Table 1.2. Threshold wind velocities of Saharan dust activation

Studies	Average Threshold Value, m/s	Threshold Range, m/s
Fernandez-Partagas et al., 1986	8	5 – 12.5
Chomette et al., 1999	-	6.63±0.67 – 9.08±1.08
Sokolik, 2002; Seinfeld, 2006	6.5	-

Threshold wind speed range differs from 5 to 12.5 m/s. The differences in thresholds may have resulted from the precisions of the different methods used (Engelstaedter, 2006).

1.2.4. Removal Mechanisms of Dust: Dry and Wet Deposition. As well as the initiation of the dust transport, finale of the transport process: removal mechanism of the dust has remarkable importance. Dust can be removed from the atmosphere by three mechanisms: sedimentation, dry deposition, and wet deposition.

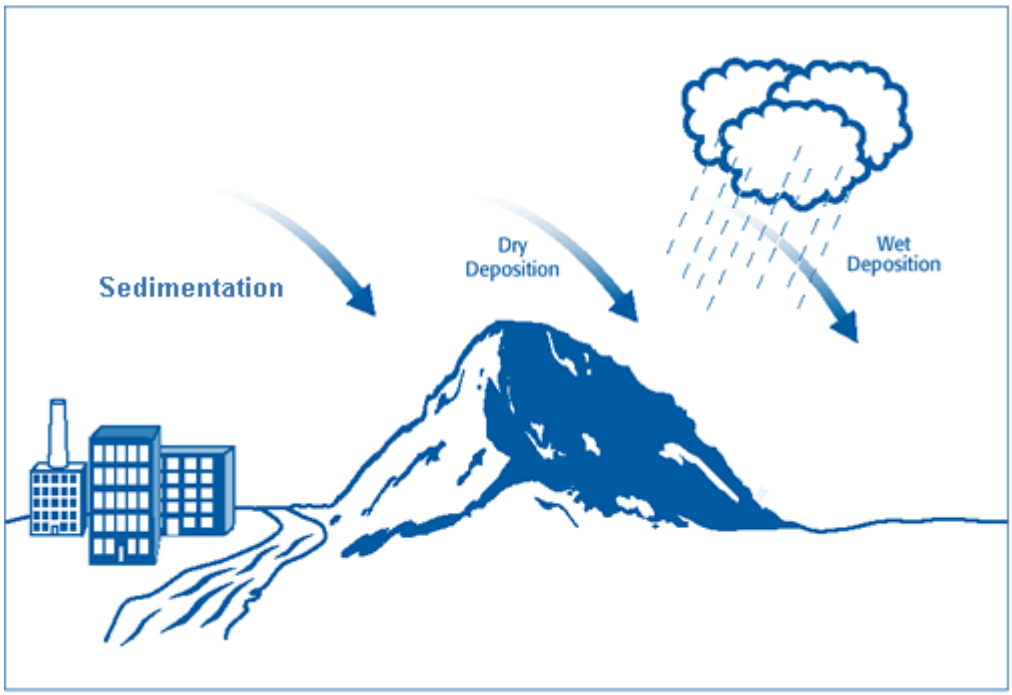

Figure 1.8. Representation of removal mechanisms of aerosols.

Sedimentation is the removal mechanism of aerosols by sinking due to the force of gravity (Jacobson, 2005). Dry deposition is the transport of gaseous and particulate species from the atmosphere onto surfaces in the absence of precipitation (Seinfeld et al., 2006). It occurs when gases or particles contact a surface and stick to or react with the surface (Jacobson, 2005). However, sedimentation is the process by which particles contact surfaces. Wet deposition is the natural process by material is scavenged by atmospheric hydrometeors (rain, snow, cloud and fog drops) and is delivered to the Earth's surface (Seinfeld et al., 2006).

1.3. Major Dust Source Areas of Saharan Desert

1.3.1. Saharan Dust Source Identification Methods

The natural dust source regions of Sahara generally lie in remote desert areas where the installation and maintanence of equipment for continous long-term measurements is not currently possible (Engelstaedter, 2006). At this point, remote observations, either at the surface or downwind of sources, or from satellites, play a significant role.

There are several ways to identify the source areas of desert dust in adition to the model trajectories (Engelstaedter, 2006):

1. Horizontal visibility measurements
2. Satellite derived products
    a. Advanced Very High Resolution Radiometer (AVHRR)
    b. Meteosat data – Infrared Difference Dust Index (IDDI)
    c. Total Ozone Mapping Spectrometer (TOMS) – Aerosol Index (AI)
    d. Moderate Resolution Imaging Spectroradiometer (MODIS)
    e. Multi-angle Imaging Spectroradiometer (MISR)

These meassurements are discussed below:

1.3.1.1. Horizontal Visibility Measurements. In desert areas, visibility reductions generally occur as a result of aerosols in the atmosphere**.** Therefore, it can be considered as an indirect method for measuring the dust loadings near the surface air layer. The reduction of visibility below specific thresholds (e.g. 1 km, 5 km and 10 km) may be used as a classification scheme to get frequency distributions of atmospheric dust events according to their relative intensity (Engelstaedter, 2006). Visibility reduction analyses have been used as the direct measurement method of dust before the new technologies such as satellite retrievals have been found. Although they have been used for years, they have some disadvantages. Their usage is limited because of the sparse distribution of meteorological stations (up to approximately 2000km) and the incomplete records due to the underdeveloped infrastructure or political instability.

On the other hand, satellite derived products of atmospheric aerosols overcome the coverage problems characteristic of surfaced based observations from meteorological stations, but experiencing the problems of unsolved errors induced by land surface reflectance and cloud cover, low frequency of measurements, the lack of long term measurements and sensitivity to height of dust layers (Engelstaedter, 2006).

1.3.1.2. Satellite-derived Products. Satellite observations in the visible range as measured from the Advanced Very High Resolution Radiometer (AVHRR) and Meteosat data are used to retrieve aerosol content over the oceans (Engelstaedter, 2006).

The retrievals from the Total Ozone Mapping Spectrometer (TOMS) from November 1978 to May 1993 on board of the Nimbus 7 satellite (from July 1996 on the Earth Probe satellite) can be used to determine absorbing aerosols by looking at the spectral contrast of two UV channels (340 nm and 380 nm for Nimbus 7; 331 and 360 nm for Earth Probe), resulting in the TOMS absorbing aerosol index (TOMS AI). The advantage of TOMS method is to be able to see the dust distribution both over the land and ocean, likewise the AVHRR and meteosat data. The disadvantage of TOMS is being weak to represent the distribution of dust near the surface at heights lower than about 1 km.

The Moderate Resolution Imaging Spectroradiometer (MODIS) and the multi-angle Imaging Spectroradiometer (MISR) are both used to detect aerosols over land and oceans but MODIS is being restricted to land surfaces with low reflectance. Detailed data on MODIS will be represented in the following sections.

Infrared Difference Dust Index (IDDI) of Meteosat IR-channel measurements has also been used to find out the atmospheric dust distributions. Another disadvantage for TOMS AI and IDDI index method is that they are sensitive to the biomass burning aerosols and biomass burning aerosols and dust can not be easily distincted from each other (Engelstaedter, 2006).

1.3.2. Identified Saharan Dust Source Areas

A recent study (Schepanski et al., 2009) has identified the dust source areas of Saharan Desert by using the fifteen-minute Meteosat Second Generation (MSG) Spinning Enhanced Visible and Infrared Imager (SEVIRI) infrared dust index images. In addition to the dust areas, major meteorological processes that cause activation of Saharan Desert dust have also been determined. This topic will be reviewed in a detailed way in the later sections (section 1.4.3).

According to the study, regions with similar topographic conditions and dust source activation (DSA) behaviour are divided into nine parts (Fig 1.9). The group of regions can be defined as: the Atlas Mountains (AT), Akhdar Mountains (AK), Western Sahara (WS), Air Mountains (AI), Adrar Mountains (AD), Bodélé Depression (BO), Quaddai Mountains (OU), Kordofan (KO) and The Red Sea and Nubian Mountains (NU).

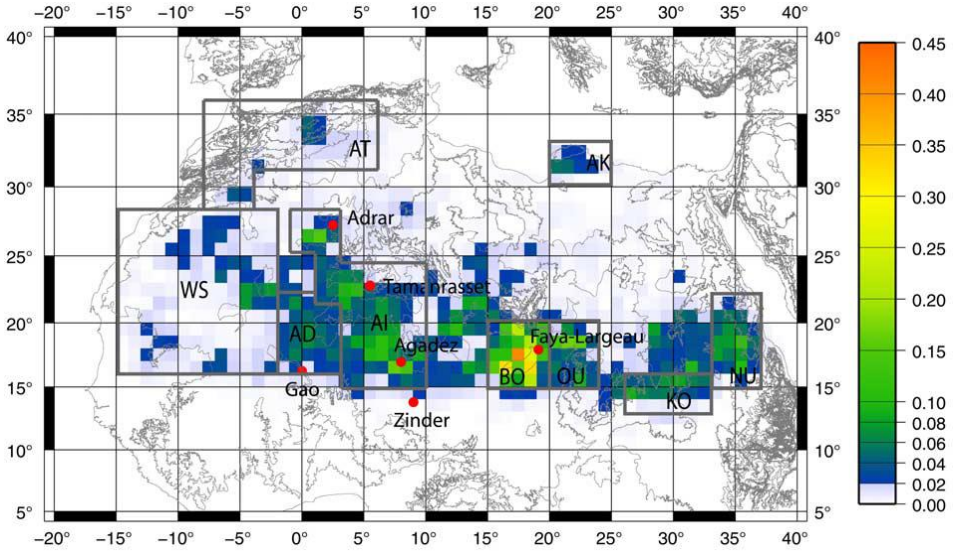

Figure 1.9. Daily fraction of dust source activations derived from MSG IR dust index during March 2006 to February 2008 (Schepanski et al., 2009).

The output graphics of the WRF backward trajectory analyses, which indicates the desert dust sources of Sahara, have been compared with these literature data to check the consistency of the results.

1.4. Theoretical Background of Atmospheric Dynamics

Almost all atmospheric processes; synoptic, regional, local and turbulent scales may be responsible for atmospheric mixing of the aerosol particles for Saharan dust mobilization (Schepanski et al., 2009). In addition, causes of aridity may depend on the global circulation behaviour of wind (Warner, 2004). Therefore, before identifying the local meteorological processes leading to Saharan desert dust activation, the general circulation patterns over the Earth are described in this section.

1.4.1. Large-Scale Wind Circulations

Large-scale weather activities across the latitudes can be represented by a simple conceptual model. Although complicated effects of the spatial distribution of the continents, mountains and ocean-surface temperatures cause many exceptions to the model, it is still convenient to mention the general characteristics of the global wind and pressure systems of the world (Figure 1.10).

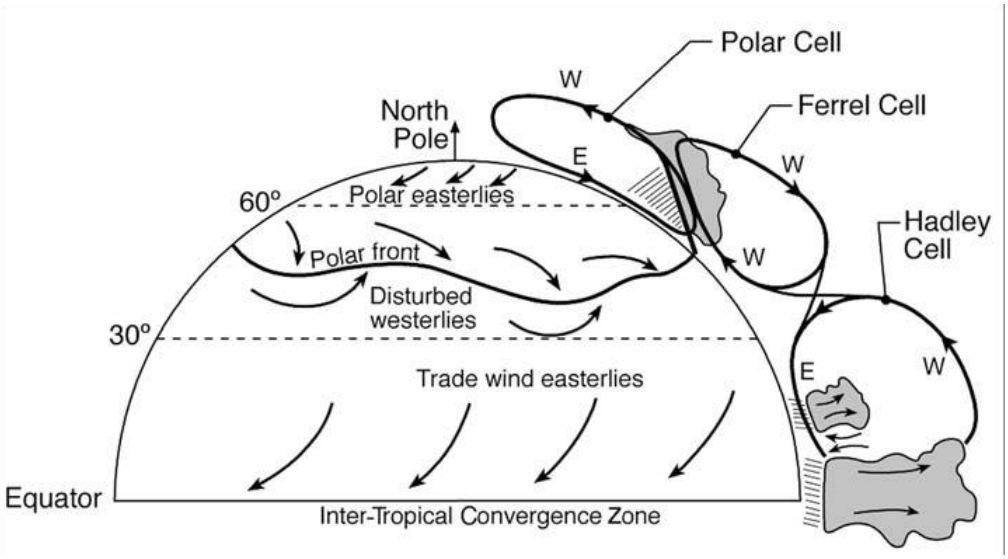

Figure 1.10. The large-scale horizontal winds of the surface and vertical structure of the north-south circulations for the Northern Hemisphere (Warner, 2004).

The very regular northeasterly winds to the north of the Equator between the Equator and approxiametely 30° latitude are called Trade Winds. In this area, horizontal wind flow

is dominated by the trade winds. The Inter-Tropical Convergence Zone (ITCZ) is known as the region where these trade winds (Northern and Southern Hemisphere trade winds) converge. Vertical circulation of winds between the Equator and 30° latitude is represented by the Hadley Cell. Scheme of Hadley Cell shows the upward motion of air, cloudiness and rain near the Equator. On the other hand, near the 30° latitude the subtropics experience subsidience and cloud-free conditions (Warner, 2004). With height the easterly low-level trade winds turn out to be westerlies. This mechanism is called thermally direct effect because the Equator is the area of the greatest heating where the upward motion of airmasses are observed.

In mid-latitudes, between 30 and 60°, eastward moving extratropical cyclones (low-pressure anomalies) and anti-cyclones (high pressure anomalies), with related rotation in the winds, produce a disturbed flow area (Warner, 2004). The horizontal temperature contrast across the polar front creates the energy of the extratropical cyclones. Polar front seperates warm air masses to the south from cold air masses to the north. The cross-section of the latitudes between 30 and 60° indicates that there is an upward motion, precipitation and cloud related with the polar front and the cyclones along the north side of the Ferrel Cell (Fig 1.10). Although direction of wind is very variable in this region, the average direction is westerly at low and particularly at high levels.

Polar easterlies at low levels are in higher latitudes and, with a weak vertical circulation called Polar Cell.

One of the mechanisms that causes aridity is related with the large scale circulations. The global circulation of the atmosphere suppresses rain between about 10° and 30-40° latitude, because of the persistent and widespread subsidence resulted by the downward branch of the Hadley Cell and the related subtropical belt of high pressure. Most of the World's greatest desert occur within this latitude belt, including the Desert of Sahara.

1.4.2. The Winds Originated from Saharan Desert

The local Saharan dust-bearing winds and their properties can be examined from the Table 1.3.

Table 1.3. Local Saharan wind systems

Name	Area Affected	Season	Direction (from)	Meteorological Conditions	Reference
Irifi	Western Sahara		SE	Frontal	Morales (1946)
Ghibli	Tripolitania			Pre-frontal	Sivall (1957)
Guebli	Tunisia & Algeria	All year but most prevalent May-October	S	Pre-frontal with katabatic effects from interior uplands to coastal plains	N.I.D (1943)
Sahel	Morocco		SW	Frontal	Mainguet (1980)
Harmattan	Bilma/Faya Largeau area plus much of West Africa South of 20°N	October-April	ENE	Pressure surge after cold air outbreaks from mid-latitudes	Kalu (1979)
Brume sè che	West Africa	October-April		Harmattan baze in light winds	Bertrand et al. (1979)
Haboob	Sudan	May-July		Single cell thunderstorm downdraft	Freeman (1952)
Khamsin	Egypt	Spring		Pre-frontal	Fisher (1978)
Chili	Tunisia & Algeria	Spring	SW	Pre-frontal	N.I.D (1943)
Shekheli	Algeria	Spring			Borushko (1972)
Chergui	Moroccan Sahara	Summer	NE		N.I.D (1943)
Dschani	Southern Sahara	June-September			Goudie (1978)
Kharif	Somalia		SW		Brooks (1920)
Gobar	Ethiopia				Goudie (1978)
Sirocco	Southern Europe	Spring	S	Frontal	Conte et al. (1996)
Leveche	Spanish Mediterranean coast Malaga-Alicante	Spring	SE-SW	Frontal	Tout and Kemp (1985)
Leste	Madeira			Frontal	Goudie (1978)
Levanto	Canary Islands				Nalivkin (1983)

Some of the commonly observed wind systems are reviewed as the following:

1.4.2.1. Harmattan. Harmattan is a dust-bearing northerly to easterly wind that is formed over the desert and extends, at the surface, as far south as the Intertropical Convergence Zone (ITCZ). It is forced by the pressure gradient to the south of the Sahara high in winter and to some extent by the gradient to the southeast of the Azores high in summer (Fig 1.11).

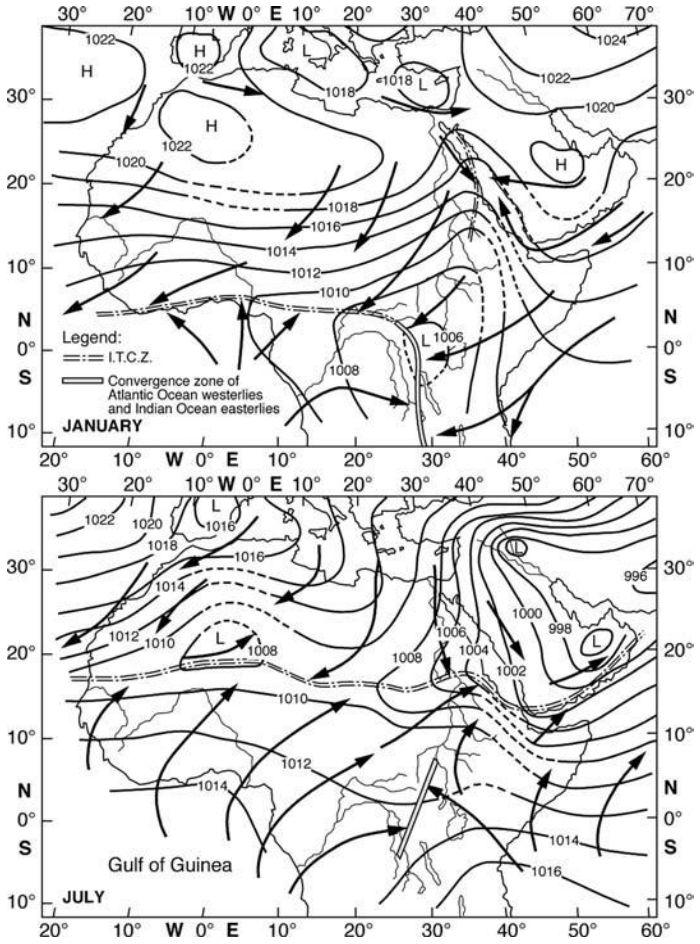

Figure 1.11. Large-scale weather patterns over North Africa in January and July (Warner, 2004).

During the summer, the cooler, maritime, southerly monsoon flow undercuts the northerly Harmattan, which keeps on flowing southward over the Gulf and Atlantic at higher elevations (Warner, 2004). Synoptic processes contol the strength of Harmattan wind. The processes are based on the pressure gradient which is generally strongest from

late December through early February. Harmattan winds are, in some areas, known as northeasterly trade winds.

1.4.2.2. Sirocco or Khamsin. It is a southerly or southeasterly wind along the Mediterranean coast of North of Africa. Khamsin is observed primarily in the spring, and also to a lesser degree in the fall. It includes the continental tropical airmasses that are in the warm sector to the south and east of eastward moving depressions (Warner, 2004). The track of the depressions has moved south to the North African coast or inland during these seasons. Although the storms are smaller than the winter Mediterranean ones, the southerly winds can be strong and lead to severe dust storms, particularly related with cold-frontal passages.

1.4.2.3. Haboob. The word meaning of Haboob is "to blow" or "strong wind" which is usually used to refer to any high wind, or wind that raises sand or dust (Warner, 2004). Synoptic-scale pressure gradients and downdrafts and outflows related with thunderstorms may be responsible for the haboob events.

1.4.2.4. İrifi. The easterly wind which arises suddenly and carries dust and extreme heat from the desert in the east to the Western Sahara is called İrifi (Warner, 2004).

1.4.3. The Meteorological Causes behind the Saharan Dust Transport

As it is stated in the previous sections, all processes synoptic, regional and local ones play roles for the mobilization of the Saharan dust. Here, the important meteorological mechanisms that lead activation of the dust source areas of Sahara are described (Schepanski et al., 2009). These mechanisms can be roughly divided into three main groups : the turbulent mixing of momentum from from nocturnal low-level jets (LLJ), the Mediterranean cyclone and convective activity (Schepanski et al., 2009).

1.4.3.1. Nocturnal Low-level Jet. The horizontal wind speed maximum in the nearest few kilometers of the atmosphere is called Low-Level Jet**.** Typically, LLJs occur at night and can lie over hundred kilometers long terrains. Under clear skies and low surface wind speed conditions, LLJs are observed over the Saharan region. They can be seen together

with the northeasterly Harmattan flow and the southwesterly monsoon flow (Schepanski et al., 2009). The causes of the LLJ generation can be listed as; baroclinity related with sloping terrain, ducting, splitting and confluence around mountain barriers, valley and mountain winds, and inertial oscillation (Schepanski et al., 2009).

During calm nights, the surface wind speeds are low. This causes near-surface air layers to be well stratified and turbulence to be suppressed. After sunrise, the solar heating starts. This enables the start of the convective turbulence mechanism. The air layer aloft, which is decoupled during the night, turns out to be frictionally coupled to the surface. The LLJ momentum is mixed downward. As a result of breakdown of the nocturnal low-level jet, high surface wind speeds are generated. These high wind speeds enable the exceedance of the threshold wind velocity to lift the desert dust and therefore, favorable conditions for dust transport may be observed.

LLJs occur over many parts of North Africa. Bodélé Depression is one of well known area that experiences LLJs. Commonly, LLJs happen under specific synoptic conditions of anticyclonic ridging.

1.4.3.2. Mediterranean Cyclone. During spring, the temperature contrast between the North African coast and the Mediterranean Sea produces a boundary layer (BL) baroclinity (Schepanski et al., 2009). Cyclones, related with this baroclinity, are commonly observed during spring because of the strong temperature gradients. These cyclones are called as Sharav Cyclones (Sharav Depression or Khamsin Depression). The mechanism that produce these cyclones are: large-scale interior baroclinity, BL baroclinity and jet stream related circulations (Schepanski et al., 2009). The cyclone, characterized by an active warm front, is generally related with very high surface temperatures, strong dust storms and low visibilities, and a shallow cold front, which is well defined at the surface by changes in temperature of 10-20 K (Schepanski et al., 2009). Winds flow quickly eastward (usually with a higher speed than 10 m/s) generally following the North African coast. On the leeward east and south part of the Atlas Mountains, this cyclone type is frequently observed. Both lee effect of the mountains and coastal thermal gradient effect may explain the spring cyclogenesis, started by the presence of an upper level trough to the west.

1.4.3.3. Convective Activity. During the summer of the northern hemisphere, a heat low generally occurs over North Africa with a mean position centered near 20°N and 0°E (Schepanski et al., 2009). The ITCZ can reach to 15°N. Large-scale sinking of airmasses related with the Hadley circulation is weak and the boundary layer deep (Schepanski et al., 2009). Deep moist convection occurs (with maximum activity in the afternoon) because of solar heating and moist air flowing from the Gulf of Guinea northward by the southwest monsoon flow (Schepanski et al., 2009). Due to the moist convection, cold humid air sinks over the area and causes high surface wind velocities (Schepanski et al., 2009). These systems can cause dust emissions related with the haboob events.

Deep moist convection can be observed in mountain areas, especially near the Atlas Mountains due to the orographic effects and blocking situations (Schepanski et al., 2009). Large-scale density currents with evaporative cooling of precipitation or cloud particles may be observed. This can cause high surface wind speeds. During daytime, evaporation makes the air cool. Cloud droplets carried by high winds in cloud top levels evaporate in dry suroundings. Therefore, temperature decreases. A dense air is produced and sinks down while the surrounding air has a lower density. On the mountain regions located orthogonally to a strong general flow, convective clouds are formed on the top of mountain ridges and the foehn effect enables a dry and warm air mass on the leeward side of mountain ridge (Schepanski et al., 2009). These make high differences between the air parcel and its surroundings. The cool, dense air produce high surface wind velocities which can intiate the dust mobilization. Density currents resulted by blown out clouds are special for the mountain areas. Because of transport of the moist air toward the mountains within the usually westerly circulation, this process can be observed in the Atlas Mountains over the Sahara. Dry convection associated with the Saharan heat low is also another cause of the mobilization of the Saharan Desert dust (Schepanski et al., 2009).

1.5. Transport Pathways of Saharan Desert dust

Atmospheric dust concentration measurements and satellite retrievals indicate that aerosols activated from the desert areas can travel over large distances within the atmosphere (Engelstaedter, 2006). In this context, studies point out three major pathways

which represent the transportation of the Saharan Desert dust over the Northern Hemisphere (Fig 1.12).

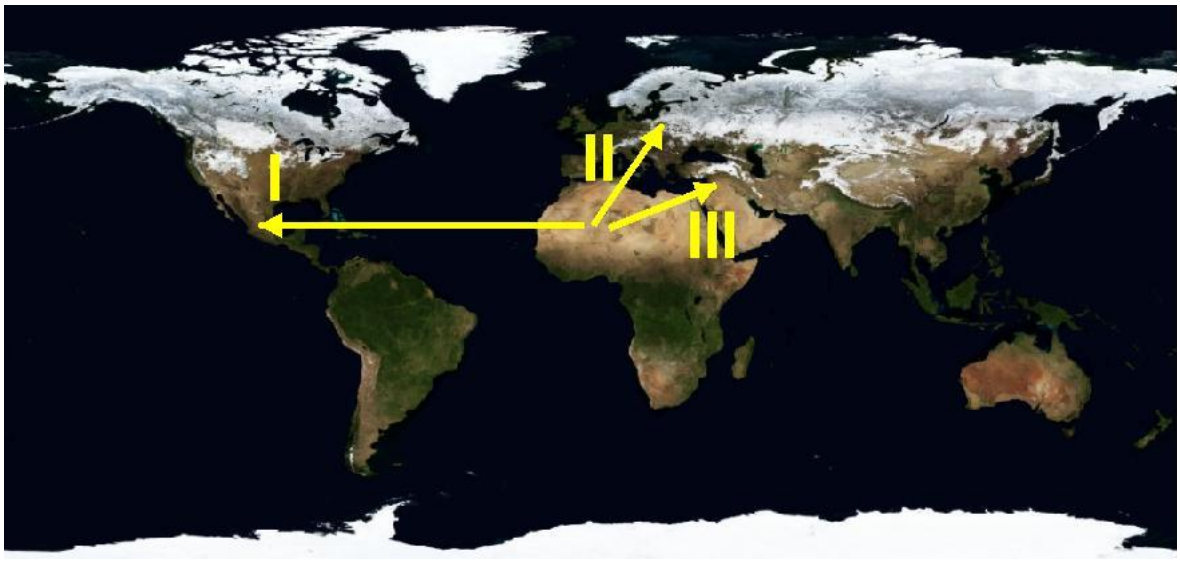

Figure 1.12. Major transport pathways of Saharan originated dust.

First, a significant transport pathway of Saharan dust can be observed across the Atlantic Ocean to the United States, the Caribbean and South America (I). Second way is defined towards the Mediterranean and Europe (II). Lastly, Saharan Desert dust transportation towards the eastern Mediterranean and the Middle East (III) has been identified (Engelstaedter, 2006). In addition to these major paths, a transcontinential dust transport from North Africa and the Middle East to the East Asia has been determined (Tanaka et al., 2005).

1.5.1. Transport Pathway across the Atlantic Ocean to the United States, the Caribbean and South America

Transport and deposition of dust across the North Atlantic Ocean has been studied by several researchers (Chen et al., 2008; Schuetz, 1979; Swap et al., 1992; Chiapello et al., 1995; Ellis and Merrill, 1995; Gatz and Prospero, 1996; Moulin et al., 1997; Prospero and Lamb, 2003).

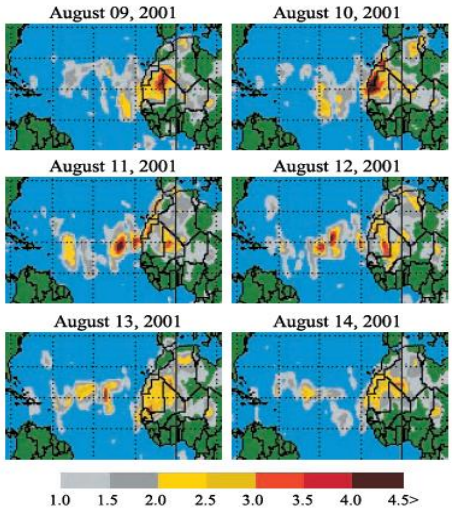

Figure 1.13. TOMS images that represent the dust blowing off the Sahara and crossing the tropical Atlantic (Chen et al., 2008).

Studies on aerosol concentrations at Barbados, Bermuda and Miami indicate that several regions of the North Atlantic Ocean are influenced by atmospheric aerosols, with a maximum in June-July and a minimum in December-February (Prospero, 1996). Dust plumes originating from west coast of the North Africa continent, related with the passage ways of easterly waves crossing North Africa from east to west, reaches there within 3 or 5 days in summer season. The transport of dust from North Africa to Caribbean lasts one week. During winter, aerosols travel more southward driven by strong northeasterly winds (Harmattan), carrying dust to most parts of Nigeria, the Gulf of Guinea (Washington et al., 2006) and the Amazon Basin in South America (Swap et al., 1992; Kaufman et al., 2005). Low level aerosols in the Saharan Air Layer (SAL) prevents the strengthening of weak tropical waves or disturbances and weakens pre-existing tropical cyclones (Dunion and Velden, 2004).

1.5.2. Transport Pathway towards the Mediterranean and the Europe

The generation and transport of dust from the Sahara towards the Mediterranean Basin has been identified previously (Israelevich et al., 2002). The study indicates that in spring and summer, low pressure systems called Sharav cyclones start the mobilization of dust over the North Africa and carry dust northwards and eastwards along the Mediterranean coast (Engelstaedter, 2006). Dust events, generally firstly observed in the

West Mediterrenean Sea and travels approxiametely 890 kilometers per day eastwards, mostly across the eastern Mediterrenan coast. For the eastern Mediterrenean, three major periods of dust events have been identified (Israelevich et al., 2002). Spring (March-May), summer (July-August), and autumn (September-November) periods show different characteristics hence, they have different particle size distributions and refractive indices.

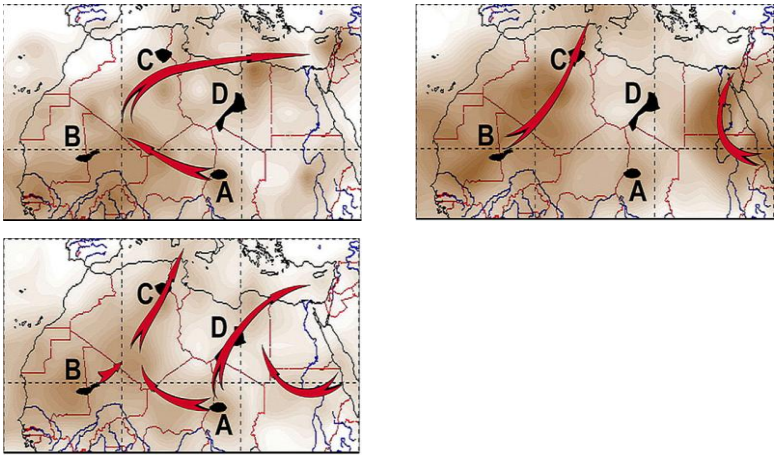

Figure 1.14. Distribution of greatest TOMS AI values observed at North Africa. Arrows of schemes indicate trajectories of dust transport for the periods of March-May, July-August and September-November, respectively (Engelstaedter, 2006).

In spring period, transportation of dust starts from Chad and maybe also from Algeria and ends in the eastern Mediterranean. This is related with the Sharav cyclones (Israelevich et al., 2002). In summer, dust may be carried from both sides of the Red Sea. Determination of the origins of the autumn period is rather complex. From Libyan coast to eastern Mediterranean, transportation has been observed (Israelevich et al., 2002). Dust seems to be transported to the Libyan region from the areas of Chad.

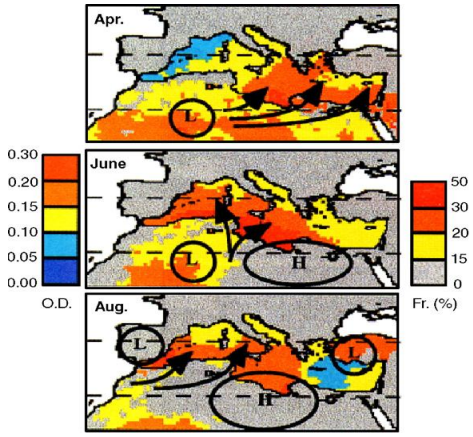

Figure 1.15. Major meteorological synoptic situations for the transport of Saharan dust during spring and summer.

Another study (Moulin et al., 1998), which is based on Meteosat retrievals of dust optical depths, indicates that the northward transport of desert dust has a seasonal pattern, shifting from eastern Mediterranean to the eastern Mediterranean basin during March to August. On the other hand, during autumn and winter minor dust concentrations have been observed. Three cyclogenesis conditions are considered to be responsible for this pattern.

Southern Europe frequently experiences dust from the Saharan region (Mattson and Nihlen, 1996; Carinanos et al., 2004; Rogora et al., 2004; Lyamani et al., 2005). Also, central Europe receives aerosols transported from the Saharan Desert (Bücher and Dessens, 1992; Schwikowski et al., 1995; Coen et al., 2004; Vukmirovic et al., 2004). Even far distances such as England (Thomas, 1982; Burt, 1991; Ryall et al., 2002) and Scandinavia (Franzen et al., 1994) observes Saharan dust.

1.5.3. Vertical Transport of the Saharan Desert Dust

The researches on vertical distribution of mineral desert dust (Alpert et al., 2004) indicates that Mediterranean dust is determined within a wider range of altitudes, generally in higher altitudes in the troposphere. On average, aerosols over the Atlantic travel up to ≤5 km while over the Mediterranean they can be found up to ≤8 km.

Over the latitudes between 10 and 30°N, dust is transported from Sahara to the Atlantic within a mixed layer called the Saharan Air Layer (SAL) (Karyampudi and

Carlson, 1988; Karyampudi et al., 1999). SAL typically reaches to 500 mb (~ 5 km). Its base is located over the Western Sahara. In a westward direction, SAL quickly rises and reaches 850 mb (~ 1.5 km) at longitude ~ 25°W. The top of dust layer over the Atlantic is at 4.5-5.5 km. The dry and hot air enables a temperature inversion near the base of SAL. Convective activities over the Mediterranean may destroy this low-level inversion and redistribute dust over the Atlantic.

2. STATEMENT OF THE PROBLEM

2.1. Identification of the Study

An air pollution episode is the term used to represent the periods of abnormally high concentrations of air pollutants that can cause several effects on human health and environment (definition from EPA). Since these extreme concentrations of the constituents lead favorable conditions for illnesses and death, the underlying mechanisms which play roles for the formation of episodes should be identified in a clear way.

As a considerable air pollutant source, particularly particulate matter pollution has been focus of several studies. To be able to find solutions to particle pollution, analyses of particulate matter episodes come into prominence. Therefore, in this study, meteorological analysis of a potential transport pathway; Saharan Desert dust transport pathway to Anatolian Peninsula, has been identified.

Data, provided from Department of Environmental Protection & Development of Istanbul Metropolitian Municipality (IMM), points out that Istanbul had experienced four significant PM_{10} episodes during the month April in year 2008 (Fig 2.1). Daily coarse particulate matter concentrations have been transformed from the average hourly PM10

data, from to IMM's 10 weather observation station. These stations are; Alibeykoy, Besiktas, Esenler, Kadikoy, Kartal, Sarachane, Sariyer, Umraniye, Uskudar, and Yenibosna.

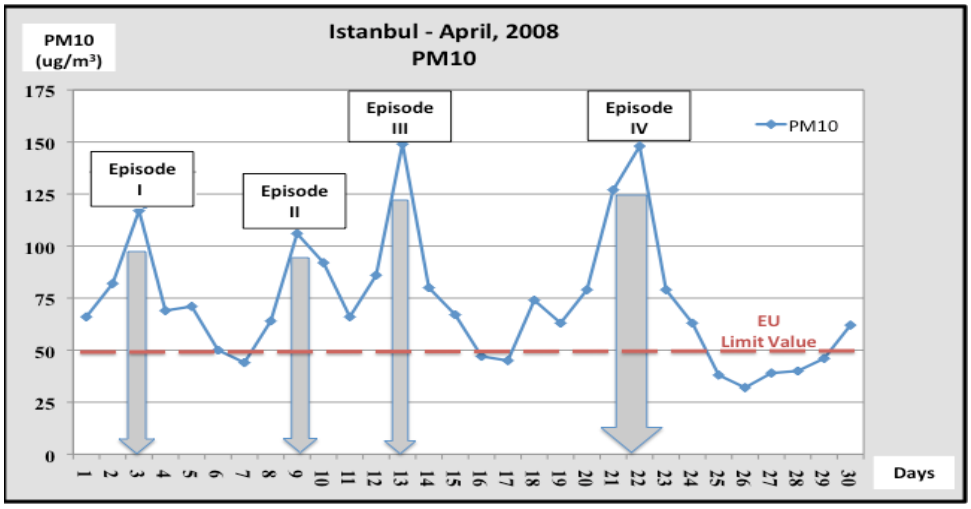

Figure 2.1. Daily average PM_{10} concentrations of Istanbul during the month of April in year 2008.

Although anthropogenic aerosols comprise appreciable part of Istanbul's ambient particulate matter concentrations, there is a potentiality of contribution of Saharan Desert dust to high levels of Istanbul particle pollution. In order to find out the possible mineral dust contribution of Saharan Desert, a numerical meteorological model called Weather Research and Forecasting (WRF) has been run.

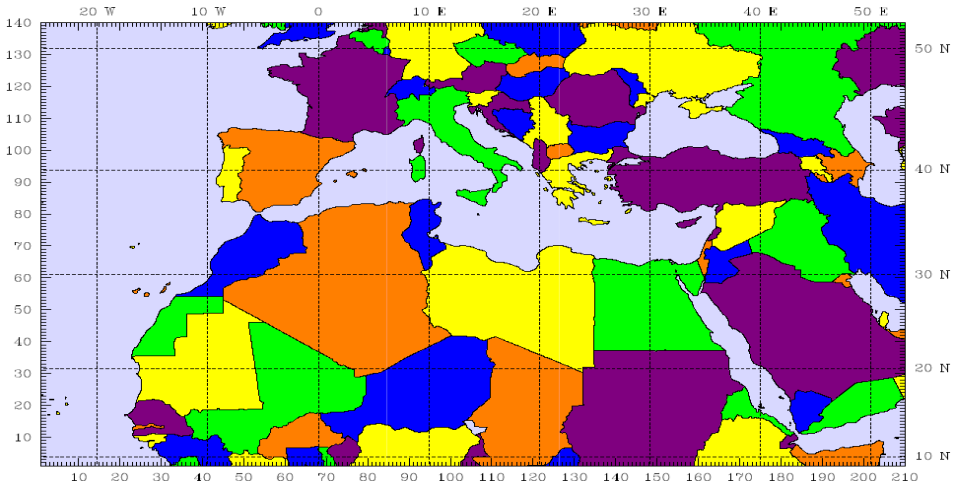

Figure 2.2. The WRF model domain, area of interest.

Figure 2.2 shows the WRF model domain. Based on the huge study domain, covering both Saharan region and Turkey, model has produced output graphics of certain meteorological parameters for the area of interest. These parameters can be listed as; temperature, horizontal wind circulation, vertical wind circulation, and precipitation. Besides these, backward trajectory analyses of WRF model have been used to find out the origins of the transported Saharan Desert dust. In addition to model results, additional data that support the transportation of the aerosols from Saharan region to Istanbul were analyzed. The archieved dust loading (g/m^2) and dry dust deposition (mg/m^2) graphics of The Dust Regional Atmospheric Model (DREAM) and backward ensemble trajectory analyses of Hybrid Single Particle Lagrangian Integrated Trajectory Model (HYSPLIT) have been used to verify the model (WRF) results. To be able to check the performance of the model (WRF), the results of NCEP/NCAR Reanalysis data and WRF model have been compared with the observation values of Istanbul. The hourly temperature observation values of Istanbul has been taken from Turkish State Meteorological Service. The temperature values of Florya, Sile and Kirecburnu meteorological stations have been selected to compare with the corresponding grid point temperatures of the WRF model.

Since the exceedance of the limit value of daily PM_{10} concentrations ($50\mu g/m^3$) have been frequently observed in this month (Fig 2.1), the time period of the model has been selected to cover the days of April 2008. As it can be inferred from the graph that, the study has four specific PM_{10} episodes. Each of the episode has been examined individually

so that it became convenient to analyze the synoptic system by viewing the similarities and differences of meteorological conditions and dust source areas of the episodes. The identification of the four episodes of the study can be viewed from Table 2.1.

Table 2.1. Summary of properties of the episodes.

Episode Name	Episode Date	24-h PM_{10} concentration, $\mu g/m^3$
Episode I	03.04.2008	117
Episode II	09.04.2008	106
Episode III	13.04.2008	149
Episode IV	21.04.2008 22.04.2008	127 148

For each of the four episodes, horizontal wind circulation vectors of the study domain have been plotted. With regard to the plot of the vertical wind circulation vectors, the source area of the episodes have been selected as any point on the pathway which is most suitable to represent the vertical transport. They do not follow a direct path towards the receptor areas. Therefore, generally the original source point of dust may have not be preferred to be used for the vertical wind circulation graphs. However, backward trajectory analyses of the model (WRF) shows the exact transport behaviour of the dust.

After determining the origins of the Saharan dust by the trajectory analyses, the results have been compared with the output data of MODIS, DREAM, and HYSPLIT models. The evaluation of MODIS and DREAM model data prove that the origin of Istanbul's PM levels are arising from the Saharan region for the days of the episodes. HYSPLIT backward ensemble trajectory analyses and also DREAM dust loading graphics demonstrate the potential transport pathway/s of the Saharan dust. The results of WRF have been compared with the results of these alternative models.

3. MATERIALS AND METHOD

3.1. The Weather Research and Forecasting Model (WRF)

The Weather Research and Forecasting (WRF) Model is a mesoscale numerical weather prediction system projected to serve operational forecasting and atmospheric research needs. It has multiple dynamical cores, a three dimensional variational (3DVAR) data assimilation system, and a software structure which allows for computational parallelism and system extensibility (Fig 3.1).

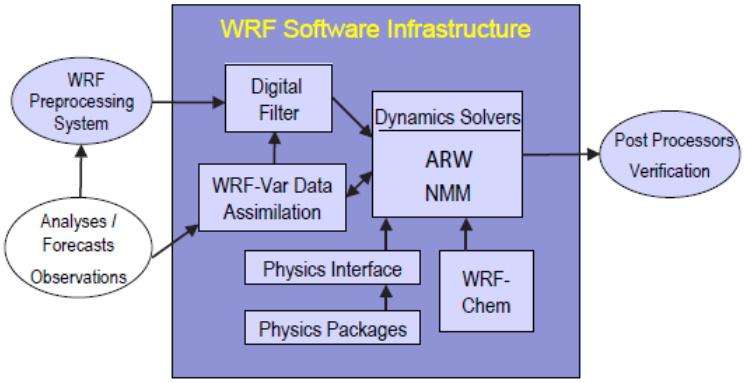

Figure 3.1. The components of the WRF system.

Several research groups took part in developing the WRF model: The National Center for Atmospheric Research (NCAR), The National Oceanic and Atmospheric Administration (NOAA), The National Centers for Environmental Prediction (NCEP), The Forecast Systems Laboratory (FSL), The Air Force Weather Agency (AFWA), The Naval Research Laboratory, The University of Oklahoma and The Federal Aviation Administration (FAA).

The two dynamical solvers, supported by the current WRF software framework (WSF), are the Advanced Research WRF (ARW) and the nonhydrostatic Mesoscale Model (NMM). The ARW is developed and maintained by the Mesoscale and Microscale Meteorology Division of NCAR. The NMM is developed by the National Centers for Environmental Prediction with user support provided by the Developmental Testbed Center. Dynamical cores include advection, pressure-gradients, Coriolis, buoyancy, filters, diffusion and time-stepping.

The ARW is convenient to be used for several applications; idealized simulations, regional and global applications, parameterization research, data assimilation research, forecast research, real-time Numerical Weather Prediction (NWP), hurricane research, coupled model applications and teaching. The ARW dynamical core has also been the selected core of the model in the study.

3.1.1. Modeling System Overview

The WRF ARW solver has an equation set which is fully compressible, Eulerian and nonhydrostatic with a run-time hydrostatic option. It is conservative for scalar variables. The model has terrain following, hydrostatic-pressure vertical coordinate (Fig 3.2) with the top of the model being constant pressure surface.

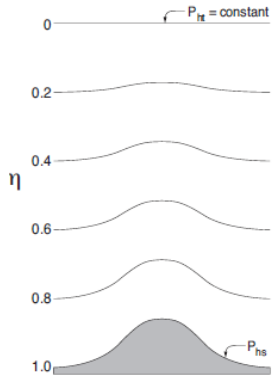

Figure 3.2. ARW η coordinate.

The Arakawa-C grid type is used for horizontal gridding (Fig 3.3). The third-order Runge-Kutta scheme is used for the time integration scheme of the model. The spatial discretization employs 2nd to 6th order schemes. Both idealized and real-data applications with several lateral boundary conditions options can be used by the model. The WRF ARW also supports one-way,two-way and moving nest options. It can be run on single-processor, shared- and distributed-memory computers.

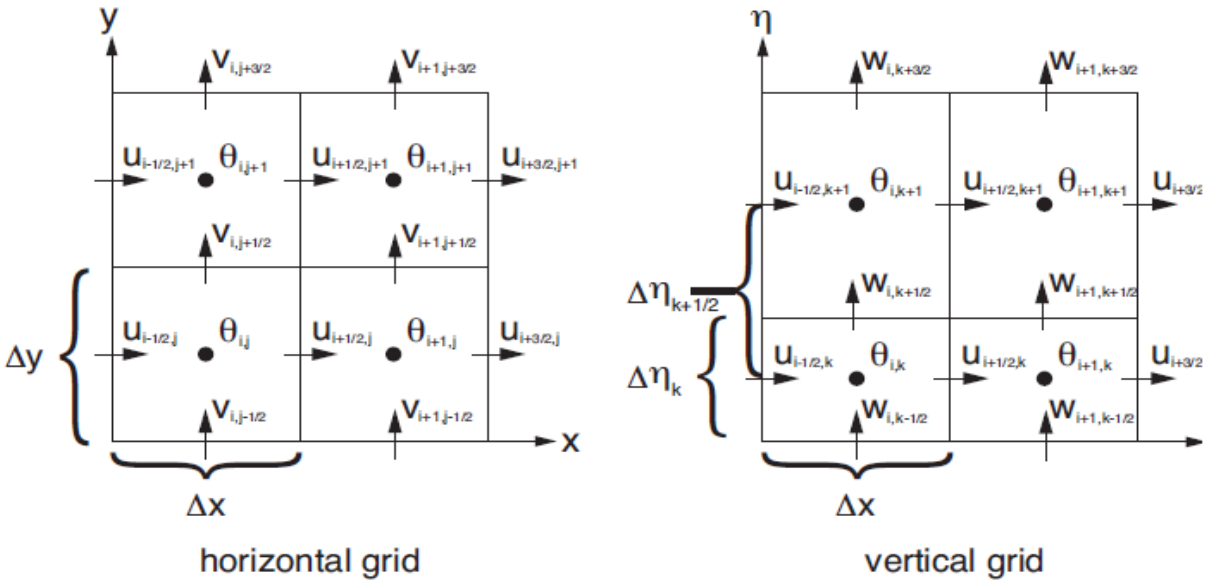

Figure 3.3. Horizontal and vertical grids of ARW.

The software requirements to run the model WRF are: Fortran 90 or 95 and c compiler, perl 5.04 or better. If MPI and openMP compilation is desired, it requires MPI or openMP libraries. WRF I/O API supports netCDF, pnetCDF, PHD5, GRIB 1 and GRIB

2 formats hence one of these libraries needs to be available on the computer where one compiles and runs WRF.

The latest WRF code (version 3) includes (Fig 3.3); *WRF Software Framework (WSF)*, *The WRF Preprocessing System (WPS)*, *Advanced Research WRF (ARW)* dynamic solver, *WRF Data Assimilation (WRF-DA)* system which currently supports 3DVAR, 4DVAR and hybrid data assimilation capabilities, *Post Processing & Visualization Component/s* and numerous *physics packages* contributed by WRF partners and the research community.

3.1.2. Functionalities of Model Components

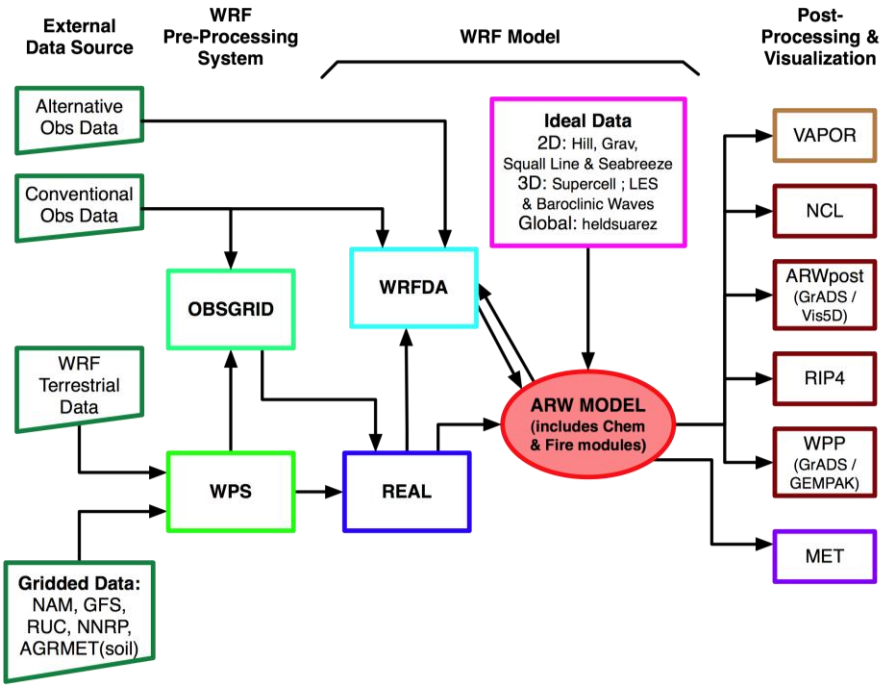

Figure 3.4. WRF modeling flowchart.

The WRF modeling system includes these major programs:

- The WRF Pre-processing System (WPS),
- Real Program,
- ARW solver,
- Post-processing and Visualization tools.

These programs are described in the following sections:

3.1.2.1. WRF Pre-processing System (WPS). The WRF pre-processor is primarily used for real-data simulations. Its major functions are: defining simulation domains, interpolating terrestrial data (e.g. landuse, terrain and soil types) and degribbing and interpolating meteorological data from another model to the simulation domain. The major features of WPS are; GRIB 1/2 meteorological data from several centers around the world, USGS 24 category and MODIS 20 category land datasets, map projections for 1) Polar stereographic , 2)Lambert-Conformal, 3)Mercator 4)latitude – longitude, nesting and user interfaces to input other static data as well as meteorological data.

The WPS includes three independent programs: *geogrid*, *ungrib* and *metgrid*.

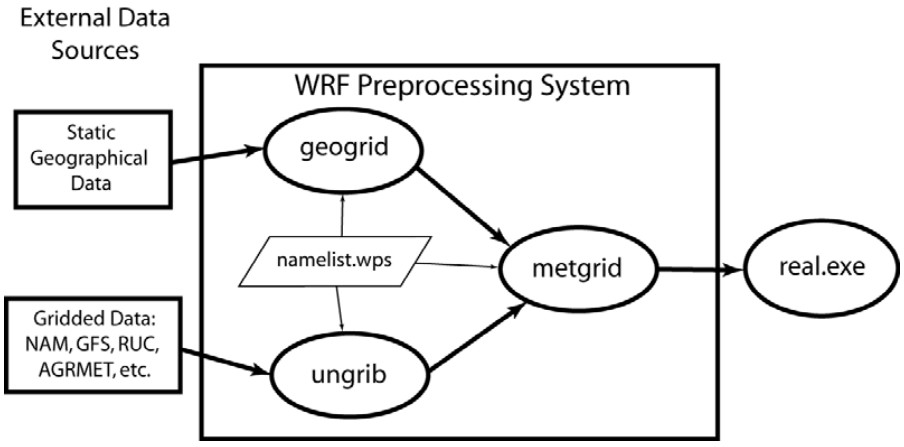

Figure 3.5. The data flow between the programs of WPS.

The Program *Geogrid* defines the simulation domains and interpolates terrestrial datasets to the model grids. It computes the latitude and longitude, and map scale factors at every grid. Also, it interpolates soil and landuse categories, terrain elevation, annual mean

deep soil temperature, monthly vegetation fraction, monthly albedo, maximum snow albedo and slope category to the model grids by default.

The Program *Ungrib* reads GRIB files, degribs the data and writes the data in a simple format called the intermediate format. GRIB is a type of file which contains time-varying meteorological fields. It is typically taken from another regional model e.g NCEP's NAM or GFS models. The Ungrib can read GRIB Edition 1 and, if compiled with a GRIB 2 option, GRIB edition 2 files. GRIB format use several codes to determine the variables and levels in the GRIB file. It use tables of these codes, called Vtables (variable tables) (Fig 3.6), to identify which fields to extract from the GRIB file and write to the intermediate format.

GRIB1 Param	Level Type	From Level1	To Level2	UNGRIB Name	UNGRIB Units	UNGRIB Description
11	100	*		T	K	Temperature
33	100	*		U	m s-1	U
34	100	*		V	m s-1	V
52	100	*		RH	%	Relative Humidity
7	100	*		HGT	m	Height
11	105	2		T	K	Temperature at 2 m
52	105	2		RH	%	Relative Humidity at 2 m
33	105	10		U	m s-1	U at 10 m
34	105	10		V	m s-1	V at 10 m
1	1	0		PSFC	Pa	Surface Pressure
130	102	0		PMSL	Pa	Sea-level Pressure
144	112	0	10	SM000010	kg m-3	Soil Moist 0-10 cm below grn layer
144	112	10	40	SM010040	kg m-3	Soil Moist 10-40 cm below grn laye
144	112	40	100	SM040100	kg m-3	Soil Moist 40-100 cm below grn lay
144	112	100	200	SM100200	kg m-3	Soil Moist 100-200 cm below gr lay
85	112	0	10	ST000010	K	T 0-10 cm below ground layer (Uppe
85	112	10	40	ST010040	K	T 10-40 cm below ground layer (Upp
85	112	40	100	ST040100	K	T 40-100 cm below ground layer (Up
85	112	100	200	ST100200	K	T 100-200 cm below ground layer (B
91	1	0		SEAICE	proprtn	Ice flag
81	1	0		LANDSEA	proprtn	Land/Sea flag (1=land,2=sea in GRI
7	1	0		HGT	m	Terrain field of source analysis
11	1	0		SKINTEMP	K	Skin temperature (can use for SST
65	1	0		SNOW	kg m-2	Water equivalent snow depth
223	1	0		CANWAT	kg m-2	Plant Canopy Surface Water
224	1	0		SOILCAT	Tab4.213	Dominant soil type category
225	1	0		VEGCAT	Tab4.212	Dominant land use category

Figure 3.6. A Vtable example.

The Program *Metgrid* horizontally interpolates the intermediate-format meteorological data which are extracted by the ungrib program onto the simulation domains identified by the Geogrid program. It correctly rotates the winds to the WRF model map projection. Then, the output of Metgrid can be read by the WRF Real program. For each Metgrid run a new simulation is initialized because the work of metgrid is time-dependent.

3.1.2.2. Real Program. The data taken from WPS needs to be transformed before it is read by the ARW solver. The program real.exe is the pre-processor of ARW WRF model for this purpose. It selects the realistic static fields of topography, land use, vegetation and soil category data. The major function of real.exe is to vertically interpolate 3D meteorological fields to the model grids.

3.1.2.3. Advanced Research WRF Dynamic Solver. It is the key component of the system which is made up of various initialization programs for idealized, and real-data simulations, and the numerical integration program. It has also a program to do one-way nesting. The ARW solver includes the following features:

- fully compressible nonhydrostatic equations with hydrostatic options
- regional and global applications
- complete coriolis and curvature terms
- two-way nesting with multiple nests and nest levels
- one-way nesting
- moving nests
- mass-based terrain following coordinate
- vertical grid-spacing can vary with height
- map-scale factors for these projections:
    - Polar stereographic
    - Lambert-Conformal
    - Mercator
    - Latitude – longitude
- Arakawa C-grid staggering
- Runge-Kutta 2nd and 3rd order time integration options
- scalar-conserving flux form for prognostic variables
- 2nd to 6th order advection options (vertical and horizontal)
- monotonic transport & positive-definite advection option for moisture, scalar & TKE
- time-split small step for acoustic and gravity-wave modes
- small step horizontally explicit, vertically implicit
- divergence damping option and vertical time off-centering
- external-mode filtering option

- upper boundary absorption and Rayleigh damping
- lateral boundary conditions
- idealized cases: periodic, symmetric and open radiative
- real cases: specified with relaxation zone
- full physics options for land-surface, planetary boundary layer, atmospheric and surface radiation, microphysics and cumulus convection
- a single column ocean mixed layer model
- grid analysis nudging using separate upper air and surface data, and observation nudging
- spectral nudging
- digital filter initialization
- gravity wave drag
- a number of idealized examples

3.1.2.4. Post Processing & Visualization Components. There are several visualization tools to display model data. 5 main programs in this category are listed as:

- Read/Interpolate/Plot (RIP4)
- NCAR Graphics Command Language (NCL)
- ARWpost (converter to GrADS and Vis5D)
- Visualization and Analysis Platform for Ocean, Atmosphere and Solar Researchers (VAPOR)
- Model Evaluation Tools (MET)
- WPP

Model data which is in Network Common Data Form (netCDF) can be displayed by any of the listed tools above. NetCDF is an independet platform, regardless of where the file was created. Within the context of this study, RIP4 has been used to display the output graphics of the model. Therefore, RIP4 is described in the following section.

The RIP4 program is a Fortran program that needs NCAR Graphics routines in order to visualize the output data from gridded meteorological data sets, primarily from mesoscale numerical models. Previously, it was prepared for sigma-level coordinate output from the

PSU/NCAR Mesoscale Model (MM4/MM5). Then, it was generalized to handle data sets with any vertical coordinate, output from the WRF modeling system.

RIP is a "quasi interactive" program. One can specify the desired plots by editing a formatted text file. Then, the program is executed, and an NCAR Graphics CGM file is created. CGM file can be viewed with any one of various different metacode translator applications.

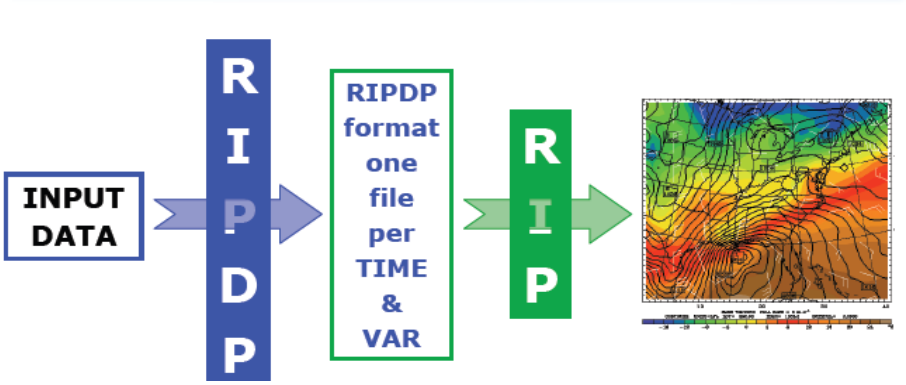

Figure 3.7. RIP flowchart diagram.

Basic features of RIP are:

- RIPDP: a preprocessing program which reads model output, and converts this data into standard RIP format data files that can be ingested by RIP. Two versions of RIPDP are provided. One for output from all components of the MM5 Modeling System, and one used in this study for output from the mass-coordinate version of the WRF model.
- It makes Lambert Conformal, Polar Stereographic, or Mercator map backgrounds, with any standard parallels
- It makes horizontal plots of contours, color-filled contours, vectors, streamlines, or characters
- It makes horizontal plots on model vertical levels, as well as on pressure, height, potential temperature, equivalent potential temperature, or potential vorticity surfaces
- It makes vertical cross sections of contours, color-filled contours, full vectors, or horizontal wind vectors

- It makes vertical cross sections using vertical level index, pressure, log pressure, Exner function, height, potential temperature, equivalent potential temperature, or potential vorticity as the vertical coordinate
- It makes skew-T/log p soundings at points specified as grid coordinates, lat/lon coordinates, or station locations, with options to plot a hodograph or print sounding derived quantities
- It calculates backward or forward trajectories, including hydrometeor trajectories, and calculates diagnostic quantities along trajectories
- It plots trajectories in plan view or vertical cross sections
- It makes a data set for use in the Vis5D visualization software package
- It allows for complete user control over the appearance (color, line style, labeling, etc.) of all aspects of the plots

3.1.3. The Model Approach

3.1.3.1. Physical Options. The WRF is an atmospheric model and has been widely used to generate meteorological data by mesoscale modelers. Here, a single domain with a horizontal resolution of 36 km was used, and there were 210, 140, 31 grid intervals in the east-west, north-south, and vertical directions, respectively. The physics options of the chosen model were the RRTM (Rapid Radiative Transfer Model) radiation scheme (Mlawer et al. 1997) to represent long-wave radiation and Dudhia scheme (Dudhia 1989) to represent short-wave radiation, Grell 3D ensemble cumulus parameterization (Grell et al., 2002), the YSU boundary layer parameterization (Hong et al., 2006), the Ferrier (new ETA) microphysics scheme, the Monin - Obukhov surface layer scheme (Monin et al., 1954) and the Unified Noah land-surface model scheme. The National Centers for Environmental Prediction (NCEP) Global Data Assimilation System (GDAS) data (with 1 degree by 1-degree resolution) were used for WRF boundary and initial conditions. The model integrated 30 days starting from 00:00 UTC April 1 2008.

3.1.3.2. The Meteorological Input Dataset: NCEP/NCAR Reanalysis. The meteorological input data of WRF has been selected as the *ds083.2 NCEP FNL (final) Operational Model Global Tropospheric Analysis data, continuing from July 1999*. These data are on 1.0 x 1.0 degree grids continously at every six hours. It is taken from the Global Forecast System

(GFS) which is operationally run four times a day in near-real time at NCEP. The analyses are found on the surface, at 26 mandatory (and other pressure levels) from 1000 mb to 10 mb, in the surface boundary layer and at some sigma layers, the tropopause and a few others. Parameters of data are: surface pressure, sea level pressure, geopotential height, temperature, sea surface temperature, soil values, ice cover, relative humidity, u- and v-winds, vertical motion, vorticity and ozone.

Table 3.1. Information on the dataset ds083.2 NCEP FNL (final) Operational Model Global Tropospheric Analysis data

Properties	Descriptions
Periods	1999-07-30 18:00 +0000 to 2010-08-11 18:00 +0000
Data format	WMO GRIB 1 - WMO GRIB 2
Type of data	Grid
Coverage	Longitude Range: Westernmost=180W, Easternmost=180E Latitude Range: Southernmost=90S, Northernmost=90N
Sources	DOC/NOAA/NWS/NCEP National centers for Environmental Prediction, National Weather Service, NOAA, U.S. Department of Commerce
Volume	1171.47 (Entire Dataset)

3.2. The Moderate Resolution Imaging Spectroradiometer (MODIS)

Giovanni is an acronym for the GES-DISC (Goddard Earth Sciences Data and Information Services Center) Interactive Online Visualization and Analysis Infrastructure. It is a web-based application that presents a simple way to analyze, visualize and access great amounts of Earth Science remote sensing data without having to download them.

From the operational website of Giovanni, the section of “aerosol daily” enables to view images which represent aerosol optical depth measurements of Terra and Aqua MODIS, Terra MISR and Aura OMI and GOCART model data. One can select the area of interest by entering the longitude and latitude values.

Within the context of this study, Terra MODIS (2000/02/24-2010/04/14) measurements (1X1 Degree) have been used to display the aerosol optical depth at 550 nm for the domain, covering the Sahara and Turkey. The data product name is MOD08_D3.005.

3.3. The Dust Regional Atmospheric Model (DREAM)

DREAM is a regional model to simulate and/or predict the atmospheric cycle of mineral aerosols. The model is divided into two parts: 1) atmospheric modeling system and 2) the dust concentration module. The atmospheric modeling system of DREAM is known as the SKIRON forecasting system. DREAM is based on the 1997 version of the ETA/NCEP model. It solves the Eularian partial differential nonlinear equation for dust mass continuity.

The concentration equation of DREAM simulates all main processes of the atmospheric aerosol cycle (Fig 3.8). The surface dust injection fluxes is made over the model grids mentioned as deserts, during the model integration. The important atmospheric model variables of the model are; turbulent parameters in the early stage of the process when dust is transported from ground to upper levels, model winds in the later phases of the process when dust becomes away from the source, thermodynamic processes and rainfall of the model and landcover features that provide wet and dry deposition of dust over the Earth surface.

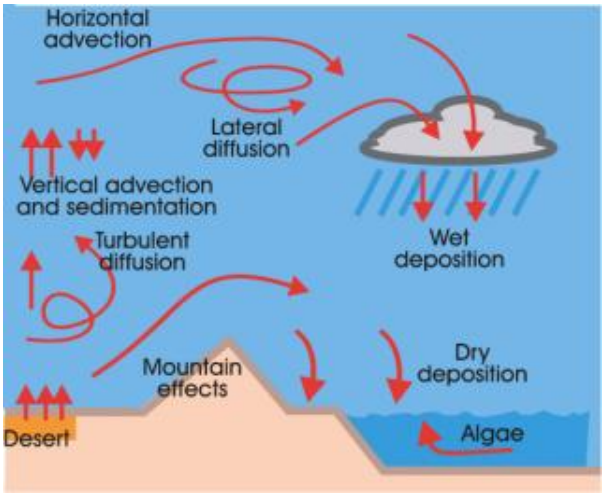

Figure 3.8. Major processes of the atmospheric dust cycle.

The model identifies the dust sources by using arid and semi-arid categories of the global USGS 1-km vegetation dataset. Particle size parameters are evaluated from FAO 4km global soil texture dataset. In the model, concentration is used as a surface condition. The structure and state of the soil and turbulent regime of the lower atmosphere affects the released surface concentration of activated dust particles and the corresponding vertical flux. This corresponding flux is also a function of friction speed and soil moisture.

DREAM model is operated by the Barcelona Supercomputing Center (BSC). From the operational website of the DREAM in the Earth Sciences division of the BSC, data and images of the mineral dust forecast system can be accessed. The archieved data and images of dust load & cloudliness, optical depth&cloudliness, deposition, surface concentration, vertical cross sections and vertical profiles can be obtained for three different domains of Euro-Mediterranean, Sahara-Sahel and Spain.

Within the context of this study, the archieved dust loading (g/m^2) and dry dust deposition (mg/m^2) graphics of Euro-Mediterranean domain(covering both Sahara and Turkey) have been used to evaluate the dust transport from the Saharan Desert region to the Anatolian Peninsula.

3.4. The Hybrid Single Particle Lagrangian Integrated Trajectory Model (HYSPLIT)

The model HYSPLIT is a system for computing simple air trajectories to complex dispersion and deposition simulations. It is initially developed as a result of a joint effort between NOAA and Australia's Bureau of Meteorology (ABM). The dispersion of the pollutants is calculated by the puff or particle dispersion method. The puff model is based on the assumption that puffs expand until they exceed the size of the meteorological grid cell (either horizontally or vertically) and then divided into several new puffs, which represents the certain fraction of the original pollutant mass. The particle model assumes that a fixed number of particles are advected about the model domain by the mean wind field and spread by the turbulance. The model configuration supposes a 3D particle distribution.

The major features of the model are:

- Trajectories
  - Single or multiple (space or time) simultaneous trajectories
  - Optional grid of initial starting locations
  - Computations forward or backward in time
  - Default vertical motion using omega field
  - Other motion options: isentropic, isobaric, isopycnic
  - Trajectory ensemble option using meteorological variations
  - Output of meteorological variables along a trajectory
  - Integrated trajectory clustering option

- Air Concentrations
  - 3D particle dispersion or splitting puffs (top-hat or Gaussian)
  - Instantaneous or continous emissions, point or area sources
  - Multiple resolution concentration output grids
  - Fixed concentration grid or dynamic sampling
  - Wet and dry deposition, radioactive decay, and resuspension
  - Emission of multiple simultaneous pollutant species
  - Automated source-receptor matrix computation
  - Ensemble dispersion based on variations in meteorology, turbulence, or physics
  - Concentration probability output for multiple simulations

- Integrated dust-storm emission algorithm
- Define rate constants to convert one species to another
- Mass can be transfered to a Eularian module for global-scale simulations

- Meteorology
  - Model can run with multiple nested input data grids
  - Links to ARL and NWS meteorological data server
  - Access to forecasts and archives including NCEP/NCAR reanalysis
  - Additional software to convert MM5, RAMS, COAMPS, WRF, and other data
  - Utility programs to display and manipulate meteorological data

Within the context of this study, backward ensemble trajectory option of HYSPLIT has been used to determine the origins of the Istanbul's PM_{10} levels during the month April in year 2008.

The ensemble option of the model automatically starts multiple trajectories from the selected starting point. By offsetting the meteorological data by a fixed grid factor, each member of ensemble trajectory has been calculated. One meteorological grid point in the horizontal and 0.01 sigma units in the vertical comprise the default offset of the model. The configuration have 27 ensemble members in total. In this case, the starting point of the trajectories has been located at Istanbul, with a vertical height of 10m. Instead of running HYSPLIT in a usual way, in our case the output results of WRF has been adjointed to HYSPLIT as an input data.

4. RESULTS

4.1. Model Performance

Meteorological parameters, such as wind, mixing height, rain and temperature are the essentials to evaluate the dust transportation behaviour. In this context, it is worth to be mentioned that the accuracy of meteorological model outputs strongly affects the performance of the dust transport prediction. Therefore, in this section, the examination of the model performance is presented . This performance measurement is made by the comparison of NCEP/NCAR meteorological data with the WRF model data.

Although the model did not use a high resolution (36km x 36km) due to the requirement of covering a huge Saharan zone, the meteorological model remained being capable of producing realistic meteorological data which is necessary to make a compherensive evolution of dust transport for the entire domain. It can be concluded from

the comparison graphs that during the simulation period, similar wind patterns and geopotential height data are observed (From Fig 4.1 to 4.12).

Furthermore, in addition to the analysis of consistency of the model results with the NCEP/NCAR data, model results have been compared with the observation data over the area of interest. The observational temperature data, which is taken from Turkish State Meteorological Service and represents the Florya, Sile and Kirecburnu Stations of Istanbul, have been compared with the output temperature data of the WRF model (Fig 13, 14 and 15). It can be inferred from the graphs that WRF performed well in capturing the trend of the observational data. Model results have been found reasonable.

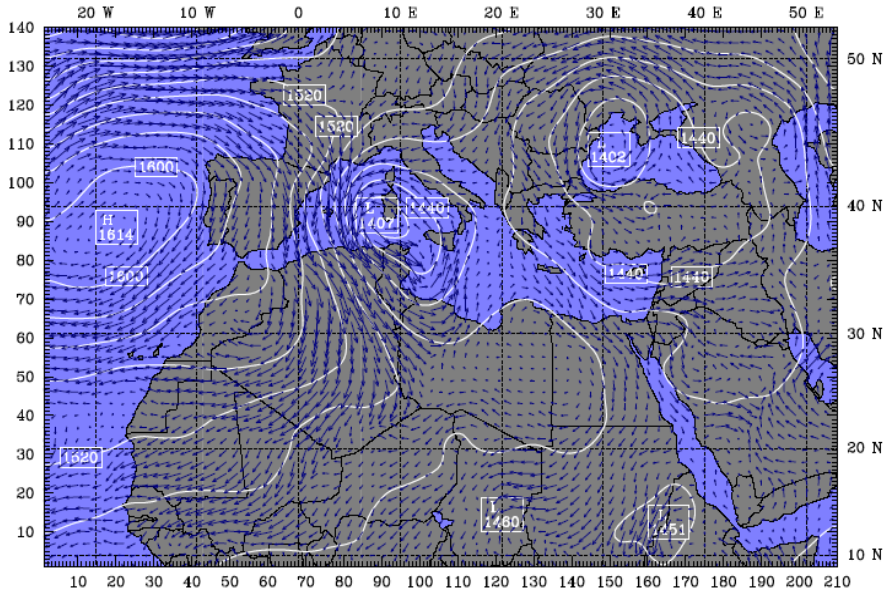

Figure 4.1. NCEP/NCAR output graphs of geopotential height and horizontal wind vectors at 850 hPa for 00UTC 01.04.2008

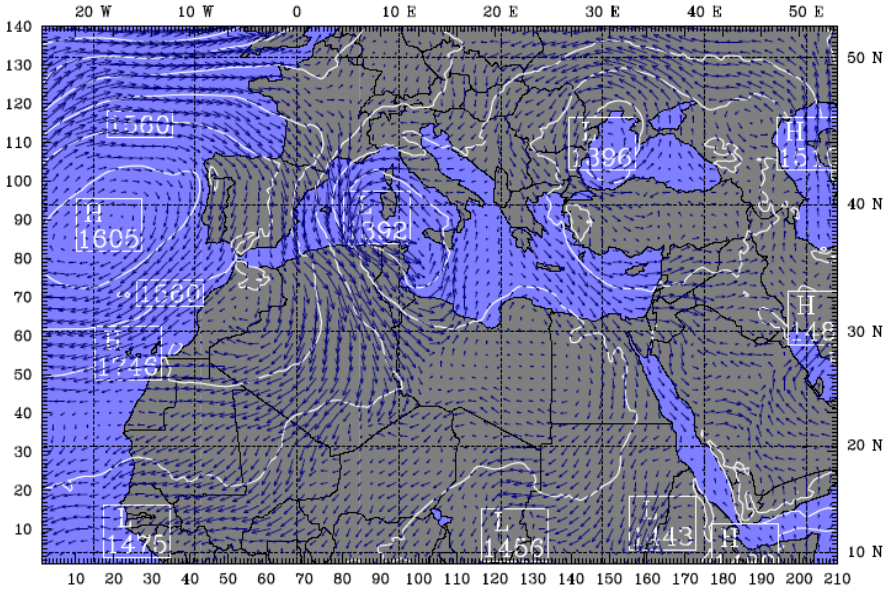

Figure 4.2. WRF output graphs of geopotential height and horizontal wind vectors at 850 hPa for 00UTC 01.04.2008

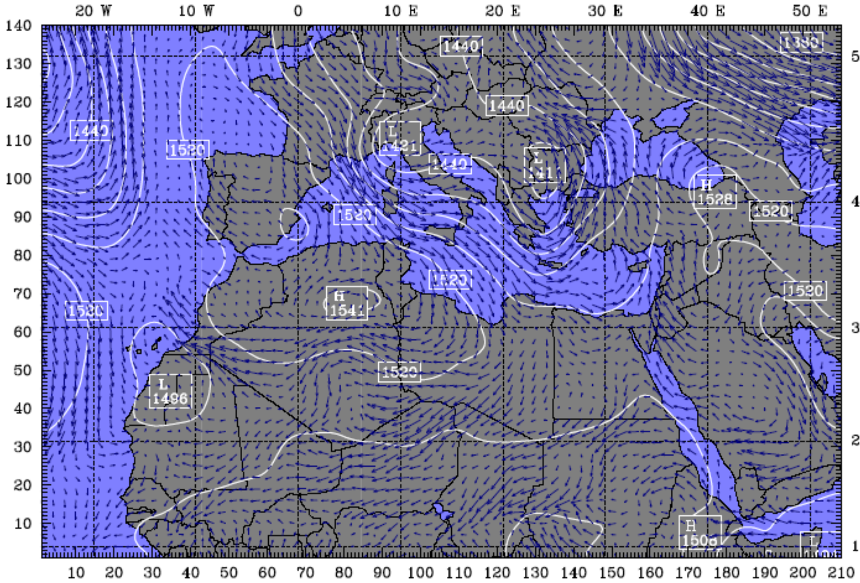

Figure 4.3. NCEP/NCAR output graphs of geopotential height and horizontal wind vectors at 850 hPa for 00UTC 15.04.2008

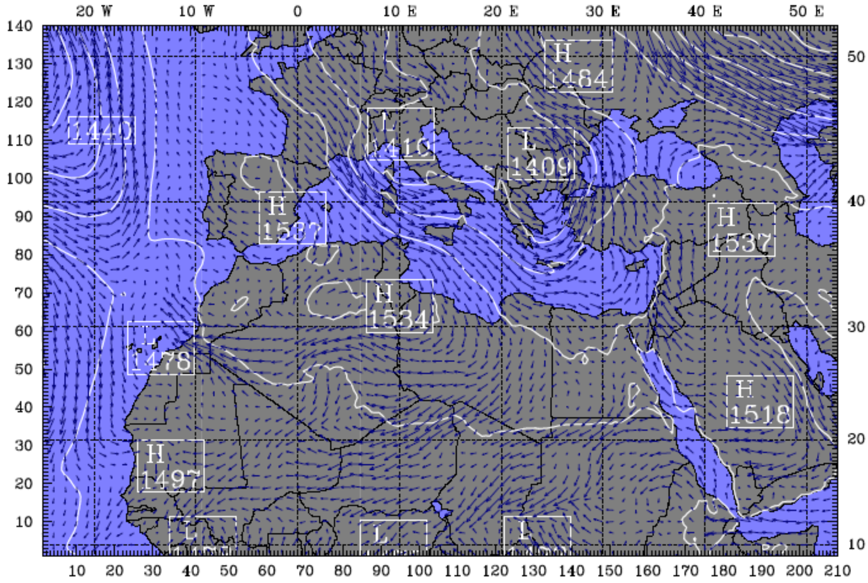

Figure 4.4. WRF output graphs of geopotential height and horizontal wind vectors at 850 hPa for 00UTC 15.04.2008

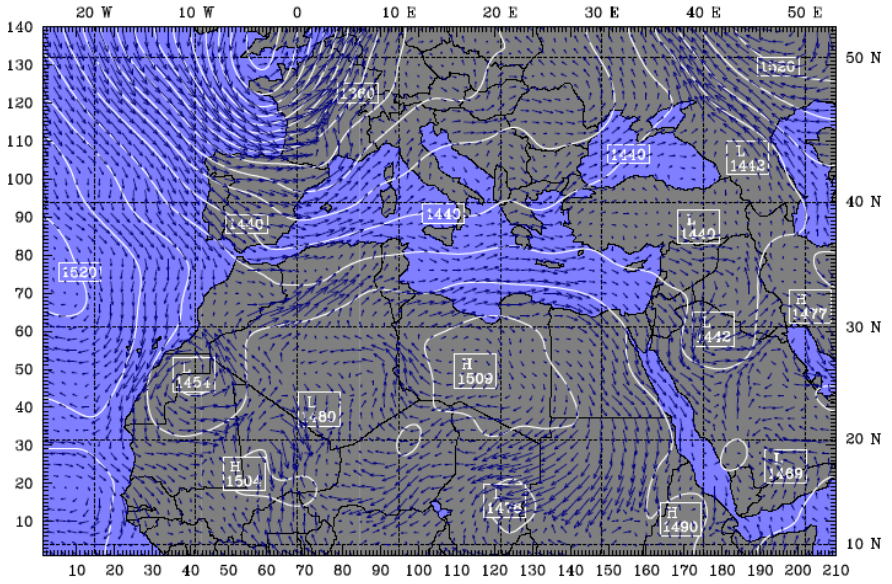

Figure 4.5. NCEP/NCAR output graphs of geopotential height and horizontal wind vectors at 850 hPa for 00UTC 30.04.2008

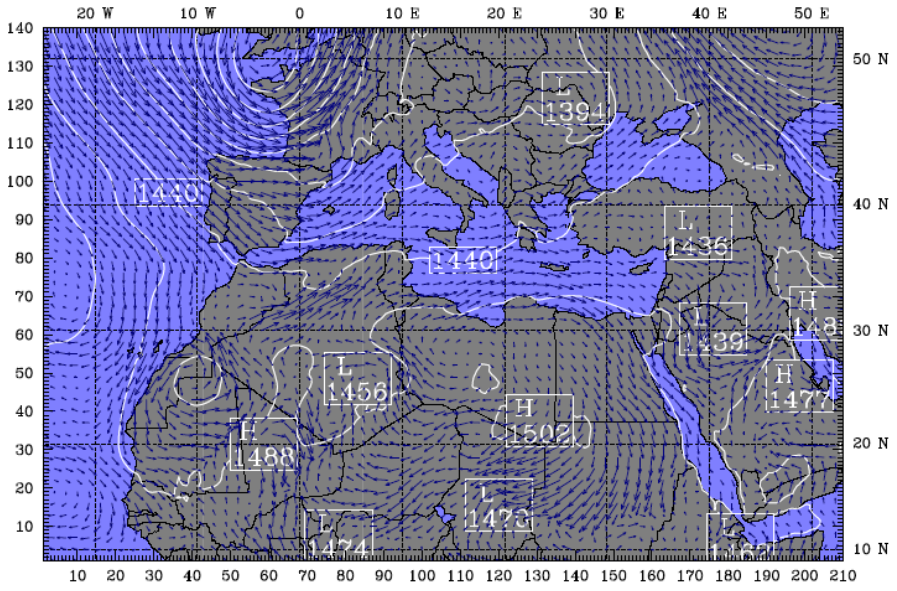

Figure 4.6. WRF output graphs of geopotential height and horizontal wind vectors at 850 hPa for 00UTC 30.04.2008

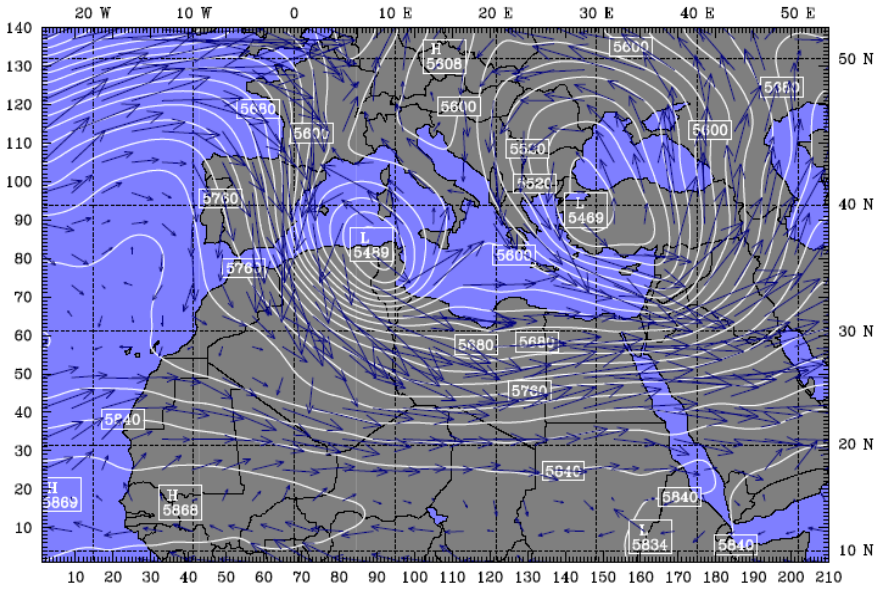

Figure 4.7. NCEP/NCAR output graphs of geopotential height and horizontal wind vectors at 500 hPa for 00UTC 01.04.2008.

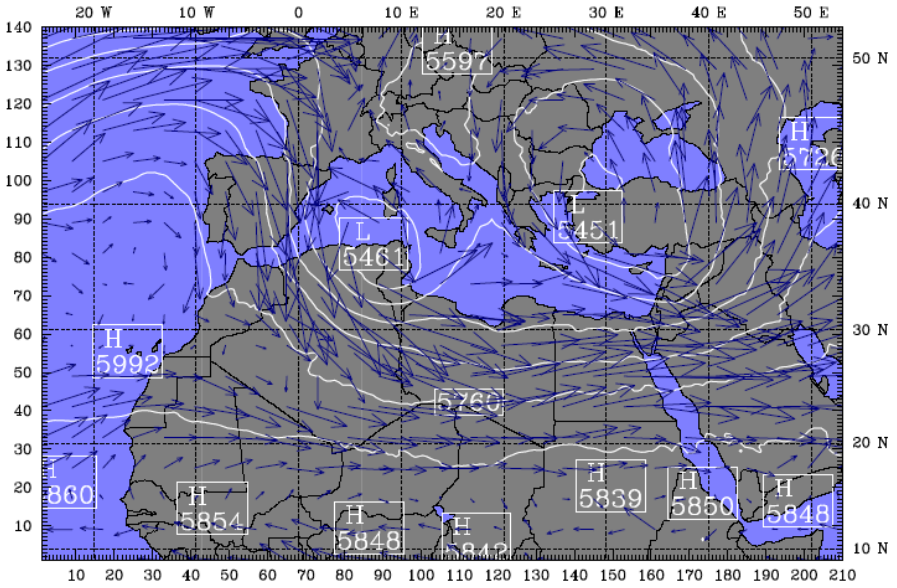

Figure 4.8. WRF output graphs of geopotential height and horizontal wind vectors at 500 hPa for 00UTC 01.04.2008.

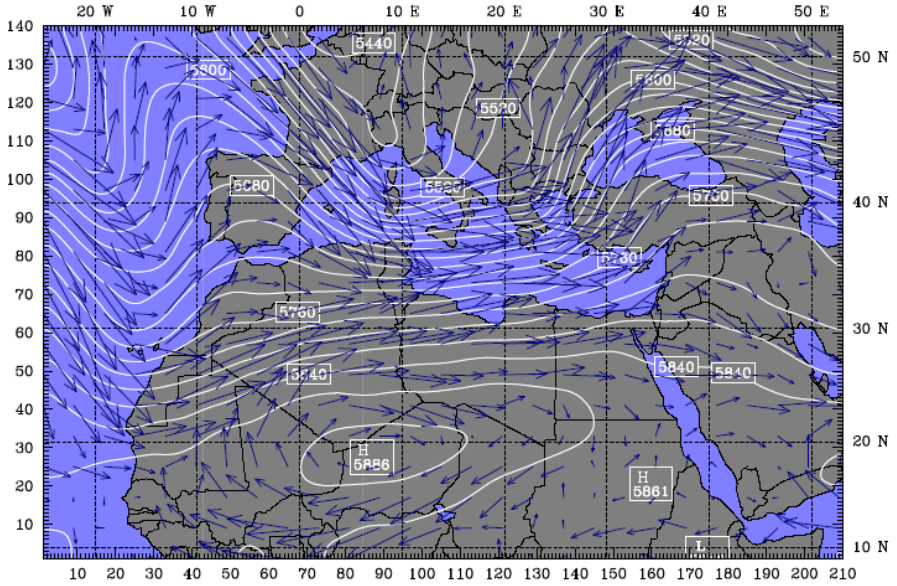

Figure 4.9. NCEP/NCAR output graphs of geopotential height and horizontal wind vectors at 500 hPa for 00UTC 15.04.2008.

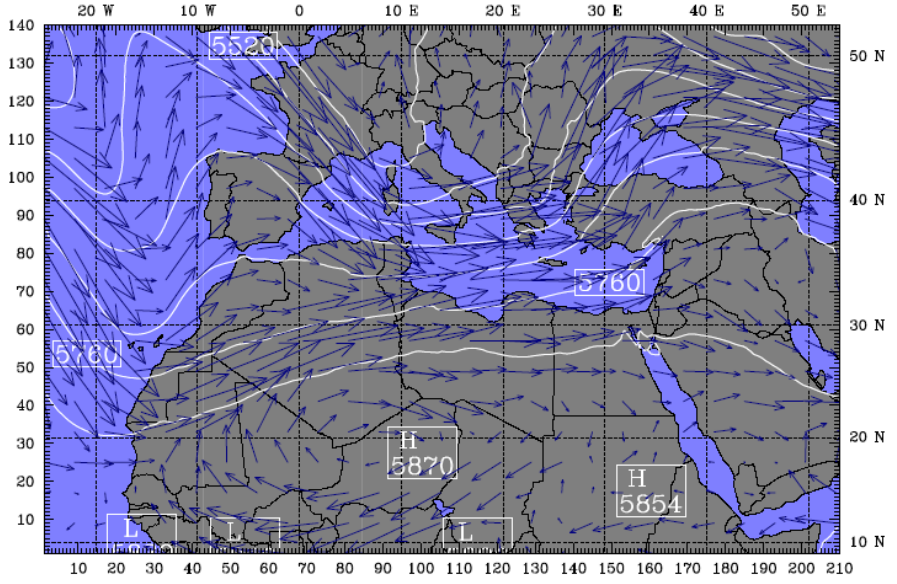

Figure 4.10. WRF output graphs of geopotential height and horizontal wind vectors at 500 hPa for 00UTC 15.04.2008.

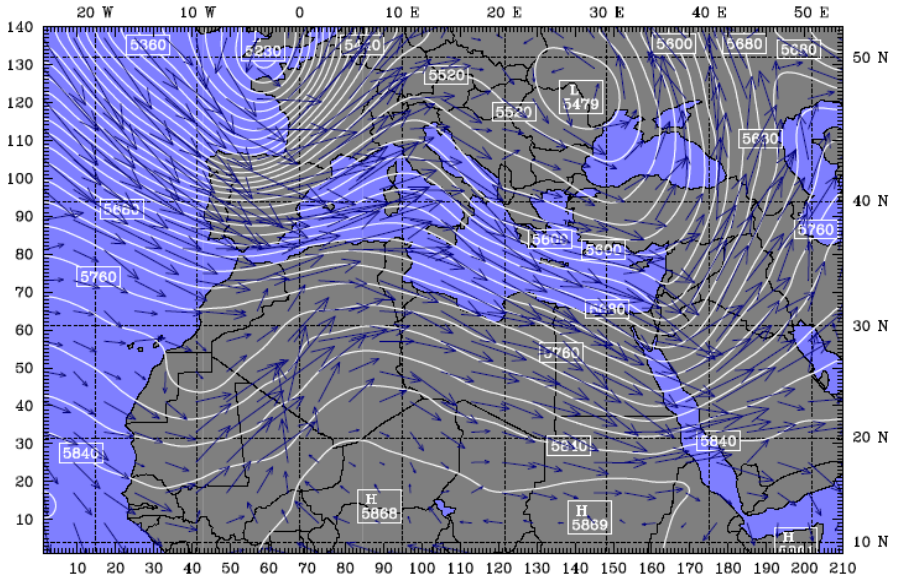

Figure 4.11. NCEP/NCAR output graphs of geopotential height and horizontal wind vectors at 500 hPa for 00UTC 30.04.2008.

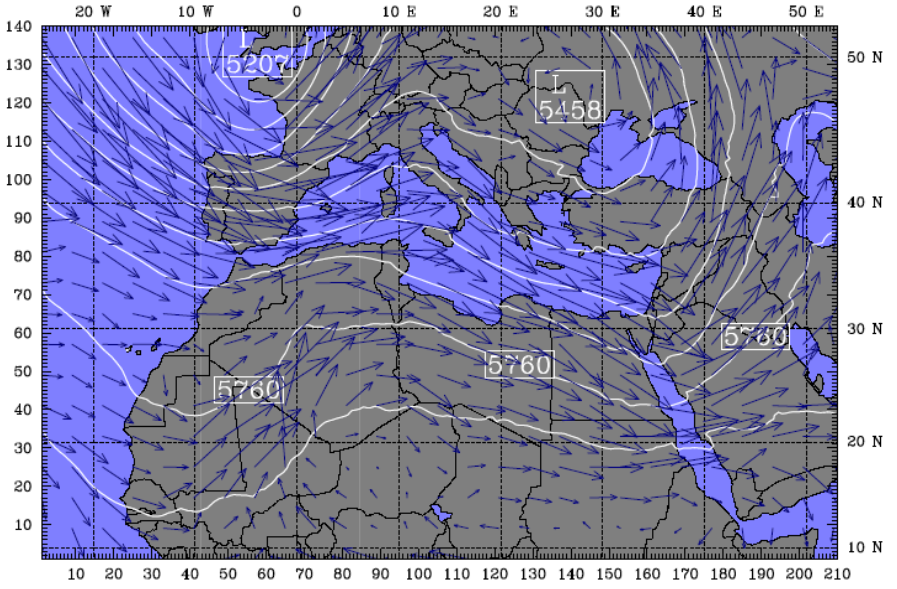

Figure 4.12. WRF output graphs of geopotential height and horizontal wind vectors at 500 hPa for 00UTC 30.04.2008.

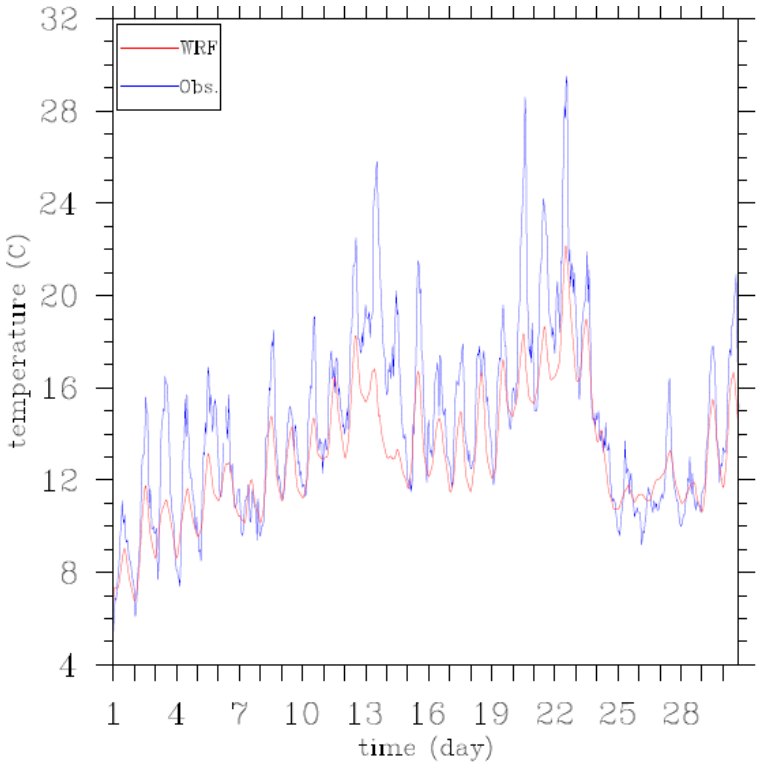

Figure 4.13. 2m temperature comparison between WRF model and observation values at Florya Station.

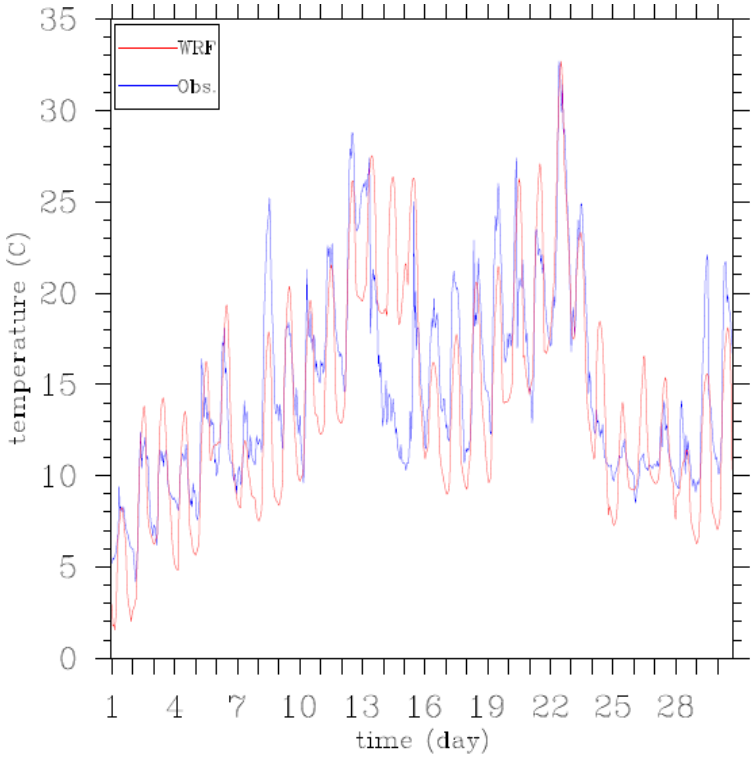

Figure 4.14. 2m temperature comparison between WRF model and observation values at Sile Station.

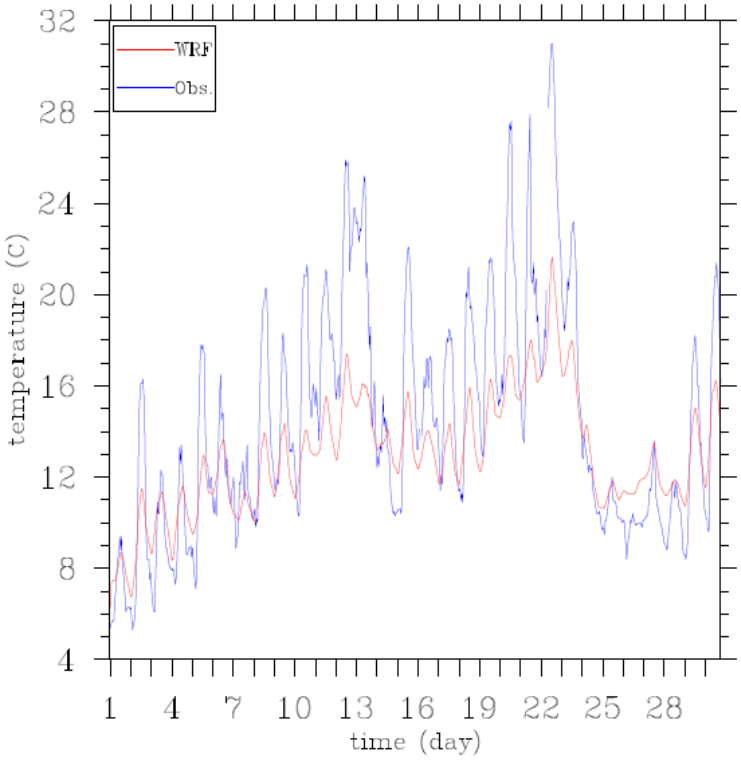

Figure 4.15. 2m temperature comparison between WRF model and observation values at Kirecburnu Station.

4.2. Results of WRF: Episode I

4.2.1. Synoptic Analysis

4.2.1.1. Distribution of Horizontal Wind Vectors. The distribution of horizontal wind speed and direction, which represents Episode I on April 2 at 18 UTC, indicates that a combined effect of a cyclone located on central Mediterranean (on the lower part of Greece), with a surface pressure of 1011hPa and a high pressure system located on eastern Mediterranean, with a surface pressure of 1016 hPa produced a transport pathway towards the Marmara Region of Turkey (Fig 4.16).

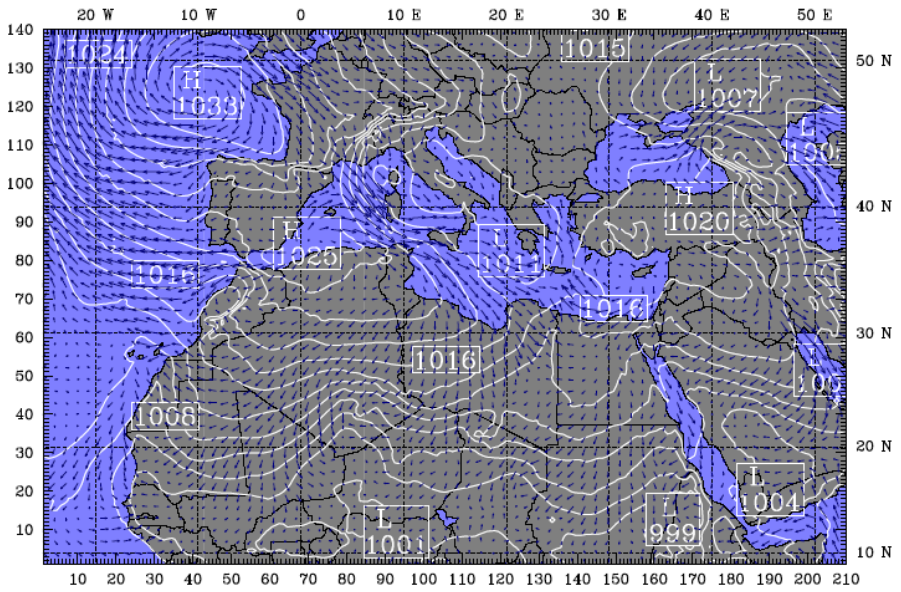

Figure 4.16. Horizontal Wind Vector Graphs of Episode I
(drawn for 18UTC 02.04.2008 at 1000 hPa).

The pressure gradient between these two systems (5hPa) reveals convenient meteorological conditions to start dust mobilization over the Akhdar Mountain region. Particularly, the low pressure system over the central Mediterranean may have a substantial role in lifting the desert dust and initiating the transportation.

4.2.1.2. Vertical Wind Circulation Vectors. In addition to horizontal wind circulation analysis, vertical wind circulation behaviour has also been examined in the study. Vertical

wind circulation graphics of the atmosphere analyzes the airflow motion on the vertical axis, between selected estimated source and receptor areas of the pollutants.

In this case, for each episode, one vertical crossline graphics has been plotted between estimated source points of Sahara and receptor points of Istanbul (Fig 4.17).

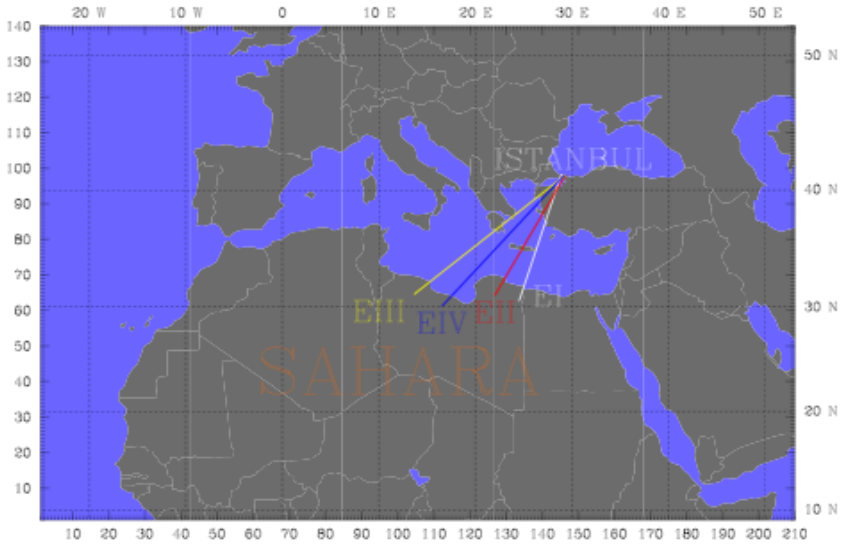

Figure 4.17. The horizontal presentation of the vertical wind circulation graphics, representing the all four episodes of the study.

As can be seen from Figure 4.17, for episode I, a point on northern Libya – Egypt border has been selected as a source point. The vertical wind graph, drawn between this area and Istanbul, points out a convection process starting from the Saharan region (Fig 4.18). As it is previously concluded from the horizontal wind plots (Fig. 4.16), the collision of the cyclone resulting from central Mediterranean and high pressure system originating from eastern Mediterranean causes a convection activity over the Akhdar Mountain region. The convective activity, which starts lifting of the dust, can be observed near the ground level (between 1000 and 925hPa). Wind vectors and potential temperature (red line) show the strong instability and convective movements over the southern part of the cross-section zone (Figure 4.18). The winds, although, are not strong along the cross sectional line, their southerly directions are able to carry the lifted-dust to the city. These atmospheric conditions are suitable for dust mobilization and transport from Sahara to Istanbul.

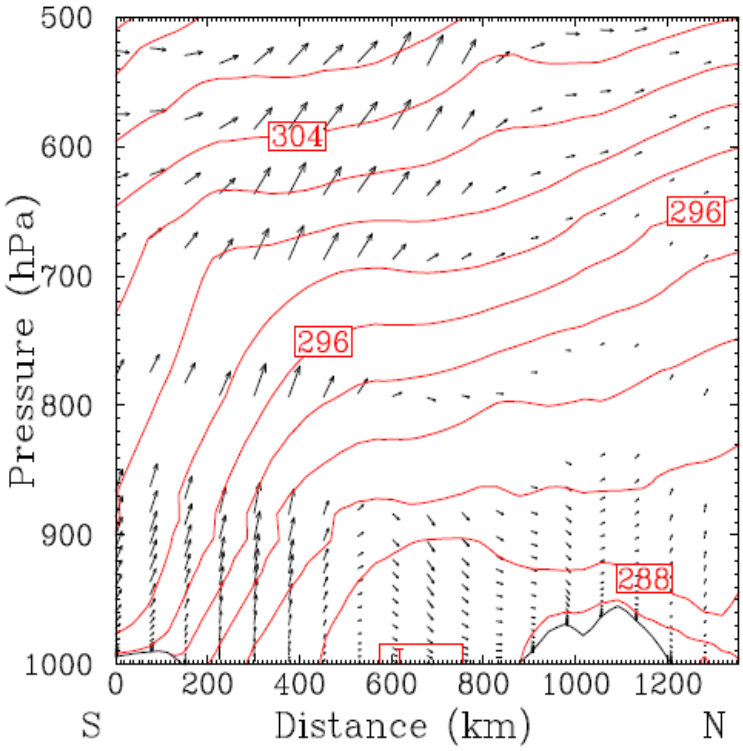

Figure 4.18. Vertical Wind Circulation Graphs of WRF Model for Episode I (drawn for 18UTC 02.04.2008).

Both, horizontal and vertical wind schemes, define the Akhdar region as the dust source activation area of dust transport towards Istanbul during the Episode I.

4.2.2. Backward Trajectory Analysis by WRF

Trajectory analyses are used to identify the source regions of the air parcels moving into a given area. Here, the origins of the high levels of PM concentrations of Istanbul have been estimated by using the backward trajectory method. Likewise the horizontal and vertical circulation graphs, backward trajectory analysis graph for Episode I (Fig 4.19) also implies that Akhdar Mountain region is the potential dust source of the episode.

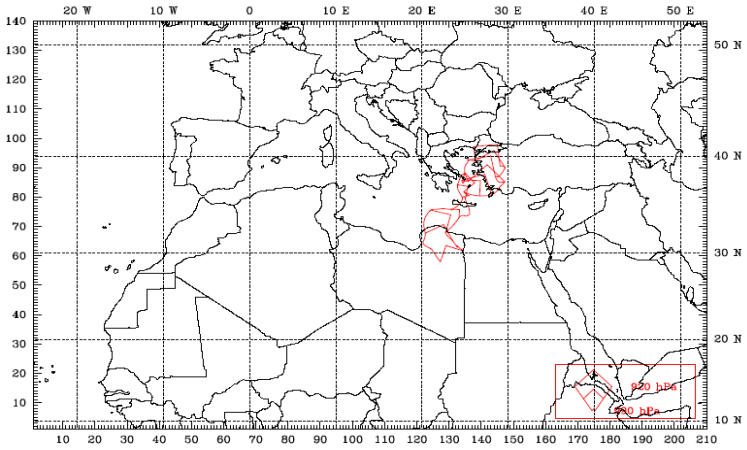

Figure 4.19. Backward trajectory of WRF model for Episode I.

Istanbul has been set as the release point of the analysis. Grid point and pressure level of the release point, time period of interest have been defined in the namelist section of WRF before the calculation. Then, program produced the graph which displays the potential source of the backward trajectories. Table 4.1. summarizes the basic features of the analysis of trajectory I.

Table 4.1. Features of Trajectory I

Trajectory Number	I
Source Area	Akhdar
Grid Number of Release Point	X = 145, Y= 98
Pressure Level of Receptor Point and Release, hPa	990 – 920
Release Time and Completion Time, h	96 – 24

4.2.3. Precipitation Graphs by WRF

24 hour precipitation graphics (Fig 4.20), which has been plotted for 4 April 2008, indicate that during Episode I the Anatolian Peninsula and Istanbul have not recieved rainfall. Consequently, dry deposition of Saharan Desert dust over Istanbul is expected.

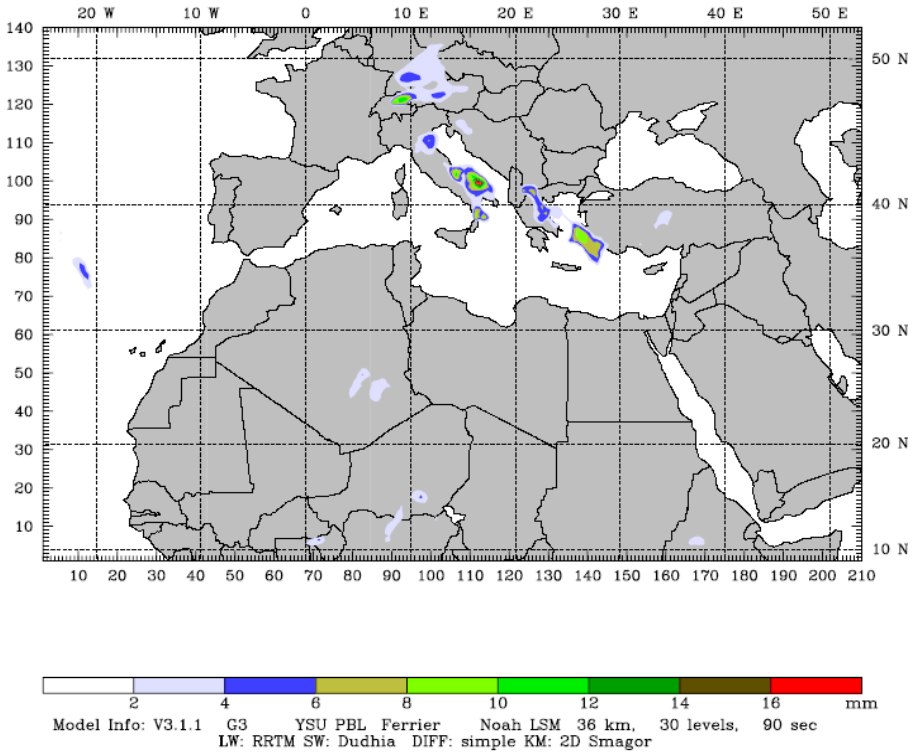

Figure 4.20. Cumulus Precipitation in past 24 hours for Episode I.

4.2.4. Aerosol & Cloud Optical Depth Images by MODIS

Besides the stated clues of Saharan dust transport acquired from the WRF model, dustiness of the study area can be identified by the satellite retrievals. The Moderate Resolution Imaging Spectroradiometer is one of these tools, for displaying the dust optical depth of the interest area. GIOVANNI, a type of MODIS application, has been used to find out the dustiness of the study domain.

Here, Fig 4.21 displays the dustiness of the domain during the deposition period of the Episode I (04.04.2008).

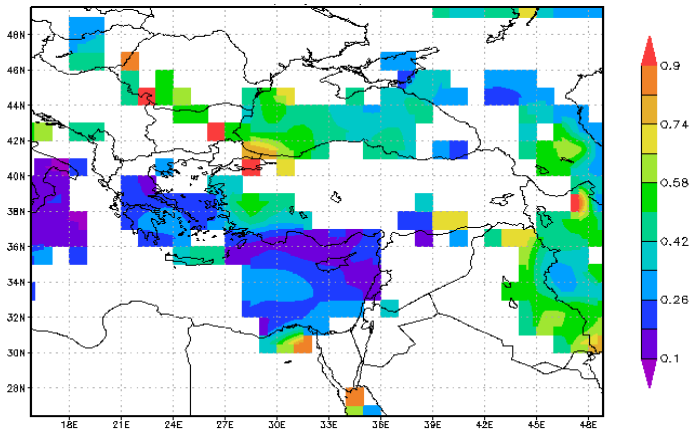

Figure 4.21. Aerosol Optical Depth graphs of MODIS for Episode I (at 550nm [unitless], during 04.04.2008).

As given in the backward trajectory analysis section (Table 4.1), the winds arrival time of Istanbul and PM peak concentration time of Episode I indicates the time period of 96th hour of the simulation period. At the end hours of April 4, winds coming from Akhdar region arrive to Istanbul and deposition of dust is expected at this period. MODIS data of aerosol optical depth supports this hypothesis. It is obtained from the graph (Fig 4.20) that Istanbul experienced high levels of dust at 4 April 2008.

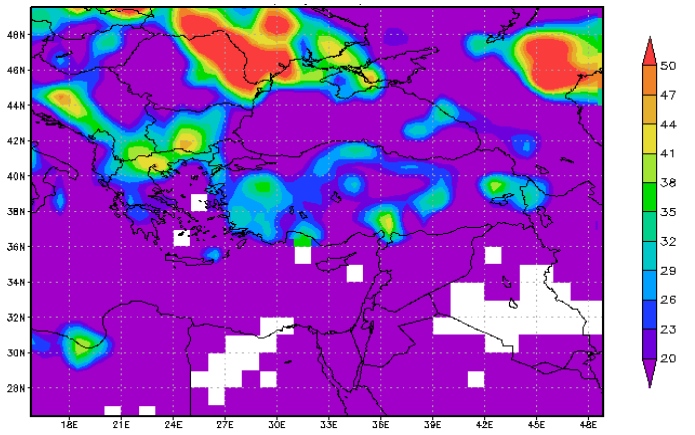

Figure 4.22. Cloud Optical Depth graphs of MODIS for Episode I (at 550nm [unitless], during 04.04.2008).

MODIS data can also identify the cloudiness of the domain. Since cloud covers prevent obtaining aerosol optical depth, the graphs of cloudiness points out the parts of the

domain where aerosol depth can not be measured in an accurate way. Figure 4.22. shows that Marmara Region has a low cloud optical depth during April 4. Therefore, aerosol optical depth of Istanbul on April 4 (Fig 4.21) has been displayed in a proper way.

4.2.5. Dust Regional Atmospheric Model (DREAM) Forecast Graphs

In order to support the dust transport from the Saharan region towards Istanbul, besides the WRF model output plots, archieved output graphs of a supporting model on behaviour of dust loadings & deposition of the study domain have been presented in this section. DREAM model plots of dust loadings (g/m^2) and dry dust deposition (mg/m^2) have been examined to find the evidence of the transport.

Figure 4.23 displays the dust loadings and wind pattern of the interest area. The combined effect of the low and high pressure systems, stated in the previous sections, can be observed from this graphics, too. Also, likewise the MODIS data (Fig 4.21), it can be inferred from Figure 4.24 that dry dust deposition has been occured over the region of Istanbul.

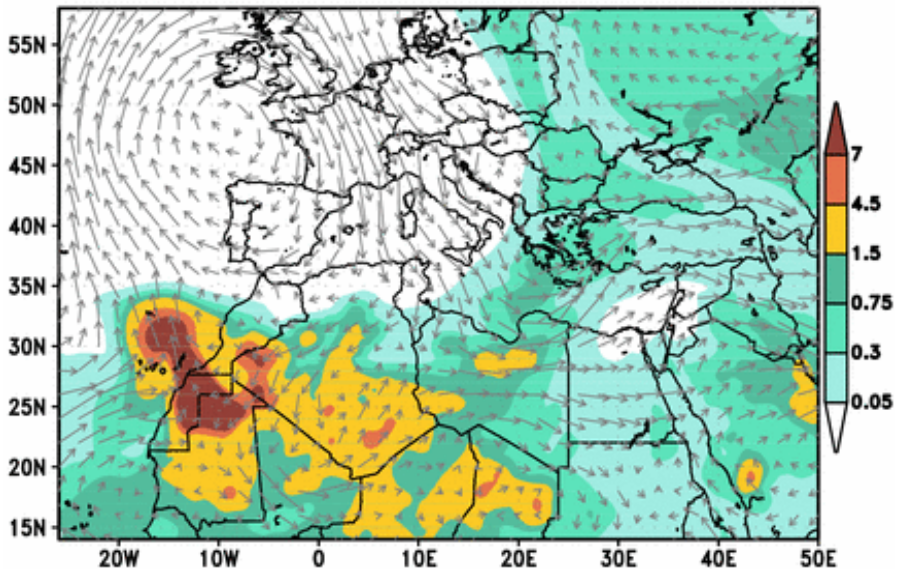

Figure 4.23. Dust loading (g/m^2) forecast graphs of BSC/DREAM for Episode I (6 hour forecast for 18 UTC 02.04.2008).

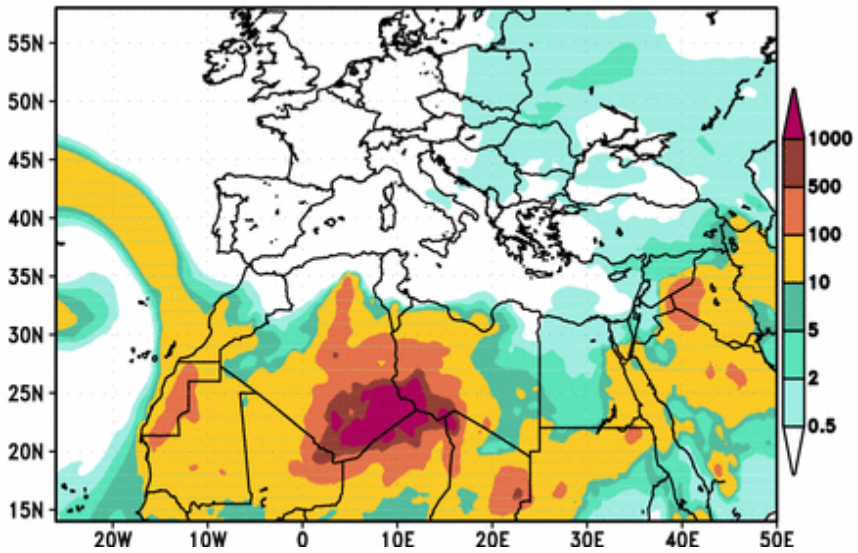

Figure 4.24. Dry Dust Deposition (mg/m^2) graphs of BSC/DREAM for Episode I (12 hour forecast for 00 UTC 05.04.2008).

4.2.6. Backward Ensemble Trajectory Analysis by HYSPLIT

Besides the trajectory analysis of the model, another model which is based on a Lagrangian transport approach has been computed to display the transport behaviour of the episodes. The advantages of the model HYSPLIT is the obtaining of 27 different trajectories for each run. Since the ensemble trajectory option of the model enables to display the additionally two neighborhood grid trajectories for each axis, for three dimensions x, y and z, model produces 3x3x3 = 27 several trajectories for every run.

Figure 4.25 represents the ensemble HYSPLIT backward trajectory analysis for Episode I. The green lines show the airmass trajectories which are travelling from the Saharan region. Supporting the WRF model data, it is obviously concluded from the graph that many trajectories are resulting from the ground level of the Akhdar region, consistent with the previous model results of Episode I.

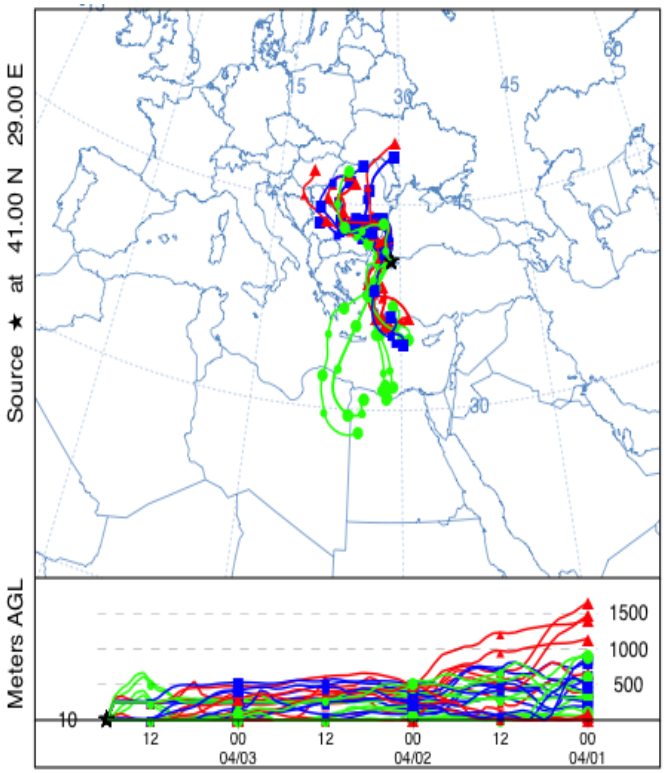

Figure 4.25. Backward Trajectories ending at 18 UTC 03.04.2008.

4.3. Episode II

4.3.1. Synoptic Analysis

4.3.1.1. Distribution of Horizontal Wind Vectors. The combined effect of cyclone, with a surface pressure of 1008hPa, occuring over the Atlantic Ocean near the West Sahara and a high pressure system over Morocco, with a surface pressure of 1013 hPa, have started the initial dust mobilization for the transport of Episode II. Winds, following the northern part of Algeria, passes over the Mediterranean and reaches to the Marmara Region of Turkey. Likewise the first Episode, a high pressure system had been located over the northern Egypt and southeast Mediterranean, with a surface pressure of 1018 hpa. This high pressure system played an important role in the synoptic system of the interest domain and changed the direction of the flow, coming from the Atlas Mountain region. Airmasses had been travelling from west to east direction. However, the high pressure system over the northern Egypt turned the direction of the flow towards the Marmara Region of Turkey (Fig 4.26).

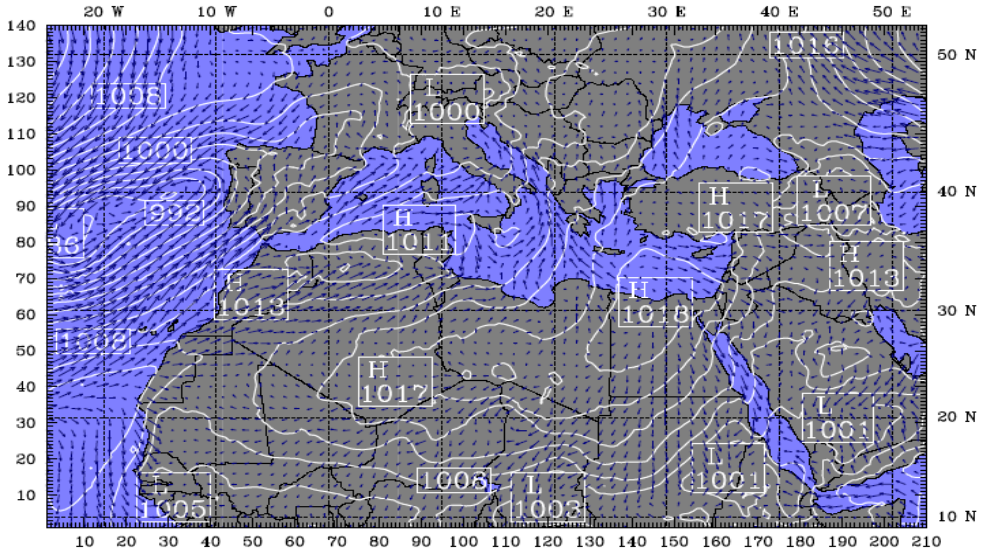

Figure 4.26. Horizontal Wind Vector Graphs of Episode II
(drawn for 18UTC 08.04.2008 at 1000 hPa).

4.3.1.2. Vertical Wind Circulation Vectors. The high-pressure system over the northern Egypt has been identified as the key factor of the Episode by changing the direction of flow towards the Marmara region (Fig 4.26). Therefore, the vertical cross section between the Akhdar region (near the high-pressure system) and Istanbul (Fig 4.27) has been selected to be analyzed (Fig 4.17).

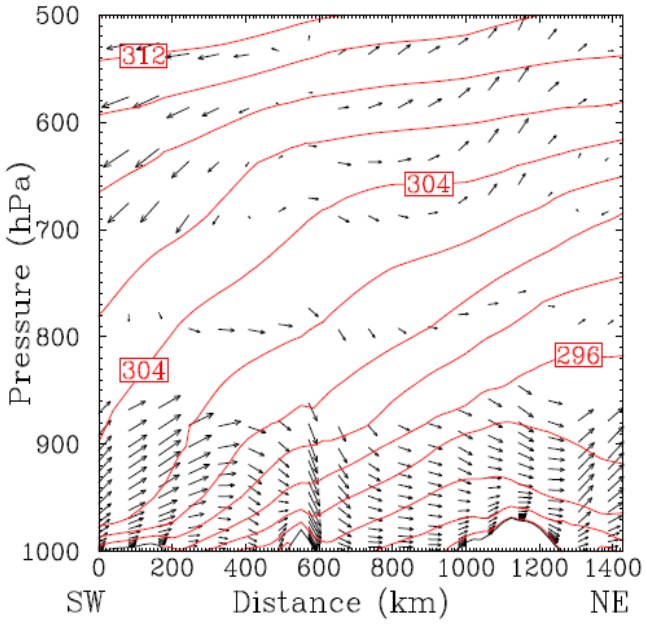

Figure 4.27. Vertical Wind Circulation Graphs of WRF Model for Episode II
(drawn for 18UTC 08.04.2008).

The airmass flow, occuring between the pressure levels of 1000 and 850 hPa can be observed from Fig 4.27. There is a significant wind flow between the Akhdar and Marmara Region at the lower layer of the atmosphere. The potential temperature indicates the strong instability over the southwestern (SW) part of the cross section.

4.3.2. Backward Trajectory Analysis by WRF

Similiar with the horizontal wind vector graphs (Fig 4.26), the dust origin of the Episode II has been determined as the Atlas Mountain Region. Winds, carrying the desert dust of the Atlas Mountain lee area, follows the Algeria-Libya border. Finally, as it is seen from the previous sections (Fig 4.26), with the effect of the high-pressure system over northern Egypt, dust is transported towards Istanbul. Trajectory analysis prove the transport (Fig 4.28).

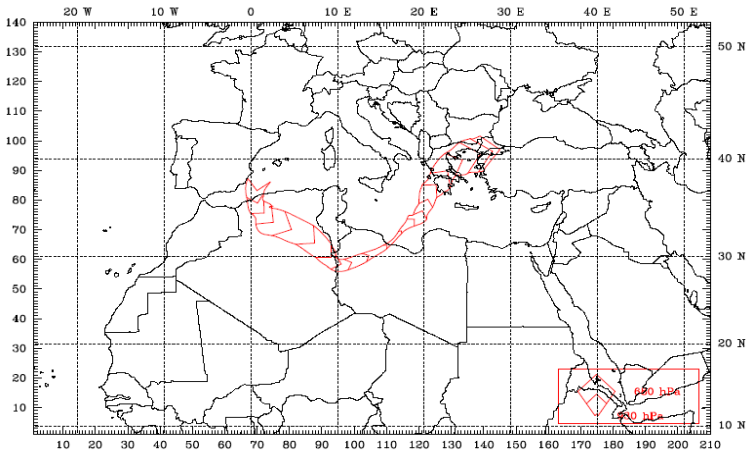

Figure 4.28. Backward trajectory of WRF model for Episode II.

Basic features of trajectory analysis of Episode II has been stated at Table 4.2.

Table 4.2. Features of Trajectory II

Trajectory Number	II
Source Area	Atlas
Grid Number of Release Point	X = 145, Y= 97
Pressure Level of Receptor Point and Release, hPa	700 – 410
Release Time and Completion Time, h	216 – 96

4.3.3. Precipitation Graphs by WRF

Figure 4.29 indicates that at 10 April 2008 Istanbul has not recieved any rainall. Likewise the first episode, dry deposition for Episode II has been expected.

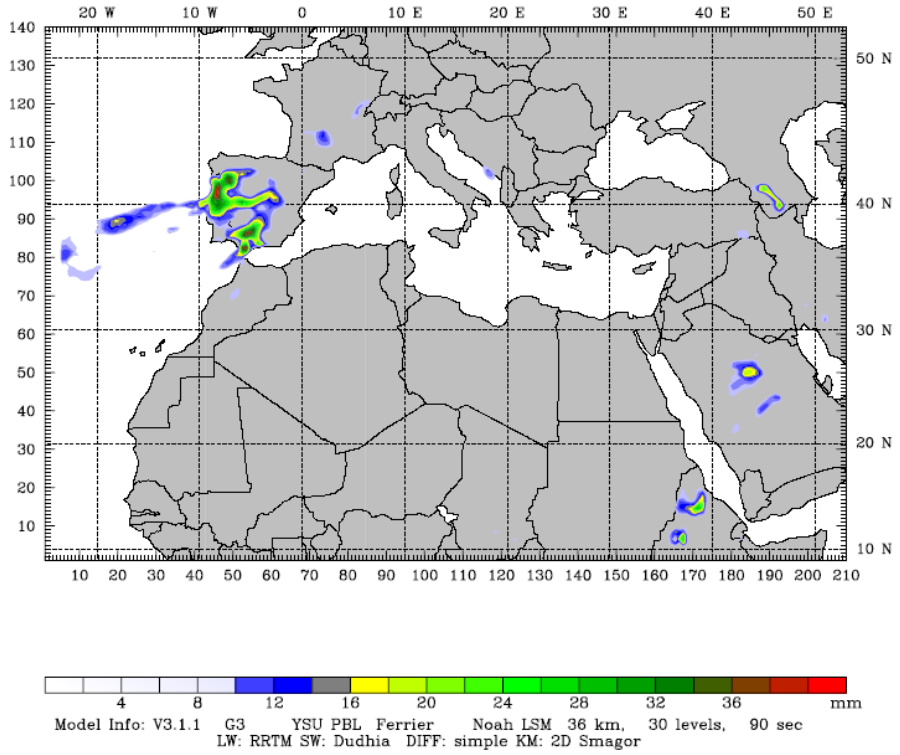

Figure 4.29. Cumulus Precipitation in past 24 hours for Episode II.

4.3.4. Aerosol & Cloud Optical Depth Images by MODIS

The MODIS graphs, plotted for the time period of dust deposition of Episode II, unfortunately does not give much information on the dustiness of the episode. Figure 4.30 points out a white region over the Marmara Region of Turkey. White region means there is a lack of information due to the cloudliness of the atmosphere above the interest area. Figure 4.31 proves the intense cloudliness of the Marmara Region, as expected.

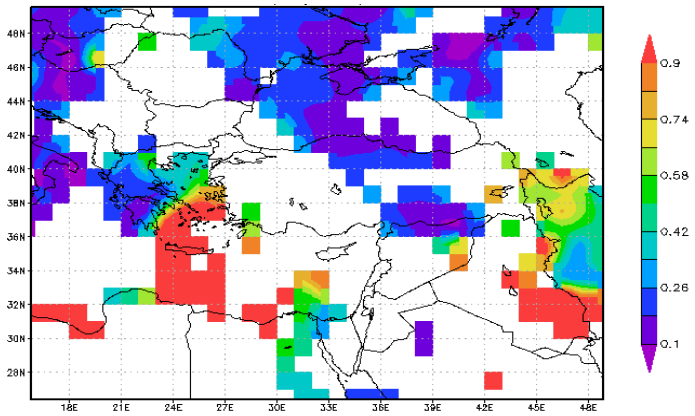

Figure 4.30. Aerosol Optical Depth graphs of MODIS for Episode II (at 550nm [unitless] during 08.04.2008).

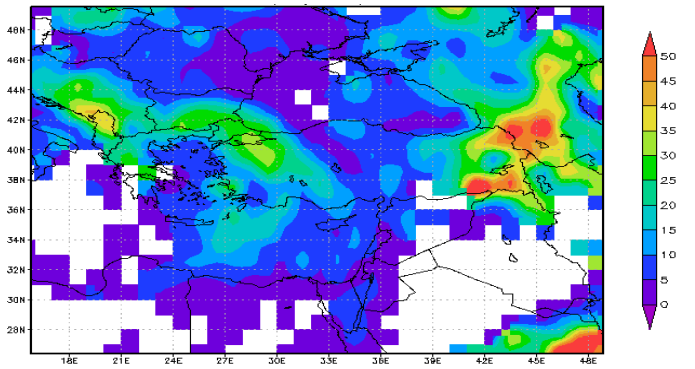

Figure 4.31. Cloud Optical Depth graphs of MODIS for Episode II (at 550nm [unitless] during 08.04.2008).

4.3.5. Dust Loadings & Dry Deposition Forecast Graphs by DREAM

The general pattern of the flow over the study domain has a significant component from southwest Sahara towards Istanbul (Fig 4.32). The wind pattern of DREAM output graph of Episode II (Fig 4.32) is in good agreement with the horizontal wind circulation graph (Fig 4.26) and the trajectory analysis graph (Fig 4.28). All graphics prove the dust transport from the Atlas and Akhdar region of Sahara to Turkey (Fig 4.26, 4.28, and 4.32).

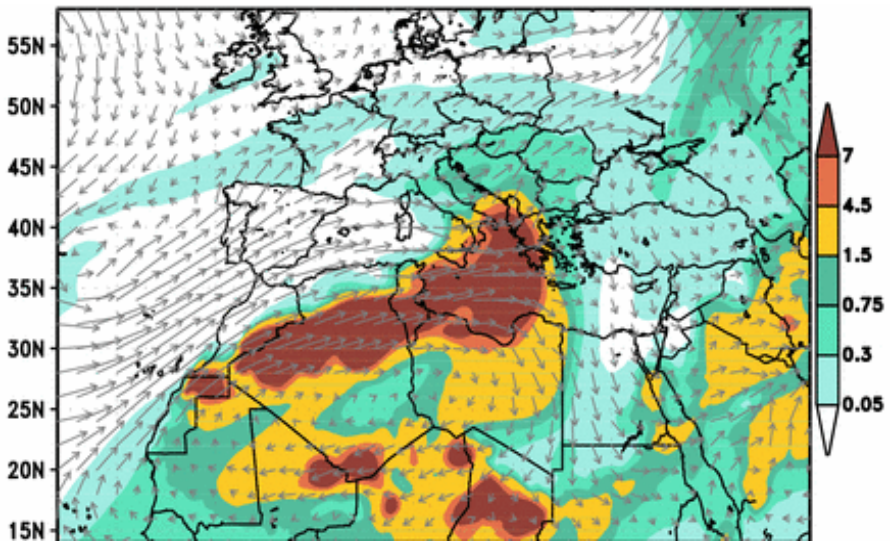

Figure 4.32. Dust loading (g/m^2) forecast graphs of BSC/DREAM for Episode II (6 hour forecast for 18 UTC 08.04.2008).

The graphic, which shows the deposition of dust at the end of Episode II, proves the contribution of Saharan desert dust to Istanbul PM levels (Fig 4.33). It is inferred from the graph that dust is significantly deposited over Istanbul which is the probable cause of the high ground level PM concentrations of Istanbul.

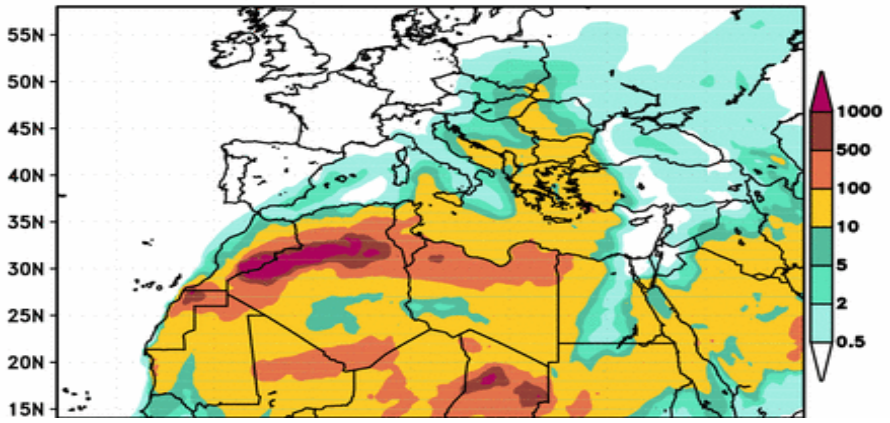

Figure 4.33. Dry Dust Deposition (mg/m^2) graphs of BSC/DREAM for Episode II (12 hour forecast for 00 UTC 10.04.2008).

4.3.6. Backward Ensemble Trajectory Analysis by HYSPLIT

The green plots of HYSPLIT plot indicates the backward airmass ground level trajectory analysis from Istanbul to Sahara (Fig 4.34). Similar with the previous data on Episode 2, HYSPLIT plot shows the Atlas Mountain area as the dust activation source of the desert. It is concluded from the plot that dust is also transported from the Akhdar region.

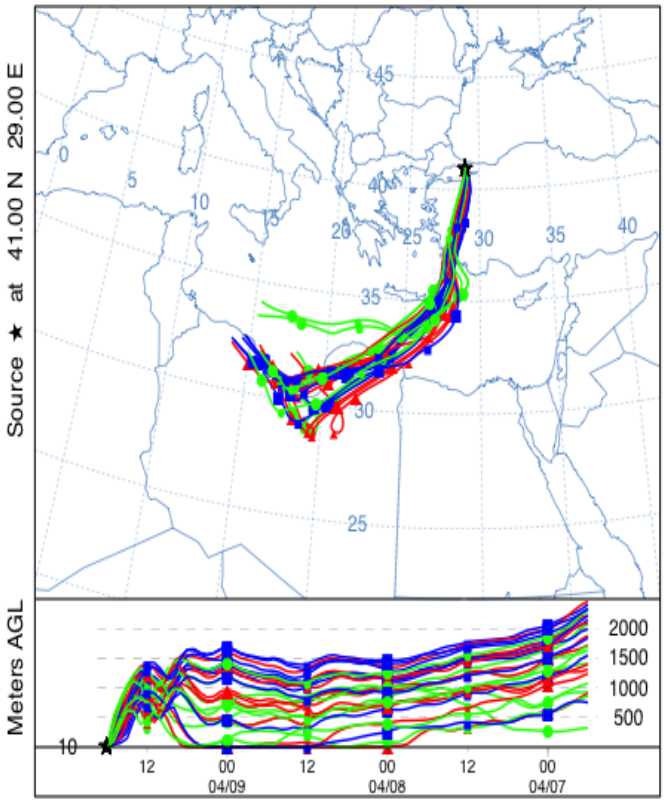

Figure 4.34. Backward Trajectories ending at 18 UTC 09.04.2008.

4.4. Results of Episode III

4.4.1. Synoptic Analysis by WRF

4.4.1.1. Distribution of Horizontal Wind Vectors. The combine effect of a high-pressure system over the southern Algeria, with a surface pressure of 1012 hPa, and a low pressure system over the Mauritania-Mali border, with a surface pressure of 1008 hPa have mobilized the desert dust (Fig 4.35). Over northern Egypt, the high-pressure system, which has a surface pressure of 1018 hPa, has been observed. Likewise to the previous episodes, the high-pressure system has the effect of turning the wind direction towards Istanbul.

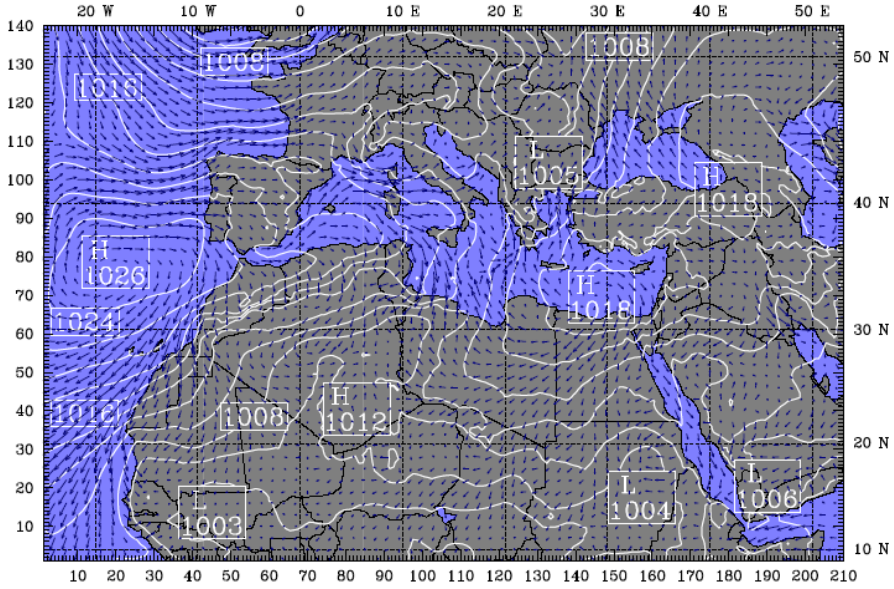

Figure 4.35. Horizontal Wind Vector Graphs of Episode III (drawn for 18UTC 12.04.2008 at 1000 hPa).

4.4.1.2. Vertical Wind Circulation Vectors. The source and receptor points of the vertical analysis of Episode III has been determined previously (Fig 4.17). Wind circulation pattern between the northwest of Libya and Istanbul has been identified in this section. The transport of dust-loaded air parcels from Sahara to the Anatolian Peninsula, vertically between the pressure levels of 900 and 1000hPa has been observed from the graph (Fig 4.36). The cross section for the episode III show strong instability over the SW zone and prevailing winds from Sahara to Istanbul.

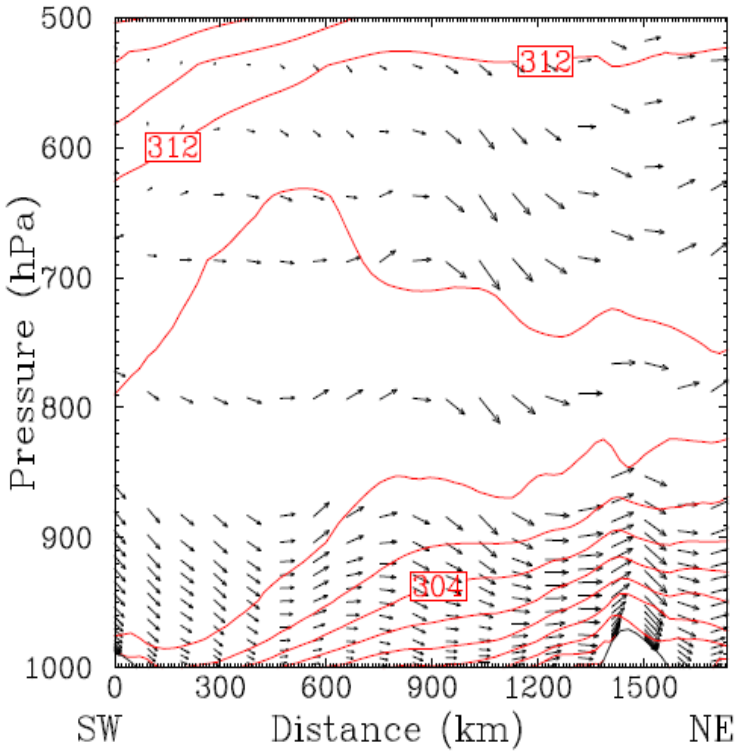

Figure 4.36. Vertical Wind Circulation Graphs of WRF Model for Episode II (drawn for 18UTC 12.04.2008).

4.4.2. Backward Trajectory Analysis by WRF

Backward trajectory analysis of WRF shows that the potential aerosol source of Episode III has been the Algeria-Libya border (Fig 4.37).

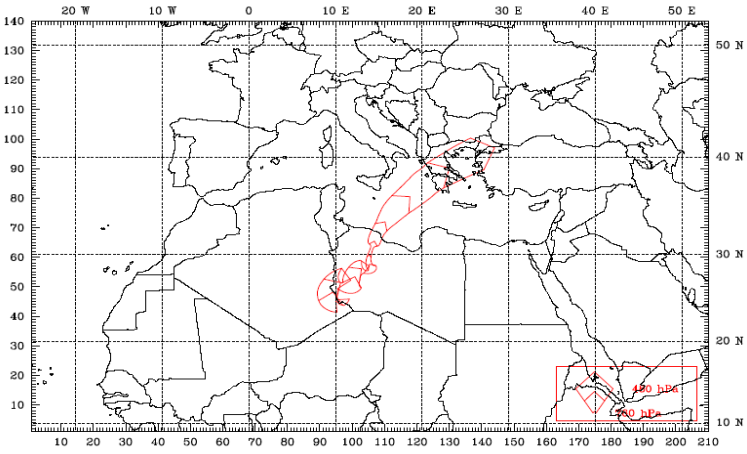

Figure 4.37. Backward Trajectory Plots for Episode III.

Table 4.3. Properties of Trajectory III

Trajectory Number	III
Source Area	Algeria-Libya border
Grid Number of Release Point	X = 144, Y= 97
Pressure Level of Receptor Point and Release, hPa	760 - 480
Release Time and Completion Time, h	306 - 228

4.4.3. Precipitation Graphs by WRF

No precipitation has been observed over Istanbul during 14 April 2008 (Fig 4.38). Similiar with the previous two episodes, dry deposition of desert dust has been expected for Episode III.

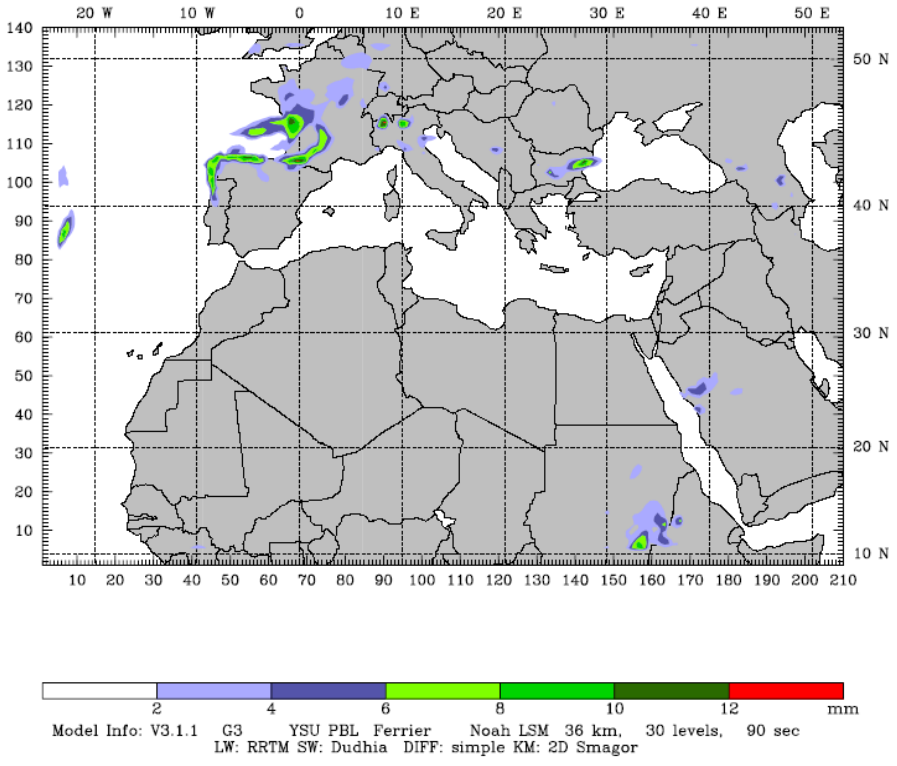

Figure 4.38. Cumulus Precipitation in past 24 hours for Episode III.

4.4.4. Aerosol & Cloud Optical Depth Images by MODIS

Aerosol and Cloud Optical Depth graphs of GIOVANNI (Fig 4.39 and 4.40), which represent the dustiness of the Episode III, demonstrate that during the days of Episode III Marmara region had a cloudy weather conditions. Therefore, there is not much information from GIOVANNI graphs about the dustiness of the area.

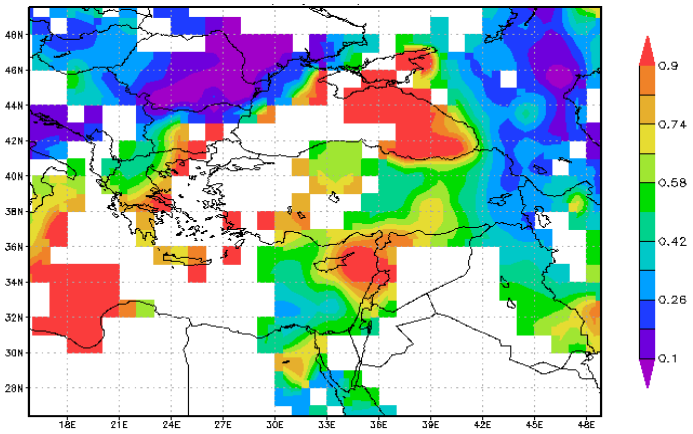

Figure 4.39. Aerosol Optical Depth at 550nm [unitless] during 13.04.2008.

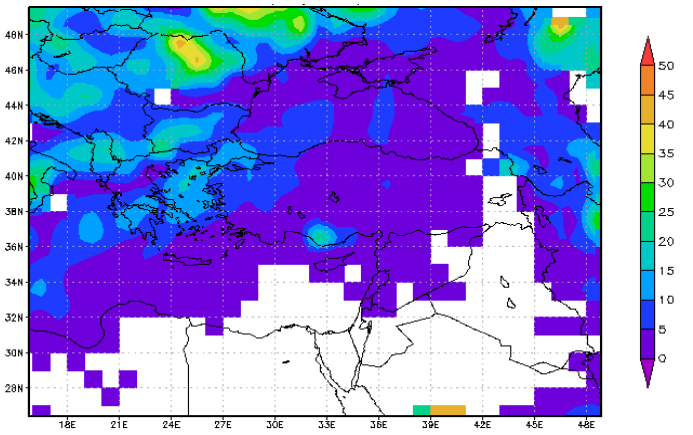

Figure 4.40. Cloud Optical Depth at 550 nm [unitless] during 13.04.2008.

4.4.5. Dust Loadings & Dry Deposition Forecast Graphs by DREAM

Dust loading graphs of DREAM indicate that the Saharan Desert dust transported to the Anatolian Peninsula. DREAM clearly supports the results of the WRF model. Western

Sahara, Atlas Mountain, Algeria-Libya border and Akhdar region are the potential dust sources of the Episode III (Fig 4.41).

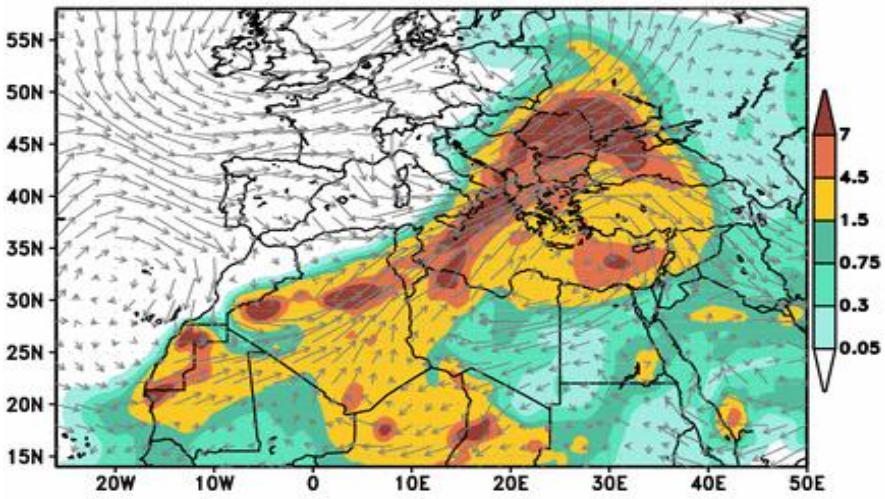

Figure 4.41. Dust loading (g/m^2) forecast graphs of BSC/DREAM for Episode III (6 hour forecast for 18 UTC 12.04.2008).

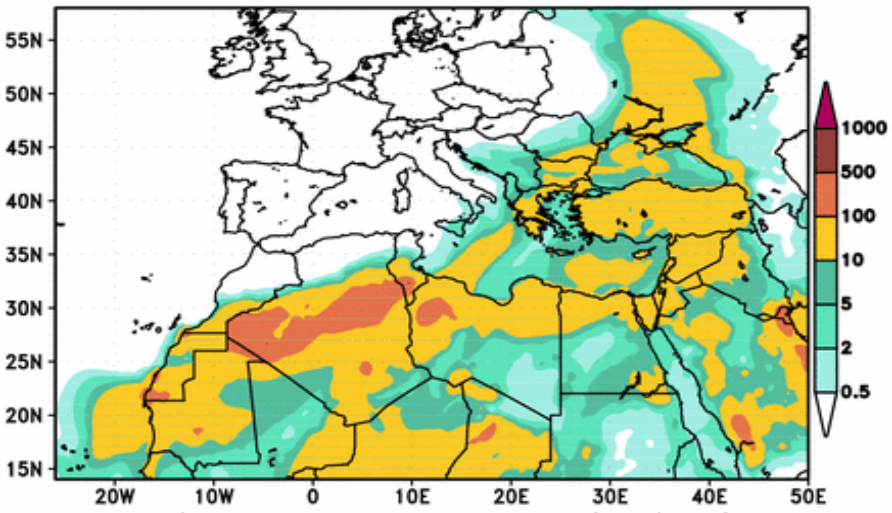

Figure 4.42. Dry Dust Deposition (mg/m^2) graphs of BSC/DREAM for Episode III (6 hour forecast for 00 UTC 12.04.2008).

Figure 4.41 demonstrate that the atmosphere, covering the Saharan Desert region and the Anatolian Peninsula, has been filled with the Saharan mineral dust. Both Figure 4.41 and 4.42 are in good agreement with the horizontal wind vector graph of Episode III (Fig 4.35).

4.4.6. Backward Ensemble Trajectory Analysis by HYSPLIT

The backward ensemble trajectory analysis of Episode III by HYSPLIT identifies the transport pathways of the Episode. Particularly, some blue plots of the graphics show the west part of the Desert as the potential aerosol source of the Episode III (Fig 4.43). The results of HYSPLIT are in good agreement with the results of the horizontal wind vector graphs of Episode III (Fig 4.35).

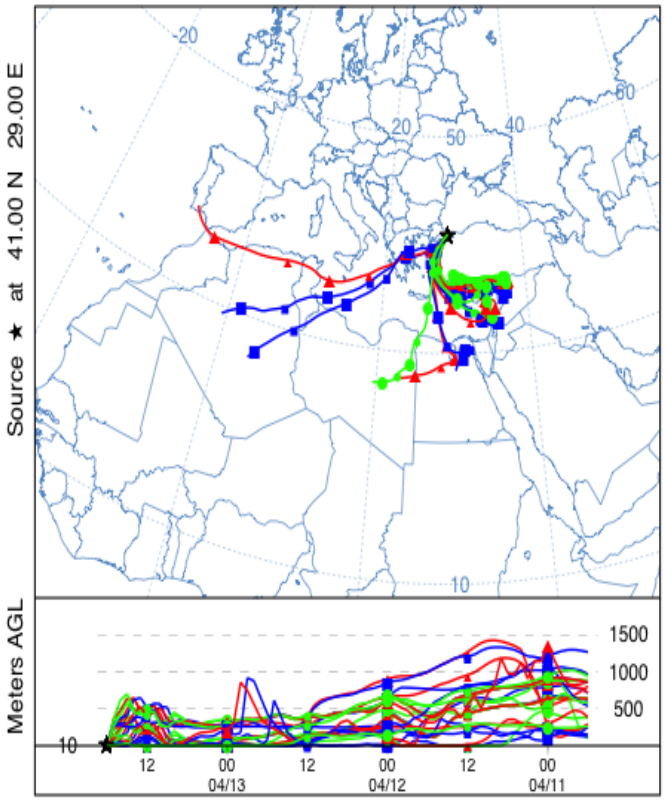

Figure 4.43. Backward Trajectories ending at 18 UTC 13.04.2008.

4.5. Results of Episode IV

4.5.1. Synoptic Analysis by WRF

4.5.1.1. Distribution of Horizontal Wind Vectors. Over the northern Atlantic, strong winds have been produced from the combined effect of a low pressure system, with a surface pressure of 993 hPa, and high pressure system, with a surface pressure of 1016 hPa (Fig 4.44). The winds have entered the Saharan domain from Western Sahara and followed an eastern path over the Algeria. Then, over the Libya, the direction of the air flow has been turned towards the Anatolian Peninsula by the effect of a high pressure system. The system has a surface pressure of 1016 hPa and it has been located over the Cyprus.

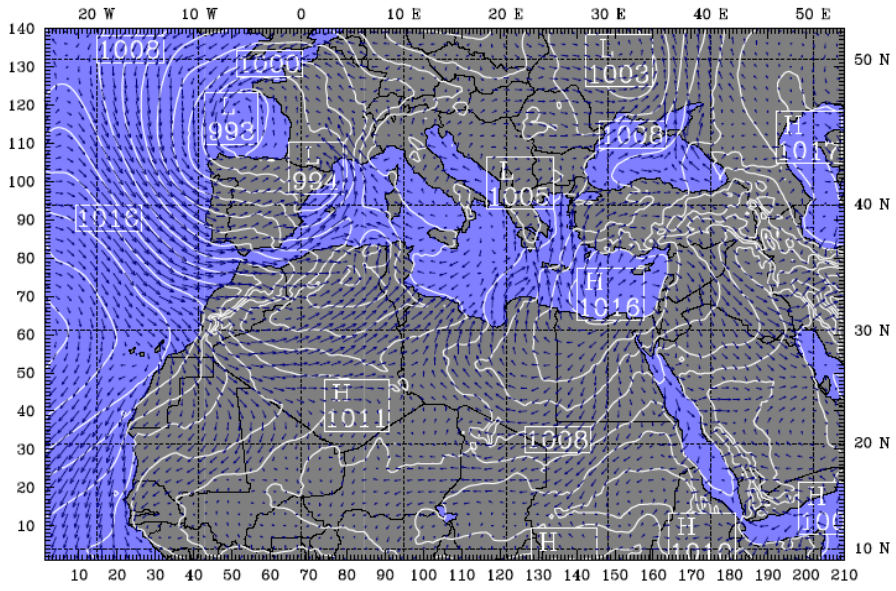

Figure 4.44. Horizontal Wind Vector Graphs of Episode IV,
(drawn for 12UTC 20.04.2008 at 1000 hPa)

4.5.1.2. Vertical Wind Circulation Vectors. From a northern point of Libya to Istanbul, vertical wind circulation pattern has been identified (Fig 4.17. and 4.45). Between 1000 and 850 hPa, transport of airmasses from Sahara to the Anatolian Peninsula can be obviously observed. The regular wind patterns prove the contribution of Saharan Desert dust to high levels of PM in Istanbul.

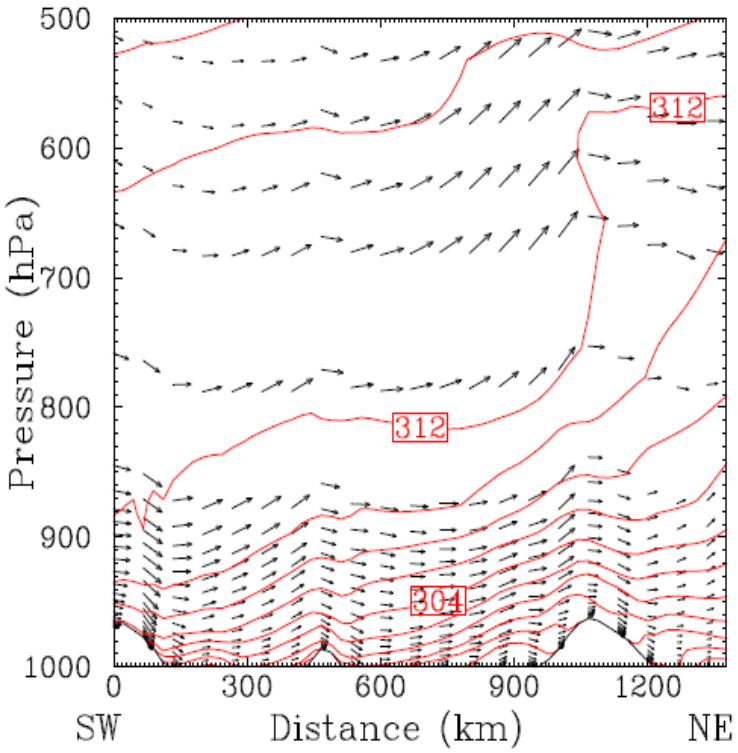

Figure 4.45. Vertical Wind Circulation Graphs of WRF Model for Episode IV, (drawn for 00UTC 22.04.2008).

4.5.2. Backward Trajectory Analysis by WRF

As consistent with the horizontal wind vector graphs (Fig 4.44), backward trajectory analysis of WRF marks that the air flow that carry the Saharan Desert dust to the Anatolian Peninsula has been originated from the Atlantic, next to the Western Sahara. By crossing the northern Libya, trajectories had arrived the Marmara region (Fig 4.46).

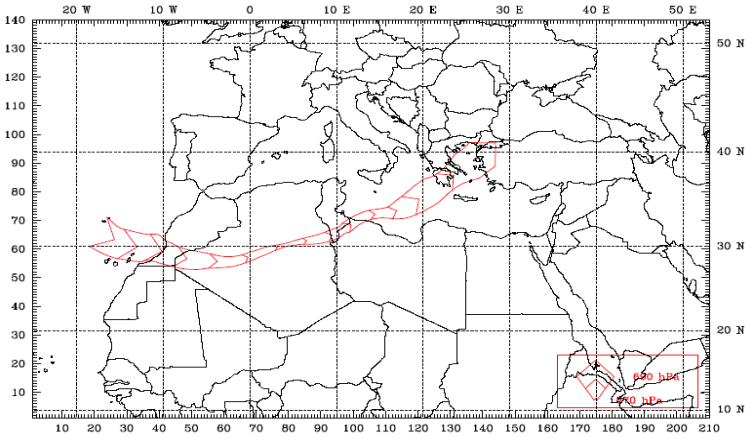

Figure 4.46. Backward Trajectory Plots for Episode IV.

Table 4.4. Properties of Trajectory IV

Trajectory Number	IV
Source Area	West Sahara
Grid Number of Release Point	X = 144, Y= 97
Pressure Level of Receptor Point and Release, hPa	870 – 690
Release Time and Completion Time, h	522 – 486

4.5.3. Precipitation Graphs by WRF

No rainfall pattern has been observed for the day of 23 April 2008 (Fig 4.47). Dry deposition has been expected for Episode IV.

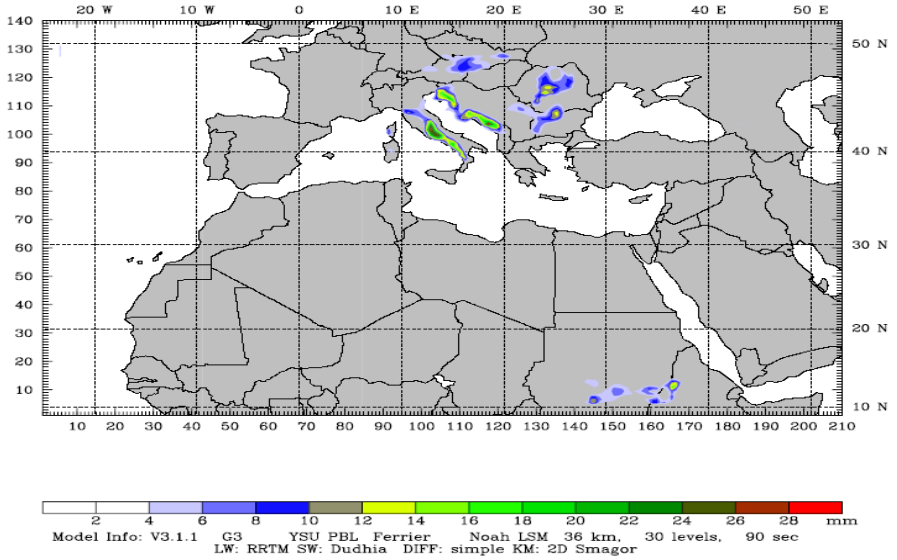

Figure 4.47. Cumulus Precipitation in past 24 hours for Episode IV.

4.5.4. Aerosol & Cloud Optical Depth Images by MODIS

The intensity of aerosols over the Marmara Region of Turkey can be inferred from the graphics (Fig 4.48 and 4.49). Atmosphere has been filled with the aerosols.

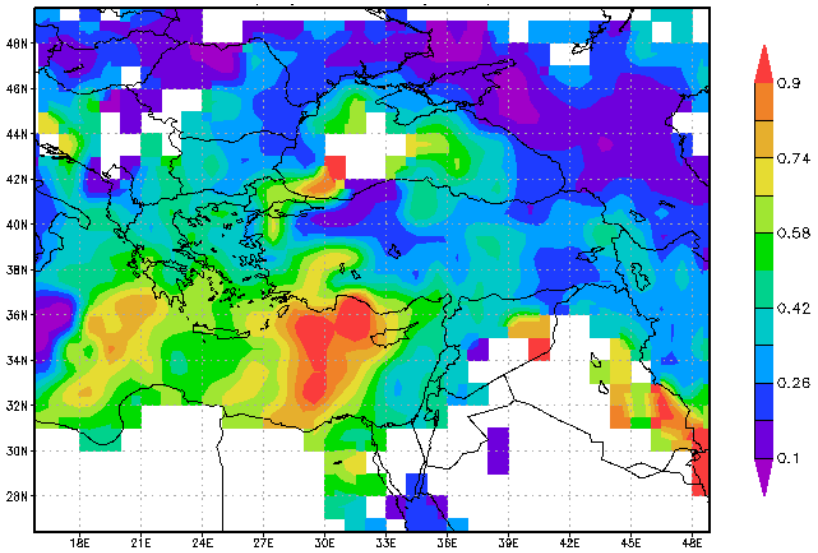

Figure 4.48. Aerosol Optical Depth (at 550nm [unitless] during 21& 22.04.2008).

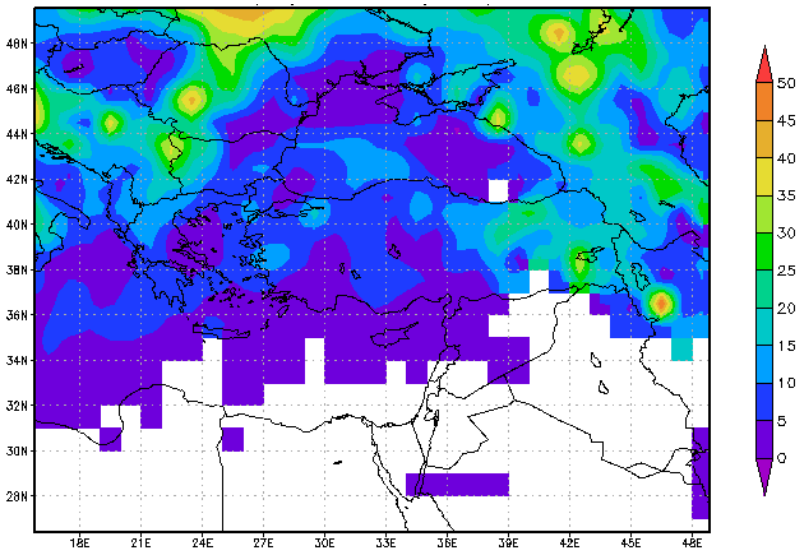

Figure 4.49. Cloud Optical Depth (at 550nm [unitless] during 21& 22.04.2008).

4.5.5. Dust Loadings & Dry Deposition Forecast Graphs by DREAM

The pathway of the Saharan Desert dust, which can be viewed from the DREAM graph (Fig 4.50), is similar with the horizontal wind vector graph of the model (Fig 4.44).

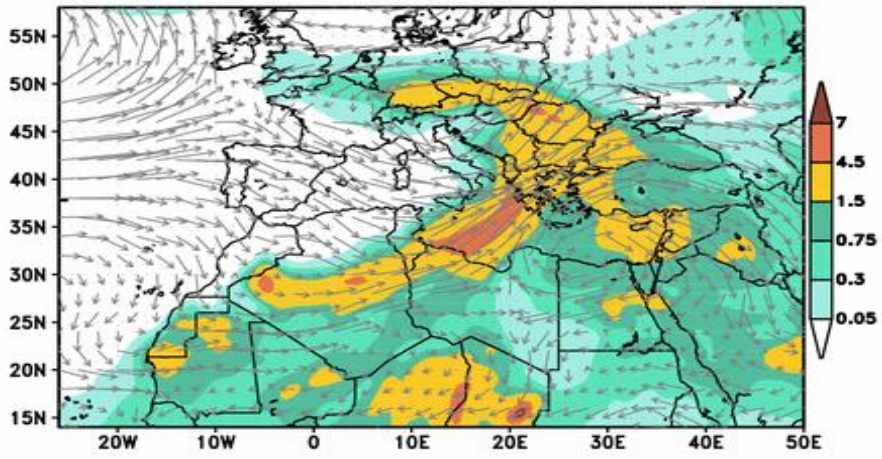

Figure 4.50. Dust loading (g/m^2) forecast graphs of BSC/DREAM for Episode IV (12 hour forecast for 00 UTC 22.04.2008).

Likewise Figure 4.44, dust has been transported from Western Sahara and passes over the northern Libya region. It can be seen from the graph that aerosols have reached the Marmara Region of Turkey.

From Figure 4.51, dry deposition of Saharan aerosols over Istanbul can be identified. The pathway of the Saharan aerosol - from West Sahara to Turkey - can be inferred from this graph too.

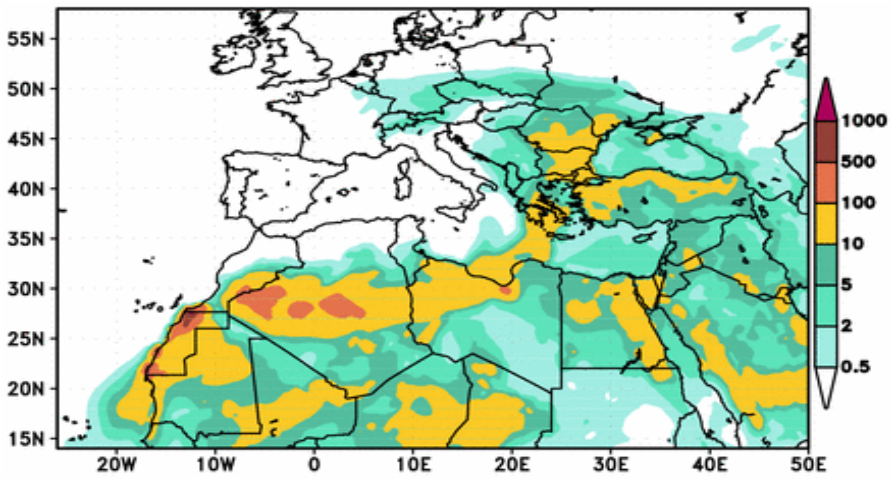

Figure 4.51. Dry Dust Deposition (mg/m^2) graphs of BSC/DREAM for Episode IV (18 hour forecast for 18 UTC 22.04.2008).

4.5.6. Backward Ensemble Trajectory Analysis by HYSPLIT

The HYSPLIT backward ensemble trajectory analysis of Episode IV (Fig 4.52) points out the Akhdar region as one of the origins of Episode IV. Some blue points demonstrate the aerosol source as the Akhdar region and northern part of the Egypt.

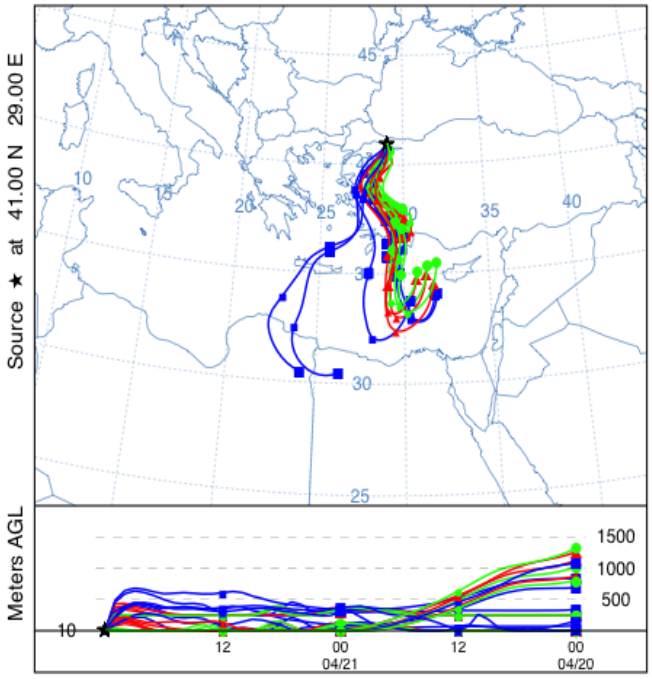

Figure 4.52. Backward Trajectories ending at 00 UTC 22.04.2008.

5. CONCLUSIONS

It is a fact that air pollution is a major concern for determining health effects and producing government regulations in many countries. Having correct and detailed information of air pollutants is becoming an essential requirement. In this study, dust transport from Saharan Region to Istanbul has been presented. The model results a significant impact of Saharan dust to particulate matter (PM) concentrations in Istanbul. An accurate identification of meteorological processes controlling dust emission is a prerequisite for correct evaluation of dust aerosol effects in the city of Istanbul. Together with the meteorological model approach and back-trajectory study; origins, routes and intensity of the PM concentrations were identified. Furthermore, DREAM model and MODIS data was used to verify our results. The new findings of the study are described below:

- Mediterranean cyclones travels quickly eastward mostly following the North African coast [Alpert et al., 1990; Alpert and Ziv, 1989]. Low-pressure systems that travel across the Mediterranean penetrating from the Atlantic and reaching to the Eastern Mediterranean are responsible for dust mobilization and advection.

- The surface high-pressure system located over northern Egypt is the key factor of Saharan dust transport and deposition to the Anatolian Peninsula and the city of Istanbul.

- Specifically, the convection zones created by these low and high pressure systems over the North Africa induce dust-loaded air parcels to the city.

- Also, new findings from this work suggest that the imposed European Union limits on PM cannot be applicable for Turkey unless the origin (natural or anthropogenic) of the PM is taken into account.

- According to EU, limit values for PM10 impose both an annual average concentration value of 40 ($\mu g/m^3$), and a daily concentration value of 50

($\mu g/m^3$) which must not be exceeded more than 35 times per calender year. This limit was exceeded for 22 days on April, 2008 in Istanbul.

- The analysis has shown that transport of Saharan dust occuring in the central part of the Mediterranean are usually rather intensive in the atmospheric mass loading capacity and take place in deeper atmospheric layers for a longer duration (approxiametely 2-4 days) than eastern Mediterranean dust events.

- The eastern transport (Akhdar zone) usually originates from Saharan Desert for short periods (approxiametely 1 day) and is restricted to a rather shallow atmospheric transport layer featured by low optical depth values.

REFERENCES

Alpert, P., Kishcha, P., Shtivelman, A., Krichak, S.O., and Joseph, J.F., 2004. Vertical distribution of Saharan dust based on 2.5-year model predictions. Atmospheric Research, 70, 109-130.

Barcelona Supercomputing Center - Centro Nacional de Supercomputación. http://www.bsc.es/plantillaH.php?cat_id=321. (accessed August 2010).

Bertrand, J., Cerf, A., Domergue, J.L., 1979. Repartition in space and time of dust haze south of the Sahara. WMO 538, 409–415.

Bodélé Depression | earthobservatory.nasa.gov. http://mm04.nasaimages.org/MediaManager/srvr?mediafile=/Size3/nasaNAS-10-NA/76059/NAfrica_AMO_2007002.jpg&userid=1&username=admin&resolution=3&servertype=JVA&cid=10&iid=nasaNAS&vcid=NA&usergroup=Earth_Observatory_(nasa)-10-Admin&profileid=46. (accessed August 2010).

Borushko, I.S., 1972. Dust storm distribution in the Tropics. Glavnaya Geofizicheskaya Observatoriya 284, 76–83 (In Russian).

Brooks, C.E.P., 1920. The meteorology of British Somaliland. Quarterly Journal of the Royal Meteorological Society 46, 434–438.

Burt, S., 1991. Falls of dust rain in Berkshire, March 1991. Weather 46, 248.

Bücher, A., Dessens, J., 1992. Saharan dust over France and England, 6–9 March 1991. Journal of Meteorology 17, 226–233.

Carinanos, P., Galan, C., Alcazar, P., Dominguez, E., 2004. Analysis of the particles transported with dust-clouds reaching Cordoba, southwestern Spain. Archives of Environmental Contamination and Toxicology 46 (2), 141–146.

Chen, S.-H., J. Dudhia, J. S. Kain, T. Kindap, and E. Tan, 2008: Development of the online MM5 tracer model and its applications to air pollution episodes in Istanbul, Turkey and Sahara dust transport, J. Geophys. Res., 113, D11203.

Chiapello, I., Bergametti, G., Gomes, L., Chatenet, B., Dulac, F., Pimenta, J., Suares, E.S., 1995. An additional low layer transport of Sahelian and Saharan dust over the North-Eastern Tropical Atlantic. Geophysical Research Letters 22 (23), 3191–3194.

Chomette, O., Legrand, M., Marticorena, B., 1999. Determination of the wind speed threshold for the emission of desert dust using satellite remote sensing in the thermal infrared. Journal of Geophysical Research, [Atmospheres] 104 (D24), 31,207–31,215.

Coen, M.C., Weingartner, E., Schaub, D., Hueglin, C., Corrigan, C., Henning, S., Schwikowski, M., Baltensperger, U., 2004. Saharan dust events at the Jungfraujoch: detection by wavelength dependence of the single scattering albedo and first climatology analysis. Atmospheric Chemistry and Physics 4, 2465–2480.

Conte, M., Colacino, M., Piervitali, E., 1996. Atlantic disturbances deeply penetrating the African continent: effects over Saharan regions and the Mediterranean Basin. In: Guerzoni, S., Chester, R. ŽEds.., The Impact of Desert Dust Across the Mediterranean. Kluwer Academic Publishing, Dordrecht, pp. 93–102.

Council of Directive 1999/30/EC of 22 April 1999 relating to limit values for sulphur dioxide, nitrogen dioxide and oxides of nitrogen, particulate matter and lead in ambient air.
http://eurlex.europa.eu/LexUriServ/LexUriServ.do?uri=OJ:L:1999:163:0041:0060:EN:PDF.

Council Directive 96/62/EC of 27 September 1996 on ambient air quality assessment and management.
http://eurlex.europa.eu/LexUriServ/LexUriServ.do?uri=CELEX:31996L0062:EN:HTML.

Daily Aerosol Optical Thickness Measurement and Model Comparison. http://gdata1.sci.gsfc.nasa.gov/daac-bin/G3/gui.cgi?instance_id=aerosol_daily. (accessed August 2010).

Definition of "Air Pollution Episode" | Terms Beginning With "A" | Terms of Environment | US EPA. http://www.epa.gov/glossary/aterms.html.

Dudhia, J., 1989: Numerical study of convection observed during the Winter Monsoon Experiment using a mesoscale two-dimensional model. J. Atmos. Sci., 46, 3077-3107.

Dunion, J.P., Velden, C.S., 2004. The impact of the Saharan air layer on Atlantic tropical cyclone activity. Bulletin of the American Meteorological Society 85 (3), 353–365.

Ellis, W.G., Merrill, J.T., 1995. Trajectories for Saharan dust transported to Barbados using Stokess Law to describe gravitational settling. Journal of Applied Meteorology 34 (7), 1716–1726.

Engelstaedter, S., Washington, R. and Tegen, I., 2006. North African dust emissions and transport, Earth Science Reviews 79 (1-2), 73-100.

European Commission - Environment - Air. http://ec.europa.eu/environment/air/legis.htm.

Fernandez-Partagas, J., Helgren, D.M., Prospero, J.M., 1986. Threshold wind velocities for raising dust in the western Sahara Desert. ARO Technical Report, vol. 19684.3-GS. United States Army Research Laboratory, Army Research Office.

Fisher, W.B., 1978. The Middle East, 7th edn. Methuen, London, 615 pp.

Franzen, L.G., Mattson, J.O., Martensson, U., 1994. Yellow snow over the Alps and sub-Arctic from dust storm in Africa, March 1991. Ambio 23 (3), 233–235.

Freeman, M.H., 1952. Duststorms of the Anglo–Egyptian Sudan. Meteorological Office, Meteorological Reports No. 11, 22 pp.

Gatz, D.F., Prospero, J.M., 1996. A large silicon-aluminum aerosol plume in central Illinois: North African desert dust? Atmospheric Environment 30 (22), 3789–3799.

G. Kallos, M. Astitha, P. Katsafados and C. Spyrou, 2007. Long-Range Transport of Anthropogenically and Naturally Produced PM in the Mediterranean and North Atlantic: Present Status of Knowledge. Journal of Applied Meteorology, 46 , 1230-1251, doi: 10.1175/JAM2530.1.

Goudie, A.S., 1978. Dust storms and their geomorphological implications. Journal of Arid Environments 1, 291–310.

Goudie**,** A.S. and Middleton, N.J. 2001. Saharan Dust Storms**:** nature and consequences. Earth-Science Reviews, 56: 179-204.

Grell, G. A. and D´ev´enyi, D.: A generalized approach to parameterizing convection combining ensemble and data assimilation techniques, Geophys. Res. Lett., 29(14), 1693, doi:10.1029/2002GL015311, 2002.

Health & Environment | Particulate Matter | Air & Radiation | US EPA. http://www.epa.gov/particles/health.html. (accessed August 2010).

Hong, S.-Y., Y. Noh, and J. Dudhia, 2006: A new vertical diffusion package with an explicit treatment of entrainment processes. *Mon. Wea.Rev.,* 134**,** 2318-2341.

HYSPLIT4 User's Guide. http://www.arl.noaa.gov/documents/reports/hysplit_user_guide.pdf. (accessed August 2010).

Israelevich, P.L., Levin, Z., Joseph, J.H., Ganor, E., 2002. Desert aerosol transport in the Mediterranean region as inferred from the TOMS aerosol index. Journal of Geophysical Research, [Atmospheres] 107 (D21) (art. no.—4572).

Jacobson**,** M. Z., 2005. Fundamentals of Atmospheric Modeling, Second Edition, Cambridge University Press, New York.

Kaufman, Y.J., Koren, I., Remer, L.A., Tanre, D., Ginoux, P., Fan, S., 2005. Dust transport and deposition observed from the Terra-Moderate Resolution Imaging Spectroradiometer (MODIS) spacecraft over the Atlantic ocean. Journal of Geophysical Research, [Atmospheres] 110 (D10) (art. no.—D10S12).

Kalu, A.E., 1979. The African dust plume: its characteristics and propagation across West Africa in winter. In: Morales, C. ŽEd.., Saharan Dust: Mobilisation, Transport and Deposition. Wiley, Chichester, pp. 95–118.

Kocak M., Mihalopoulos N., Kubilay N., 2009. Origin and source regions of PM10 in the Eastern Mediterranean atmosphere. Atmospheric Research 92, 464–474.

Kocak, M., Mihalopoulos, N., Kubilay, N., 2007. Contributions of natural sources to high PM10 and PM2.5 events in the eastern Mediterranean. *"Atmospheric Environment"*, 41, p.3806-3818.

Lyamani, H., Olmo, F.J., Alados-Arboledas, L., 2005. Saharan dust outbreak over southeastern Spain as detected by sun photometer. Atmospheric Environment 39 (38), 7276–7284.

Mainguet, M., 1980. Aeolian interdependencies of arid Saharan areas on the borders of the Sahel and the consequences for the propagation of desertification. Stuttgarter Geographische Studien 95, 107–123.

Mattsson, J.O., Nihlen, T., 1996. The transport of Saharan dust to southern Europe: a scenario. Journal of Arid Environments 32 (2), 111–119.

Mitchell, K., 2005: The Community Noah Land-Surface Model (LSM) User's Guide Public Release Version 2.7.1. http://www.ral.ucar.edu/research/land/technology/lsm/noah/Noah_LSM_USERGUIDE_2.7.1.pdf.

Mlawer, E. J., S. J. Taubman, P. D. Brown, M. J. Iacono, and S. A. Clough, 1997: Radiative trans-fer for inhomogeneous atmosphere: RRTM, a validated correlated-k model for the long-wave. J. Geophys. Res., 102(D14), 16663-16682.

Monin, A. S., and A. M. Obukhov, 1954: Basic laws of mixing in the ground layer of the atmosphere. Tr. Geofiz Inst. Akad. Nauk SSSR, 151, 163-187.

Morales, A.F., 1946. El Sahara Espan˜ol. Alta Comisaria de Espan˜a en Marruecos, Madrid, 167 pp.

Moulin, C., Lambert, C.E., Dulac, F., Dayan, U., 1997. Control of atmospheric export of dust from North Africa by the North Atlantic oscillation. Nature 387 (6634), 691–694.

Moulin, C., Lambert, C.E., Dayan, U., Masson, V., Ramonet, M., Bousquet, P., Legrand, M., Balkanski, Y.J., Guelle, W., Marticorena, B., Bergametti, G., Dulac, F., 1998. Satellite climatology of African dust transport in the Mediterranean atmosphere. Journal of Geophysical Research, [Atmospheres] 103 (D11), 13,137–13,144.

Nalivkin, D.V., 1983. Hurricanes, Storms and Tornadoes. Amerind, New Delhi, 597 pp.

Prospero, J.M., Lamb, P.J., 2003. African droughts and dust transport to the Caribbean: climate change implications. Science 302 (5647), 1024–1027.

Prospero, J.M., 1996. The atmospheric transport of particles to the ocean. In: Ittekkot, V., Schaefer, P., Honjo, S., Depetris, P.J. (Eds.), Particle Flux in the Ocean. John Wiley and Sons, Chichester, pp. 19–52.

Rogora, M., Mosello, R., Marchetto, A., 2004. Long-term trends in the chemistry of atmospheric deposition in Northwestern Italy: the role of increasing Saharan dust deposition. Tellus. Series B, Chemical and Physical Meteorology 56 (5), 426–434.

Ryall, D.B., Derwent, R.G., Manning, A.J., Redington, A.L., Corden, J., Millington, W., Simmonds, P.G., O'Doherty, S., Carslaw, N., Fuller, G.W., 2002. The origin of high particulate concentrations over the United Kingdom, March 2000. Atmospheric Environment 36 (8), 1363–1378.

Saharan Mineral Dust Experiment - SAMUM.
http://samum.tropos.de/scopeintro.html.

Sahara. http://en.wikipedia.org/wiki/Sahara. (accessed August 2010).

Schepanski K, Tegen I, Todd MC, Heinold B, Bönisch G, Laurent B, Macke A (2009) Meteorological processes forcing Saharan dust emission inferred from MSG-SEVIRI observations of subdaily dust source activation and numerical models. Journal of Geophysical Research 114(d10): D10201.

Schuetz, L., 1979. Sahara dust transport over the North Atlantic ocean: model calculations and measurements. In: Morales, C. (Ed.), Saharan Dust: Mobilization, Transport, Deposition. John Wiley & Sons, New York, pp. 267–277.

Schwikowski, M., Seibert, P., Baltensperger, U., Gaggeler, H.W., 1995. A study of an outstanding Saharan dust event at the high-Alpine Site Jungfraujoch, Switzerland. Atmospheric Environment 29 (15), 1829–1842.

Seinfeld, J. H., and Pandis, S. N., 2006. Atmospheric Chemistry and Physics: From Air Pollution to Climate Change. 2nd ed. John Wiley and Sons, Inc., Hoboken, NJ.

Sivall, T., 1957. Sirocco in the Levant. Geografiska Annaler 39, 114–142.

Sokolik, I.N., Winker, D.M., Bergametti, G., Gillette, D.A., Carmichael, G., Kaufman, Y.J., Gomes, L., Schuetz, L., Penner, J.E., 2001. Introduction to special section: outstanding problems in quantifying the radiative impacts of mineral dust. Journal of Geophysical Research, [Atmospheres] 106 (D16), 18,015–18,027.

Swap, R., Garstang, M., Greco, S., Talbot, R., Kallberg, P., 1992. Saharan dust in the Amazon Basin. Tellus. Series B, Chemical and Physical Meteorology 44 (2), 133–149.

Tanaka, T.Y., Kurosaki, Y., Chiba, M., Matsumura, T., Nagai, T., Yamazaki,A., Uchiyama,A., Tsunematsu, N.,Kai,K., 2005. Possible transcontinental dust transport from North Africa and the Middle East to East Asia. Atmospheric Environment 39 (21), 3901–3909.

The November 2001 Technical Procedures Bulletin (TPB).
http://www.emc.ncep.noaa.gov/mmb/mmbpll/eta12tpb/.

Thomas, F.G., 1982. Sahara dust-fall in Dover, Kent. Journal of Meteorology 7, 92–93.

Tout, D.G., Kemp, V., 1985. The named winds of Spain. Weather 40, 322–329.

Vukmirovic, Z., Unkasevic, M., Lazic, L., Tosic, I., Rajsic, S., Tasic, M., 2004. Analysis of the Saharan dust regional transport. Meteorology and Atmospheric Physics 85 (4), 265–273.

Warner, T. T. (2004) Desert Meteorology, Cambridge University Press, Cambridge.

Washington, R., Todd, M.C., Engelstaedter, S., Mbainayel, S., Mitchell, F., 2006. Dust and the low-level circulation over the Bodele Depression, Chad: observations from BoDEx 2005. Journal of Geophysical Research, [Atmospheres] 111 (D3) (art. no.—D03201).

WRF Model Users Site.
http://www.mmm.ucar.edu/wrf/users/. (accessed August 2010).